Synthesis, Characterization, Membrane Fabrication and Gas Transport Behaviors of Liquid Crystal Polymer Materials

Feras Hamed Rabie

A DISSERTATION SUBMITTED TO THE FACULTY OF THE GRADUATE SCHOOL
OF VIRGINA POLYTECHNIC INSTITUTE AND STATE UNIVERSITY IN PARTIAL FULLFILMENT OF THE
REQUIREMENTS FOR THE DEGREE OF

Doctor of Philosophy

In

Chemical Engineering

Stephen Martin, Co-chair

Eva Marand, Co-chair

Donald Baird

Luke Achenie

Zdenka Sedlakova

September 12, 2013

Blacksburg, VA

Keywords: Liquid crystal, polymer, membrane, gas transport

Synthesis, Characterization, Membrane Fabrication and Gas Transport Behaviors of Liquid Crystal Polymer Materials

Feras Hamed Rabie

ABSTRACT

A variety of liquid crystalline (LC) materials have been examined as potential membrane separation materials. The order present in the LC phases has measurable effects on solute sorption, diffusivity, permeability, and selectivity, and can thus be used to tune the transport and separation of different species. The current work has focused on polymer dispersed liquid crystal (PDLC), linear butadiene diol based side chain liquid crystalline polymer (LCP), and linear and crosslinked acrylate based LCP membranes. The focus was primarily on the separation of propylene and propane, a separation of significant industrial interest that is not easily achieved with current membrane technology.

Polysulfone (Psf) and 4-cyano-4'-octylbiphenyl (8CB) were used to fabricate polymer dispersed liquid crystal (PDLC) membranes. Permeation properties for propane and propylene through polysulfone membranes with increasing LC concentrations were measured at temperatures above and below the glass transition temperature and in several LC phases. The plasticization of PSf by 8CB increased permeability and selectivity with increasing temperatures below the T_g, and membranes with higher LC concentrations exhibited a higher mixed gas permeability and selectivity for propylene. Permeability selectivity decreased across the smectic to nematic phase transition. Overall, selectivities were low, and membrane stability was a significant problem, especially at higher pressures. Thus, several LCP systems were studies as candidates for membrane gas separations.

A side chain liquid crystalline poly(butadiene)diol with cyanobiphenyl mesogens was impregnated in a porous PTFE support for gas transport studies. Single gas sorption for propane and propylene in the LCP were investigated in the smectic A mesophase. Gas transport in the glassy state showed separation dominated by differences in gas diffusivity. Permeabilities and selectivities for

propylene/propane in the liquid crystal mesophase increased with increasing temperature due to an increase in the segmental motional of the mesogenic units which facilitated solubility of propylene over propane. In addition, an increase solubility differences between propane and propylene were observed with an increase in feed pressure. Mixed gas permeability measurements resulted in an increase in selectivity both below and above the glass transition temperature due to competitive sorption of the two gases. The thermal behavior of liquid crystalline poly(butadiene)diols (PBDs) containing methoxy- or butoxy-substituted azobenzene side chains was studied. A strong dependence of the viscous and dynamic moduli of the polymer with respect to frequency and degree of modification was observed, but the results suggested that prolonged membrane stability for linear poly(butadiene)diol LCPs would be difficult to achieve. As a result, a new class of cross-linkable acrylate based side-chain LCPs was developed.

A mesogenic cyanobiphenyl based acrylate monomer, in combination with a non-mesogenic comonomers and a cross-linking agent, was used was used to fabricate stable cross-linked LCP films for membrane separation applications using an *in situ* free radical polymerization technique with UV initiation. To our knowledge, this is the first reported example of a crosslinked LCP membrane. Increasing the cross-linker content resulted in a decrease in mesogen order. At temperatures in the LC mesophase permeability selectivity for propylene over propane was derived from both solubility and diffusivity selectivity and was higher for the membrane with lower crosslinker content. An increase in the temperature causes a decrease in molecular ordering and consequently decreased permeability selectivity. At temperatures approaching the nematic/isotropic transition and above, the membrane with higher crosslinker content exhibited higher propylene selectivity. Mixed gas studies of propylene/propane resulted in higher selectivities compared to the single gas runs due to the decrease of propane permeability by the presence of propylene.

To my parents and brother and sister

ACKNOWLEDGMENTS

I have been indebted in the preparation of this thesis to my advisors Stephen Martin and Eva Marand. Stephen Martin, whose patience and kindness, as well as his academic experience, have been invaluable to me. I am also extremely grateful to Eva Marand for allowing me to obtain her knowledge to achieve my academic goal.

I am also very grateful for the opportunity to work with a talented team of committee members. The support and encouragement of my committee members has been valuable to me. Thank you Donald Baird, Luke Achenie and Zdenka Sedlakova.

I am most especially indebted to my colleague, mentor and friend, Lenka Polakova, not only for her encouragement but for being an inexhaustible source of knowledge and ideas. Lenka's constant support has been instilled in the very fabric of my research.

I would like to thank the departmental staff for their help throughout my academic studies; especially Mike Vaught and Riley Chan who have helped me build my equipment. In addition, I would like to thank my labmates (past and present) for our insightful conversations and their good company.

My deepest thanks to my parents, Laila and Hamed, who have been a constant source of love and encouragement. This thesis would certainly not have existed without them. To my brother and sister Basil and Arwa for being my brother and sister.

Table of Contents

List of Figures

List of Tables

Chapter 1: Thesis Overview

Membrane separation technologies have attracted great interest due to their low energy consumption, low capital cost, and low maintenance costs compared to conventional separation techniques. Current technologies that separate gases such as olefins from paraffins and CO2 from natural gas are limited due to economic constraints. Accordingly, there are incentives to find new membrane materials capable of performing these separations. There has been limited research on the gas transport properties of liquid crystals (LCs). The unique thermal and morphological properties of liquid crystalline materials offer the ability for tuning and controlling mass transport behavior. The ordering of the LC mesogens enhanced solubilities of polar gases and diffusion of smaller penetrants. The work presented here is a study of the gas transport properties of three different types of liquid crystalline materials. Polymer dispersed liquid crystal (PDLC) membranes were fabricated to investigate the effect of liquid crystal concentration and domain size on the transport of propane and propylene. An impregnated linear liquid crystalline polymer (LCP) membrane was used to investigate the effect of material morphology and competitive permeation by studying the dependence of solubility and diffusivity on temperature and pressure. Finally, crosslinked LCPs were investigated to study the effect of ordering and free volume on gas transport as the crosslinker content changes. The contents of each chapter are described briefly below.

Chapter 2 provides a review on the topics of liquid crystalline materials and gas transport through dense films. The classes of liquid crystals are outlined and the common phases encountered are discussed. The LC phase properties as well as the most useful characterization techniques are reviewed. Fundamentals of gas transport in polymeric materials are included. This is divided into the sorption and diffusion of constituents in polymeric materials. Finally, studies pertaining to the gas transport properties of LCs are reviewed.

Chapter 3 provides a brief overview of the permeation apparatus built for gas transport measurements. The system is able to measure single and mixed gas permeation. The chapter includes necessary information that is needed to understand, build and calibrate a similar unit.

Chapter 4 describes the fabrication, characterization and gas transport properties of polymer dispersed liquid crystal (PDLC) membranes. Through the solubility differences between LC and polymers, LC molecules phase separate from an LC/polymer solution to form PDLCs. PDLC films have generated significant interest due to their unique electro-optic properties, but separation applications have been

limited to polymer/LC blend membranes. We have developed novel paraffin/olefin separation membranes using LC domains in a polymer composite. The effect of LC ordering and polymer phase behavior on olefin/paraffin transport is discussed.

Chapter 5 reports on the effect of material phase and feed pressure and temperature on the gas transport properties of several gases through linear Side-Chain (SC) LCP including thermal gravimetric analyzer and single and mixed gas permeation. The SCLCPs incorporate the cyanobiphenyl mesogenic unit laterally attached to a poly(butadiene)diol via an alkane spacer. An impregnation technique to fabricate a dense linear LCP membrane exhibiting mesomorphic phase behavior is described using field emission scanning electron microscopy and differential scanning calorimetry. The segmental motion of the polymer backbone and grafted mesogenic units play a significant role in the dissolution and diffusion of penetrate gases. The ability of LC mesogens to act as barriers for gases is described.

Chapter 6 reports on the dependence of storage and loss moduli on LC grafting densities and LC phases. To improve on the intrinsic mechanical limitations of LC material for membrane applications, an investigation of the mechanical properties were performed for linear LCPs. In addition, a time-temperature superposition has been successfully applied to predict LCP stability over long operating times. The characterizations of methoxy- or butoxy-substituted azobenzene in side chains include differential scanning calamity, polarized optical microscopy and dynamic mechanical thermal analysis. Heating linear LCP membranes above the glass transition and into the LC or isotropic states increases polymer mobility, which results in an undesirable decrease in the loss and storage moduli. For this reason, a cross-linkable LCP material have been synthesized.

Chapter 7 describes the synthesis and copolymerization of novel crosslinkable nitroazobenzene and cyanobiphenyl methacrylate liquid crystals with 2-ethylhexyl acrylate (2-EHA). By using a free radical polymerization approach, copolymer LCs were synthesized at varying copolymer ratios. Thermal properties of the homopolymers and copolymers were determined using differential scanning calorimetry, polarized optical microscopy and X-ray scattering. The use of a single reaction scheme to produce multiple LCPs with various mesogen types allows for the facile optimization of LCP membranes for specific applications.

Chapter 8 discusses the effects of LC ordering and polymer mobility on gas transport properties in crosslinked LCP membranes. A novel technique was used to fabricate crosslinked LCP films. There have been no reports of networked acrylate LCP films to date. The technique uses in situ free radical polymerization in a specifically designed reaction cell with UV initiation. The ability of cyanobiphenyl to form ordered phases attached to a network is discussed. Enhanced interactions of polar gases form with

ordered LC mesogens to produce solubility selective membranes. The LCP network showed improved mechanical stability compared to linear LCPs as the LCP network does not have macroscopic mobility.

Chapter 2 Literature Review

2.1 Liquid Crystals

Liquid crystals are known as the fourth state of matter. They represent a state of matter which is characteristic with the ordering of a solid and the mobility of a liquid.[1] Depending on the class of the liquid crystal, ordering can be a function of temperature, solvent, concentration of solution, electric or magnetic fields, shear flow, grooving of the substrate surface, as well as anchoring interactions[2]. Thermotropic liquid crystals are further classified as low molecular weight liquid crystals or polymer liquid crystals. Low molecular weight liquid crystals have rod-like molecular structures and a rigid long axis with strong dipoles.[3] Polymer liquid crystals have flexible polymer backbones and rigid mesogens, either attached to the polymer with a comb-like structure or fully incorporated in the polymer backbone and combination thereof.[4-6]

Liquid crystal materials have been studied and developed since the 1800's. Due to their anisotropic nature, liquid crystals are birefringent,[7] which is the double refraction of light in a transparent, molecularly ordered material. This leads to many applications relating to optical imaging, displays, light modulators, and thermometers as well as applications pertaining to polymer manufacturing and plasticizers. [8-10] In contrast, the intrinsic transport properties and separating abilities of these materials have not been fully investigated and further research needs to be performed to understand the effect of the molecular orientation and enhanced intermolecular interactions of the liquid crystals on the transport properties of both gases and liquids.

2.1.1 Lyotropic Liquid Crystals

In addition to lyotropic liquid crystals being temperature dependent, concentration of solution and solvent/solute interactions effect liquid crystal phase formation. Lyotropic liquid crystals were first observed in a mixture of myelin and water in the 1850's. LLCs are a class of amphiphilic surfactants with the majority having two distinct parts: a polar, hydrophilic or ionic head attached to a non-polar, hydrophobic section, often being an alkane tail. The arrangement is strongly dependent on the polarity of the solvent. At high concentrations, the tail would be strongly attracted to a nonpolar solvent or would be repelled by polar solvent, such as water. Figure 2.1 shows several lyotropic liquid crystal phases in water.

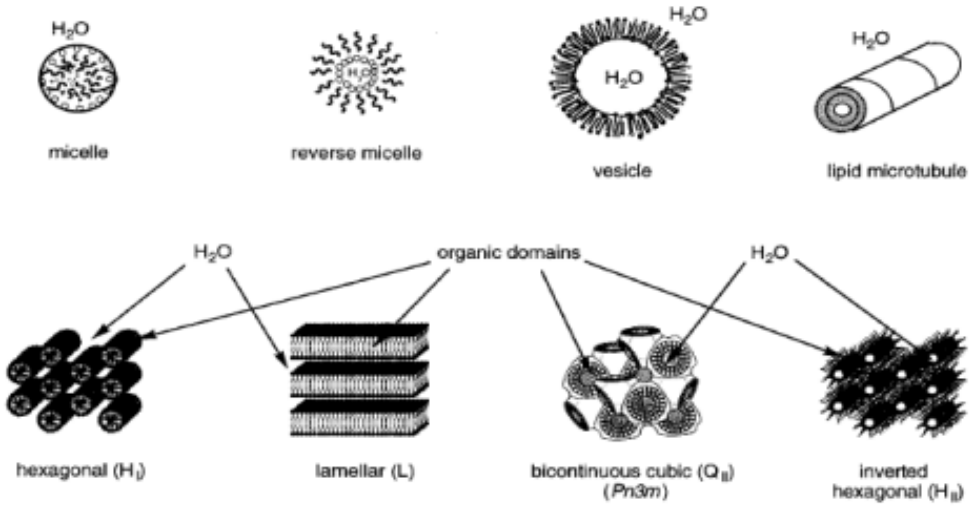

Figure 2.1: Lyotropic liquid crystal phases commonly encountered[11]

A lyotropic liquid crystal commonly known is soap. Figure 2.2 shows the phase behavior of soap, which is representative of a phase diagram of many amphiphilic molecules. Tk, the Krafft boundary, is the boundary defining the minimum surfactant concentration to achieve crystalline dispersions in surfactant-water systems and the dashed line represents the minimum concentration required to form micelles.

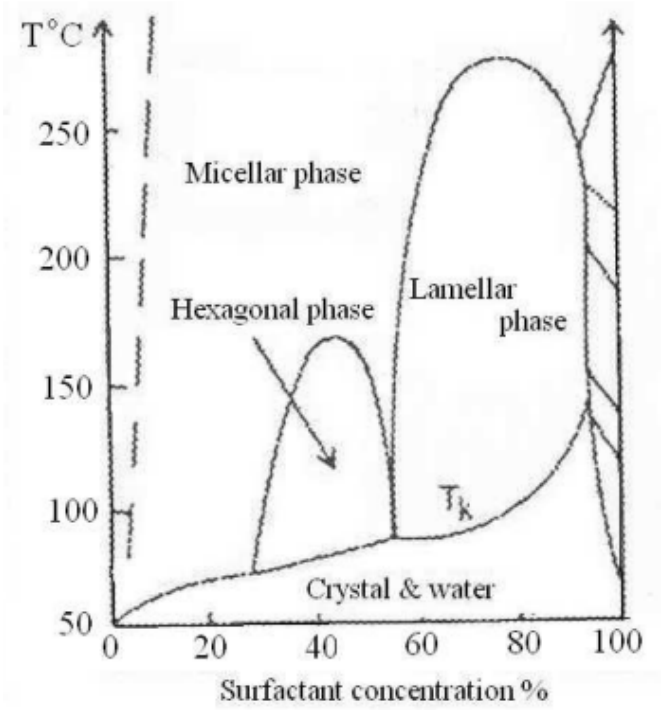

Figure 2.2: Example of lyotropic LC phase diagram.[12]

2.1.2 Thermotropic Liquid Crystals

Thermotropic liquid crystals (TLCs) are a class of liquid crystal in which molecular phases are primarily dependent on temperature, but degree of molecular ordering is also responsive to other stimuli such as: shearing, annealing, applied electric field, or anchoring effects.[13-15] The liquid crystalline phase is observed in a large number of organic compounds. Despite significant differences in chemical composition, these molecules have similar chemical structures and physical properties. Thermotropic liquid crystals encompass two categories: low molar mass liquid crystals and polymer liquid crystals. Low molar mass liquid crystals (LMMLCs) have rod-like organic mesogens which usually exhibit a length-to-diameter ratio of 3 to 8.[16] They comprise a central rigid core within a ring system connected to two terminal groups for which at least one should be an alkyl chain. Examples of a ring system would be aromatic, alicyclic, aromatic heterocyles, saturated heterocycles, or condensed ring systems. The central core, if applicable, usually is a polar group such as but not limited to azo-groups, azoxy-groups, imines, esters, thioesters, biphenyls and amides.[9] Thermotropic liquid crystals include three classes: nematic, smectic, and cholesteric or chiral liquid crystals, with each having specific phase behaviors and characteristics that lead to various applications.

Nematic liquid crystals are the simplest type of liquid crystals, which exhibit only one-dimensional order, long range orientational order. The molecules in the nematic phase are oriented on average along a particular direction. Assuming the liquid crystals to be cylindrical rods, positional ordering of nematic liquid crystals is classified by the preferred direction unit vector, n, and the orientational order parameter, s.[17] The orientational order parameter is defined as

$$S = \langle {}^{3}/_{2}\, cos^{2}(\theta) - {}^{1}/_{2} \rangle \qquad (2.1)$$

where θ is the angle between each molecular axis and the director, n (Figure 2.3).

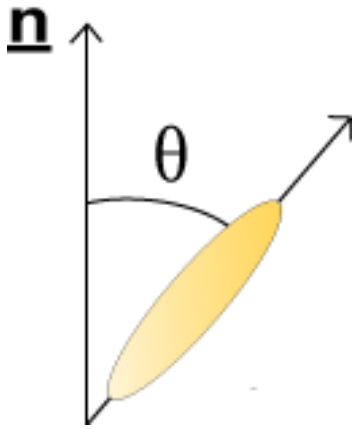

Figure 2.3: Angle between director and liquid crystal

The brackets represent the average. The degree of ordering is a function of temperature and can range from a value of 0 (purely isotropic) to 1 (purely crystalline). Madhusudana, et. al. concludedthat ordering increases with an increase in chain length for several p-n-alkyl-p'-cyanobiphenyl small chain liquid crystals (Figure 2.4).[18] Within the nematic phase, as temperature was increased, the order parameter decreased from 0.6 to 0.3.

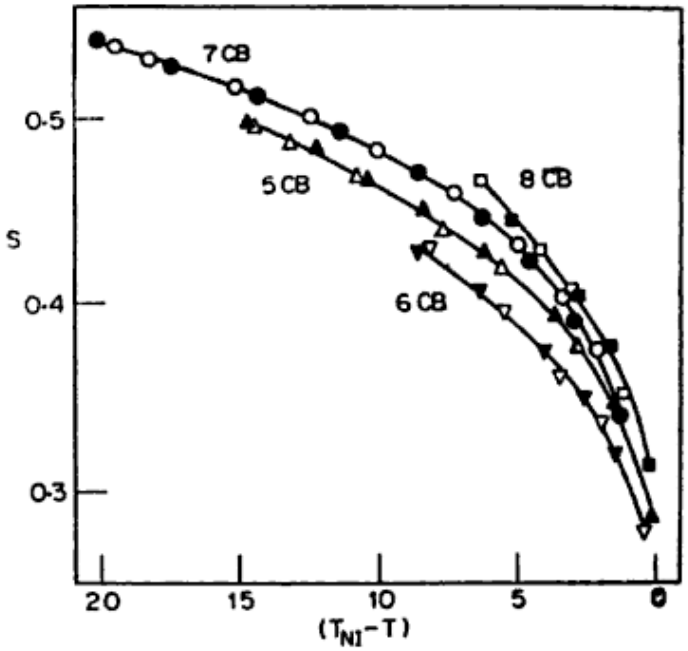

Figure 2.4: Order parameters of several para-cyanobiphenyl liquid crystals on the dependence of varying alkyl chain lengths and temperature.[18]

2.1.3 Cholesteric Liquid Crystals

A cholesteric liquid crystal is a type of liquid crystal with a helical structure. Cholesteric liquid crystals are also know as chiral nematic liquid crystals. They possess a chiral carbon and can not be racemic or be in combination with a chiral dopant (Figure 2.5).[5,6]

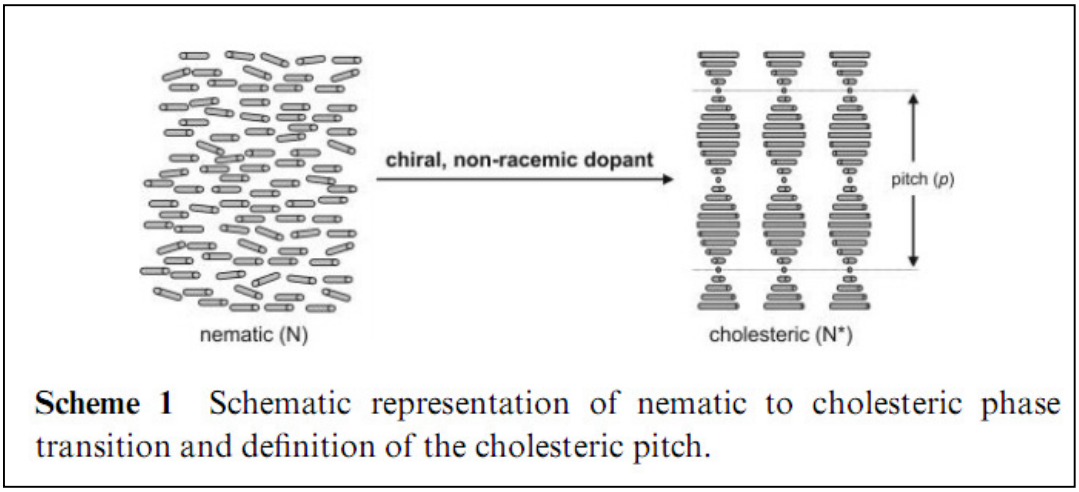

Scheme 1 Schematic representation of nematic to cholesteric phase transition and definition of the cholesteric pitch.

Figure 2.5: Chiral LC phase created by the doping of a nematic liquid crystal[19]

The rod-like molecules exhibit orientational order and no translational order, similar to that of a nematic liquid crystal. Due to the chiral center, there is a rotation of the orientational ordering of the molecules, which gives rise to a helical structure. The distance over which the director makes a full rotation is called the pitch, p and is shown in Figure 2.6.[20] This can be influenced by the temperature as well as boundary conditions of the system.

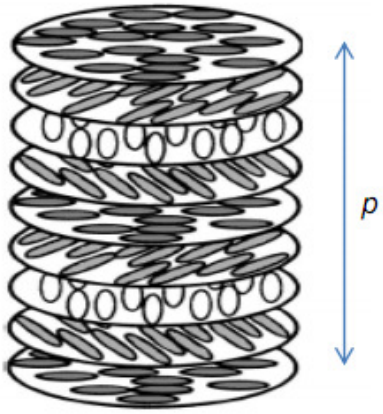

Figure 2.6: Schematic representation of the cholesteric phase. The distance needed for a 2π rotation is a pitch, p.[20]

2.1.4: Smectic Liquid Crystals

Smectic liquid crystals are often categorized as a 2-dimensional liquid crystal. Similar to the nematic phase, smectic liquid crystals have long-range directional order, but also an added translational

order, also known as a layered structure. The director can be parallel (smectic A) or at an angle (smectic C) to the layer normal (Figure 2.7).

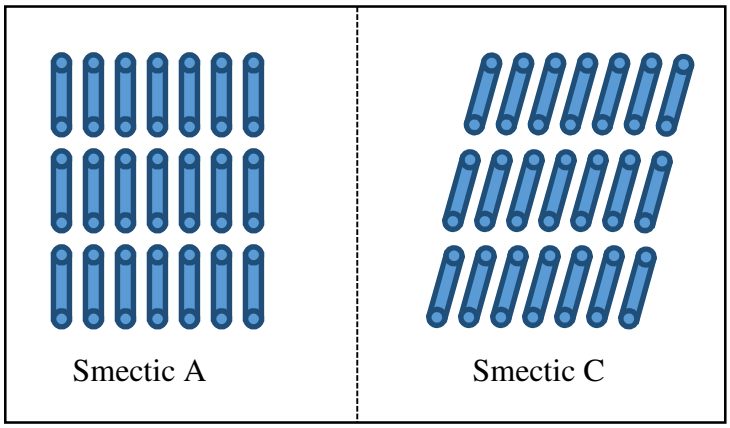

Figure 2.7: A simplistic representation of the smectic A and smectic C liquid crystal phase

2.1.5 Polymer Liquid Crystals

Polymer liquid crystals, PLCs, are a distinct class of liquid crystals where the liquid crystal mesogens are attached to a polymer network. The liquid crystal mesogens are fully incorporated in the main chain (main chain liquid crystal polymers), attached to form a comb like structure (side-chain liquid crystal polymers), or a combination thereof.[4-6] PLCs are attractive materials for photonic, ferroelectric and anti-ferroelectric applications or in non-linear optics.[10, 21-24] In side-chain liquid crystal polymers (SCLCPs), mesomorphic phase behavior is strongly dependent on the decoupling of the polymer backbone from the polar mesogen by the incorporation of spacer alkane chains.[25] A previous study showed that as the spacer length increases, a more well-ordered mesogenic phase is formed, due to the increased mobility the spacer grants the mesogen. [26] On the other hand, an increase in chain length plasticized the material and resulted in a decrease of mesogenic ordering.[27]

Certain characterization techniques are needed to investigate the phase behavior of LCP material. The most commonly used are differential scanning calorimetry (DSC), x-ray diffraction (XRD), nuclear magnetic resonance (NMR), polarized optical microscopy (POM), and dielectric measurements.[28-32]

Primary XRD techniques used for PLC morphological characterization are small angle x-ray scattering (SAXS) and wide angle x-ray diffraction (WAXD).[32-33] Depending on the phase of the liquid crystals, specific peaks arise. The Smectic phase has long-range orientational order and positional order

(translational symmetry). The translational order or the spacing between the polymer backbones (Figure 2.8) is represented by a sharp peak at smaller scattering angles and is observed while scanning the equatorial direction. The orientational order or the spacing between mesogenic side chains are shown by a diffuse peak at larger angles and is observed while scanning the meridian direction.[34,35] Scattered waves interfere constructively and allow for the use of Bragg's law of diffraction.

$$sin\theta = \frac{n\lambda}{2d} \qquad (2.1)$$

where d is the distance between polymer backbones or mesogens, λ is the wavelength of the incident x-ray beam, θ is the angle of incidence, and n is an integer.

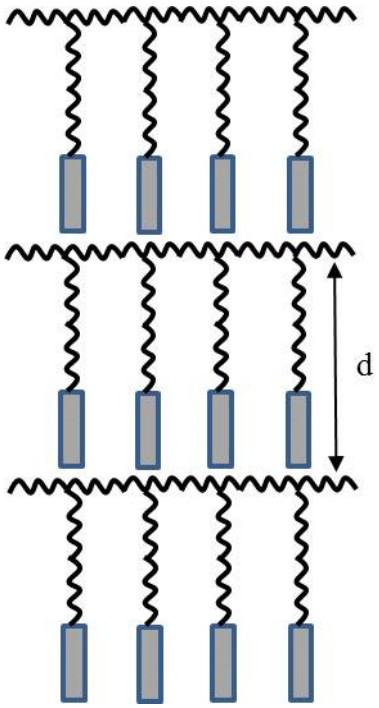

Figure 2.8: A 'tail-to-backbone' representation of spacing between "comb-like" PLCs

Various research groups have studied the dependence of the packing structure and *d*-spacing on flexible spacer groups. Silveira, et. al. concluded that increasing the spacer length motivates interdigitation between mesogenic groups. This is demonstrated by comparing the *d*-spacing, determined by SAXS, and the theoretical full length of the mesogen (Figure 2.9).[36] For polyacrylate SCLCPs, a packing structure of tail-to-tail was determined due to the measured *d*-spacing being much larger than the theoretical length of the mesogen. Increasing the tail length increases the interdigitation of the LCs. In

contrast, Zhou, et al. investigated acrylate SCLCPS with the LC attached from the mesogen and found comparable *d*-spacing values to the theoretical length, which lead to the conclusion the packing structure is arranged tail to backbone.[32]

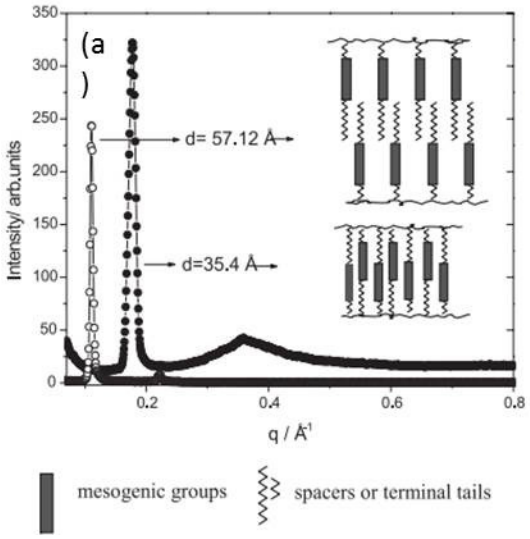

	d	*l*	*d/l*	d_2
P_{46}	52.8	31.92	1.65	5.50
P_{410}	57.12	34.20	1.67	5.26
P_{11M}	35.4	36.94	0.96	5.48
P_{11Cl}	35.3	36.94	0.96	5.27

Figure 2.9: *d*-spacing of PLCs acrylates (a) Small angle X-ray scattering of polyacrylates (b) d_2, d and l values are given in angstroms.[36]

Due to the absence of long-range translational order, nematic liquid crystals show no scattering peak on the equatorial direction, but rather exhibit a diffuse peak in the direction of the meridian that corresponds to the distance between the grafted mesogenes. To identify liquid crystal behavior, polarized optical microscopy and differential scanning calorimetry can be used in conjunction with XRD techniques.

DSC is employed to study the phase behavior and transition temperatures of liquid crystalline materials. Polymer liquid crystals typically exhibit a glass transition prior to mesomorphic states. The rubbery state of the polymer give the mesogenic units enough mobility to organize into their phases. Furthermore, liquid crystalline transition temperatures as well as the material clearing point (isotropization) can be accurately measured. In addition, monotropic characteristics can be detectable by taking isobars at both cooling and heating cycles.[37]

Birefringence of light is a consequence of anisotropic orientation in liquid crystalline polymers.[38] This is measured by means of a polarized optical microscope. Depending on the alignment process and liquid crystal molecular properties, several textures can be observed. Each phase can be identified by their characteristic defect structure or textures.

The most commonly observed textures for nematic liquid crystals are the schlieren, marble and thread textures. The schlieren texture of nematic liquid crystals is observed when the orientation of the director, n, is discontinuous (point of disclination). The strength of disclinations, s, for nematics, have values of ±1/2 (2 brushes) or ±1 (4 brushes). The sign is associated with the relative rotation of the brushes with respect to the sample. This can be seen in Figure 2.10a. Figure 2.10b represents the marbled texture with many domains, each with its own homogenous axis. It is usually observed in thin sample preparations. The thread-like liquid crystal texture is typically observed in thick layers and is shown in figure 2.10 c. The threads are line singularities, which usually connect two s=±1/2 point defects. [39]

Figure 2.10: Various textures of nematic liquid crystals (a) Schlieren texture of 4-n-caproyloxy-4'-ethoxyazoxybenzene[40] (b)Marbled texture of Azo-benzene compound after uv exposure[41] (c)Thread like nematic LC texture of Benzoic Acid, 4-(4-Pentenyloxy)-,2-Methyl-1,4-phenylene Ester[42]

Smectic A phasescan exhibit batonnets, fan-shaped and focal conic textures. Smectic C phases can exhibit schlieren, hexagonal columnar and rectangular columnar textures. Example POM images of smectic A and smectic C phases are shown in Figure 2.11. In cooperation with other methods, POM becomes a powerful tool to identify phase change and texture.

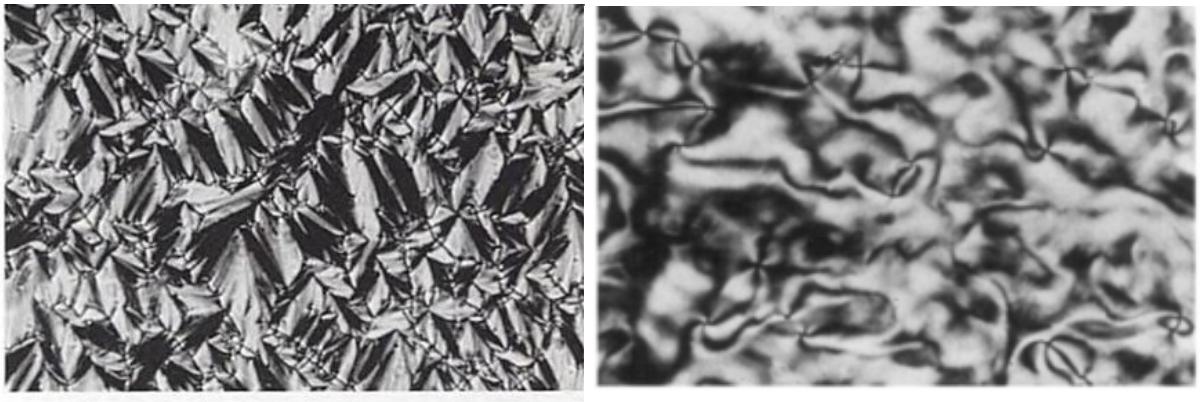

Figure 2.11: Polarized Optical Images of Smectic liquid crystals. Focal-conic, smectic A (left) [43] Schlieren, Smectic C (right).[40]

2.2 Steady-State Diffusion

Membrane separation processes are an attractive alternative to conventional separation techniques due to their relative ease of operation and low energy and capital or startup cost.[44] Interest in this field dates back to the mid 1800's, where Graham used natural rubber to enrich the oxygen content of air from 21% to 41%.[45] Graham concluded that permeation through non-porous, dense, polymer membranes followed a three-step solution diffusion mechanism. Penetrant gas or liquid molecules dissolve onto the face of the membrane (feed side), diffuse across the length of the membrane, due to a concentration gradient, and finally desorb from the permeate face of the membrane and enter the downstream low pressure side of the system. The 1-dimensional flux of gas A, through the dense membrane film can be accurately described by Fick's law.

$$N_A = -D\frac{dC_A}{dx} + W_A(N_A + N_P) \qquad (2.2)$$

where D is the gas diffusion coefficient of solute A in the material, C_A is the local concentration of dissolved gas A in the membrane, and N_P is the flux of the membrane (which is assumed to be zero). This reduces to

$$N_A = -\frac{D}{1-W_A}\frac{dC_A}{dx} \qquad (2.3)$$

This phenomenon can be effectively modeled using the time-lag method based on Fickian diffusion. By definition, the steady state permeability of a single gas molecule, P_A, is the steady state gas flux normalized by the pressure gradient between the feed and permeate side of gas molecule A and the thickness of the membrane.

$$P_A = \frac{N_A l}{p_2 - p_1} \qquad (2.4)$$

where p_2 and p_1 are defined as the upstream and downstream pressures, respectively. Combining equations 2.3 and 2.4:

$$P_A = \frac{D}{1-W_A} \frac{dC/dx}{\Delta P/l} \qquad (2.5)$$

Integrating both sides of the equation from x=0 ($C=C_2$) and x=l ($C=C_1$)

And setting

$$\overline{D} = \frac{1}{C_2 - C_1} \int_{C1}^{C2} \frac{D}{1-w_A} dC \qquad (2.6)$$

Permeability becomes,

$$P_A = \left[\overline{D}\right] \frac{C_2 - C_1}{p_2 - p_1} \qquad (2.7)$$

At low downstream pressure where $p_2 >> p_1$ and $C_2 >> C_1$, permeability can be defined with two components

$$P_A = \left[\overline{D}\right]\left[\overline{S}\right] \qquad (2.8)$$

Where $S = \frac{C_2}{P_2}$, the apparent sorption coefficient. At low pressures, S is a Henry's law coefficient and can be used with a permeability measurement (at the same pressure) to calculate the average gas diffusivity at a constant pressure.

Fick's second law is applied to model the concentration profile for the measurement of solubility and diffusivity by assuming there is no boundary layer resistance at the membrane interface and no or negligible convective flow through the membrane.

$$\frac{\partial C_i}{\partial t} = \frac{\partial}{\partial x}\left(D_{eff} \frac{\partial C_i}{\partial x} \right) \qquad (2.9)$$

C_i is the concentration of species i, D_{eff} is the effective diffusivity of the solute in the medium, x is the direction of gas transport and t is time. The boundary conditions below are applied with a membrane initially free of diffusing species.

$C(x, 0) = 0$ (2.10a)

$C(0, t) = C_o$ (2.10b) (2.10)

$C(L, t) = C_L \approx 0$ (2.10c)

A Laplace transform or separation of variables is used to obtain the concentration profile of the membrane perpendicular to its feed and permeate face.

$$C = C_o\left(1 - \frac{x}{L}\right) + \frac{2C_o}{\pi}\sum_{n=1}^{\infty}\frac{1}{n}\sin\left(\frac{n\pi x}{L}\right)\exp\left(-\frac{D_{eff}n^2\pi^2 t}{L^2}\right) \quad (2.11)$$

Fick's first law is used to obtain the flux, J.

$$J = -D\frac{\partial C}{\partial x} \quad (2.12)$$

Differentiating equation 2.11 with respect to x and combining with equation 2.12:

$$J = \frac{D_{eff}C_o}{L} + \frac{2D_{eff}C_o}{L}\sum_{n=1}^{\infty}\cos\frac{n\pi x}{L}\exp\left(-\frac{n^2\pi^2 D_{eff}t}{L^2}\right) \quad (2.13)$$

Solving the unsteady state problem results in the following equation for solute diffusivity:

$$D = \frac{l^2}{6t_{lag}} \quad (2.14)$$

The time-lag is independent of the solubility coefficient and can be determined directly from experimental permeation data shown in Figure 2.12. Permeability is calculated using the steady-state pressure increase with time. Ideal gas law is used to attain molar flow rate across the membrane. The ideal gas law is applicable due to low permeate pressures. The steady-state region is extrapolated to y = 0 and x = t_{lag}.

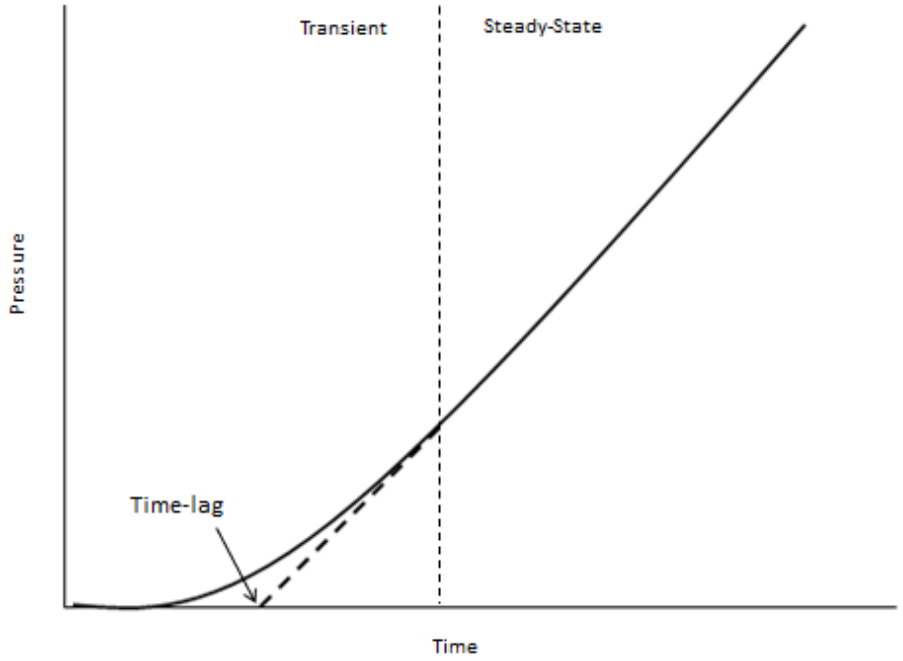

Figure 2.12: Measurement of time-lag by extrapolating steady-state pressure vs time

For a mixture of two gases permeating through a non-porous dense membrane at steady-state, the ratio of components A and B is defined as the separation factor or selectivity, α**.**

$$\alpha_{AB} = \frac{P_A}{P_B} = \left[\frac{\overline{D_A}}{\overline{D_B}}\right]\left[\frac{\overline{S_A}}{\overline{S_B}}\right] \qquad (2.15)$$

2.3 Sorption

Sorption is generally used to describe the penetration and dispersal of permeant molecules into the polymer matrix which includes adsorption, absorption, and the incorporation of permeants into microvoids in the polymer. Sorption is a responsive phenomena dependent on several factors, which include but are not limited to, temperature, permeate gas properties (size, critical temperature, etc), the materials free volume, as well as the phase of the material (glassy or rubbery polymers).

2.3.1 Effect of Material Phase

The phase of the polymer, specific polymer/gas interactions and the properties of the gas will dictate the sorption behavior of a system. Figure 2.13 shows the isotherm modes that are commonly encountered during sorption isotherm studies. Henry's law of sorption is obtained with rubbery polymers when interacting with non-condensable gases. Florry-Huggins sorption occurs when permeant/permeant interactions are strong relative to permeant/polymer interactions. Langmuir sorption represents the sorption in specific microvoids. Dual-mode sorption is a combination of Langmuir sorption and Henry's law of sorption.

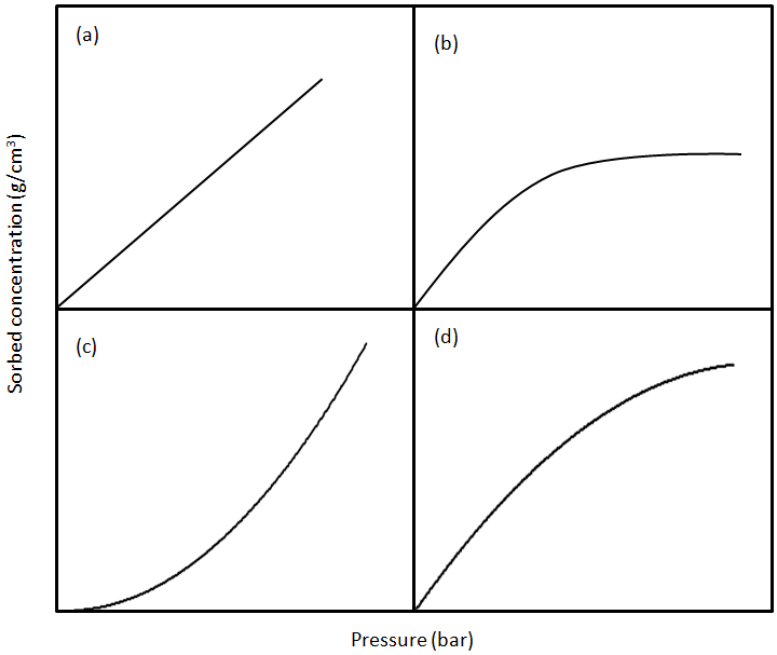

Figure 2.13: Commonly encountered isotherm modes. (a) Henry's Law of sorption (b) Langmuir (c) Flory-Huggins (d) dual-mode sorption

2.3.1.1 Rubbery Polymers

Henry's Law of sorption, Figure 2.13a, is normally obtained with rubbery polymers when interacting with non-condensable gases. Behavior is similar to sorption in an infinitely dilute liquid, which is modeled by

$$C = Sp \qquad (2.16)$$

S is the permeant solubility coefficient with respect to the polymer. The solubility coefficient is a constant, independent of sorbed concentration at a specific temperature. P is the partial pressure of the low interacting gas. In result, the sorbed concentration of the gas shows a linear relationship to the partial pressure. Pinnau, et. al. investigated the gas sorption of poly(dimethyl siloxane) with various gases.[46] Figure 2.14 shows sorption isotherms for several diatomic gases. Henry's law isotherms were observed and are typically present for systems that exhibit no specific polymer-penetrate interactions.

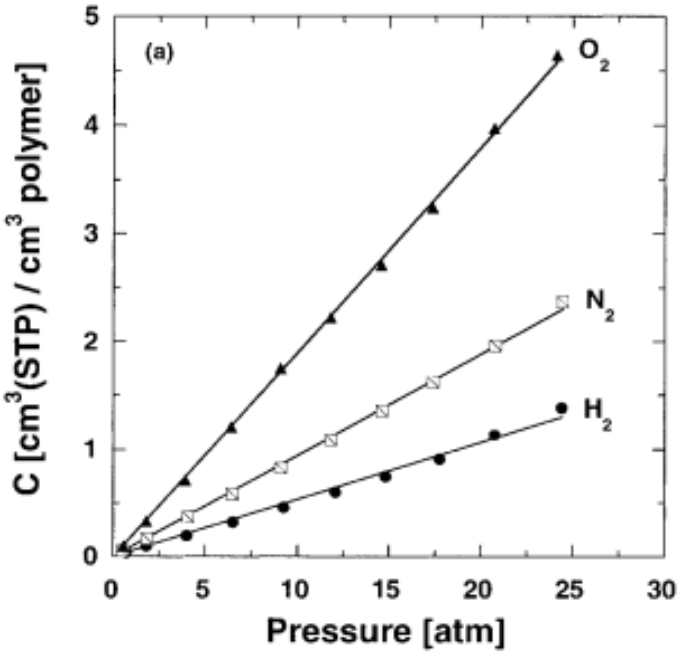

Figure 2.14: Sorption of diatomic gases following Henry's Law. [46]

Naito et. al. concluded that solubility of highly condensable organic vapors in a rubbery polymer, polybutadiene, increases with pressure as shown in Figure 2.15.[47] This type of sorption occurs when permeant/permeant interactions are strong relative to permeant/polymer interactions. This behavior is well modeled by employing Flory-Huggins Solution theory.

$$ln\frac{P}{Po} = ln\phi_1 + (1-\phi_1) + \chi(1-\phi_1)^2 \qquad (2.15)$$

Where P^o is the saturation vapor pressure, ϕ is the volume fraction of the permeant in the polymer, and X is the Flory-Huggins interaction parameter. The concentration of penetrate in the polymer exhibits a

linear relationship with the dilation of the polymer. It is concluded that there is a relationship between the magnitude of dilation and the solubility of the organic vapor in the polymer.

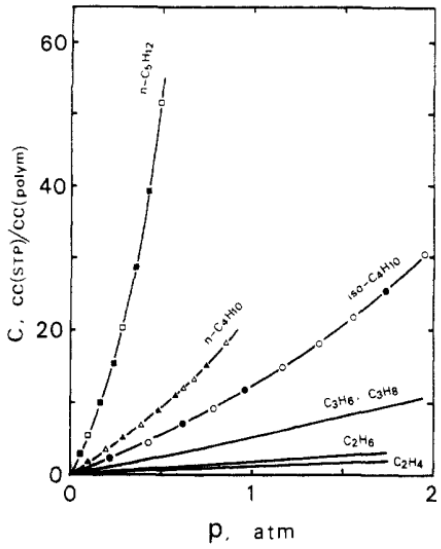

Figure 2.15: Sorbed isotherms for organic gases in polybutadiene at 25°C. Open and solid symbols correspond to sorption and desorption isotherms, respectively. [47]

2.3.1.2 Glassy Polymers

It is postulated that specific sorption isotherms arise because of the non-equilibrium nature of glassy polymers. As temperature is decreased across the glass transition, the change in specific volume with respect to temperature is decreased (Figure 2.16). These non-equilibrium, "un-relaxed" polymer chains result in the formation of micro domains in the material. These domains allow gas molecules to sorb into specific sites.

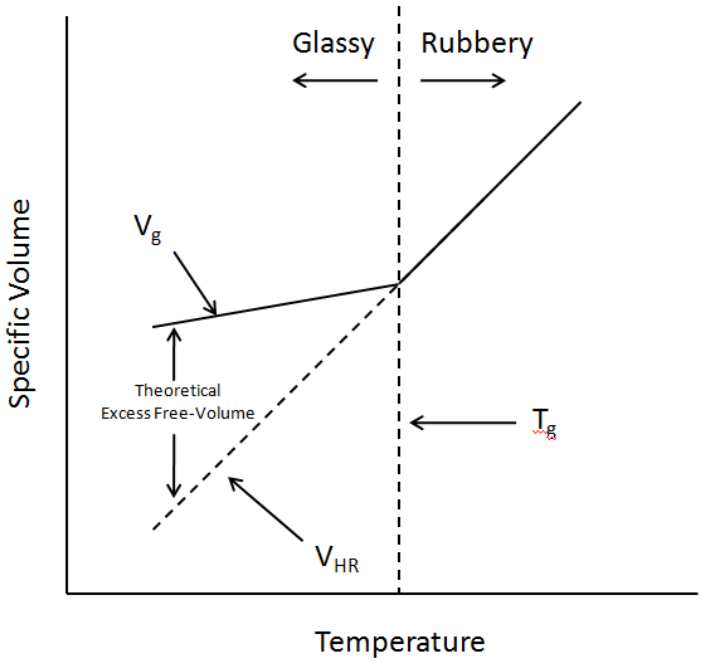

Figure 2.16: Change of specific volume vs temperature slope as the glass transition is traversed

Sorption isotherms in glassy polymers have been successfully modeled utilizing the dual mode sorption model, which is the incorporation of both Henry's Law of sorption and Langmuir-type sorption. The difference between the sorption behavior of glassy and rubbery polymers is caused by non-equilibrium behavior in the glassy state. The rearrangement of the polymer chains is hindered by the lack of mobility below the glass transition, which results in a significant decrease in the thermal expansion coefficient. This leads to the immobilization of penetrant molecules in microvoids in the polymer. Consequently, the dual phase model is represented analytically as

$$C = C_H + C_D \qquad (2.16)$$

where C is the total concentration of the penetrant in the polymer, C_H is the concentration contribution due to Henry's sorption or penetrant molecules dissolving in the polymer, and C_D is the penetrant concentration, due to Langmuir sorption, in the microvoids of the polymer.

$$C = Sp + \frac{C_H' bp}{1+bp} \qquad (2.17)$$

At constant temperature the concentration or amount of penetrant sorbed into the polymer is directly proportional to the partial pressure of the gas, p. The Henry's constant or the solubility coefficient, S, is a proportionality constant reflecting the distribution of the permeant molecules between the gas and polymer phase.

Langmuir sorption represents the initial sorption in specific microvoids in the polymer; b is the Langmuir affinity constant, C'_H is the qualitative representation of the maximum penetrant concentration able to sorb into the polymer cavities (hole saturation constant). Given by:

$$C'_H = \left(\frac{V_g - V_{HR}}{V_g}\right)\rho \qquad (2.18)$$

where V_g and V_{HR} are the specific volumes of the glassy and hypothetical rubbery polymer at a constant temperature respectfully and ρ is the penetrant molar volume.

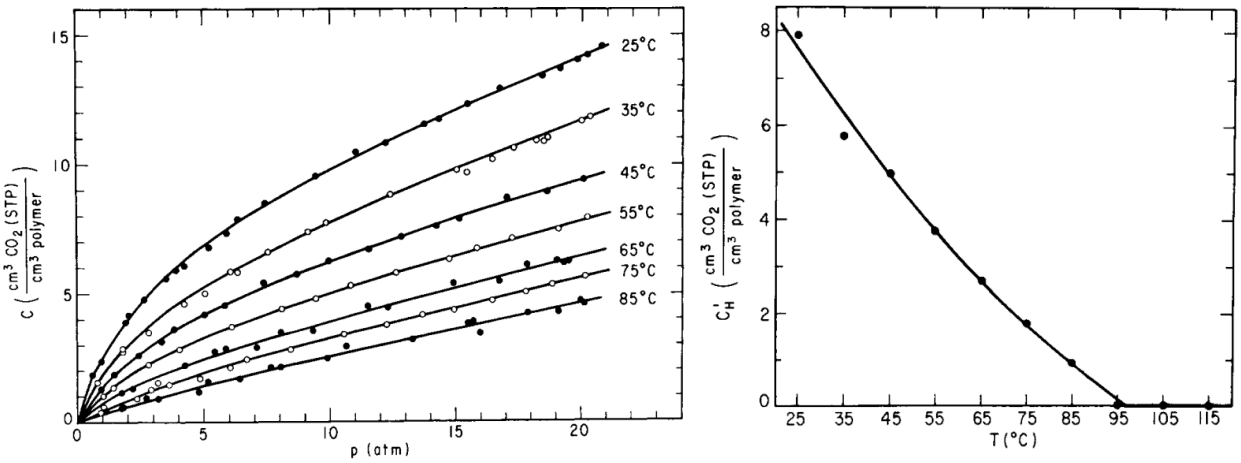

Figure 2.17: (a) Sorption of CO_2 in PET at temperatures below T_g exhibiting dual mode sorption (b) Decrease in C'_H, hole saturation constant, with increase in temperature.[48]

Figure 2.17 (a) represents the concentration of CO_2 approaching the glass transition temperature of PET. At low temperatures, in the glassy state, and low system pressures the polymer exhibits a dual mode sorption behavior, . As the pressure is increased, the polymer microvoids are occupied. This results in the remaining sorption being Henry's Law sorption. Henry's solubility constant can be measured by taking the slope of a plot of concentration and pressure at high pressures. As the system temperature increases towards the glass transition temperature, Henry's Law of Sorption dominates. This is shown by the decrease in C'_H, (Figure 2.17b) due to the increase in polymer chain mobility, which leads to a smaller

difference in actual and theoretical polymer specific volume. This subsequently decreases the number microvoids in the polymer available as penetrant sorption immobilization sites.

2.3.2 Effect of System Temperature

Solubility, over relatively small temperature changes, follows an Arrhenius-type relationship.

$$S = S_o \exp[-\frac{\Delta H_S}{RT}] \qquad (2.19)$$

where S_o is a constant and ΔH_S is the partial molar heat of solution or enthalpy of sorption, expressed as:

$$\Delta H_S = \Delta H_{cond} + \Delta H_{mix} \qquad (2.20)$$

ΔH_{cond} is the latent heat of condensation and ΔH_{mix} is the enthalpy change of solution or mixing, which is the change associated with the dissolution of the permeant in the polymer at infinite dilution.
Highly condensable gases cause the enthalpy of condensation to dominate over the enthalpy of mixing. $|\Delta H_{cond}| > \Delta H_{mix}$, which results in a decrease in solubility with an increase in temperature. For gases such as H_2, N_2, and O_2, which have critical temperatures well below room temperature, $|\Delta H_{cond}|$ is typically lower than ΔH_{mix}, resulting in a decrease in solubility, with an increase in temperature. This has been demonstrated (Figure 2.18) with sorption isotherms of tetramethyl hexafluoro polycarbonate (TMHFPC) above its glass transition temperature (150 °C).[49] Solubility decrease with temperature due to the gases exothermic heats of solution.

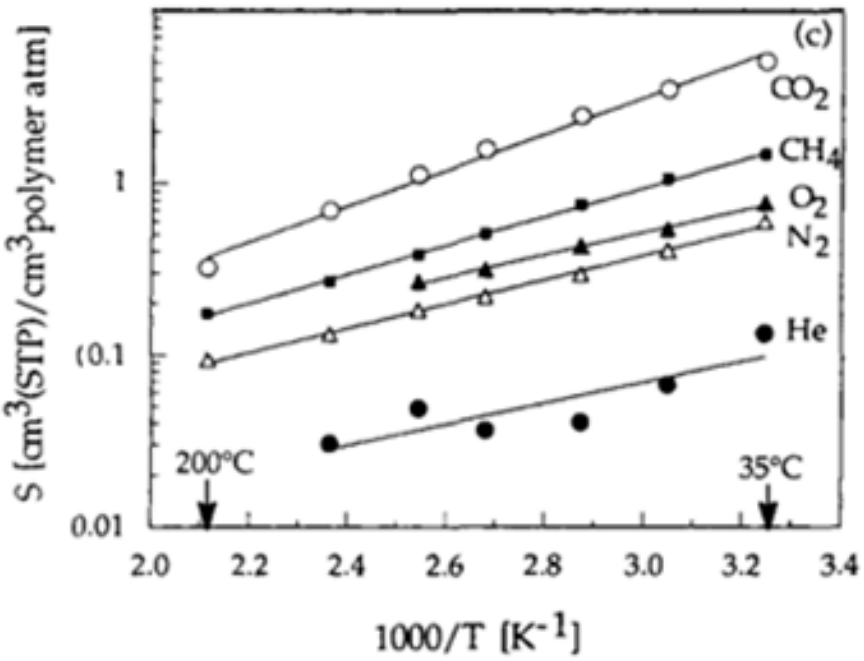

Figure 2.18: Temperature effects on solubility with TMHFPC [49]

2.3.3 Condensability

Condensability of gases is strongly connected to the critical temperature, T_c or boiling temperature, T_b of the penetrant. Consequently, sorption of gases, for both glassy and rubbery polymers, increases as the critical temperature is increased. This is shown in Figure 2.19. Sorption isotherms of several penetrants in poly(phenylene oxide) were collected at 35 ^oC for pressures between 0 and 30 atm. The penetrant concentrations decrease with decreasing critical temperature as follows: CO_2 (T_c = 31.04 ^oC) > CH_4 (T_c = -82.3 ^oC) > Ar (T_c = -122.4 ^oC) > N_2 (T_c = -146.9 ^oC).

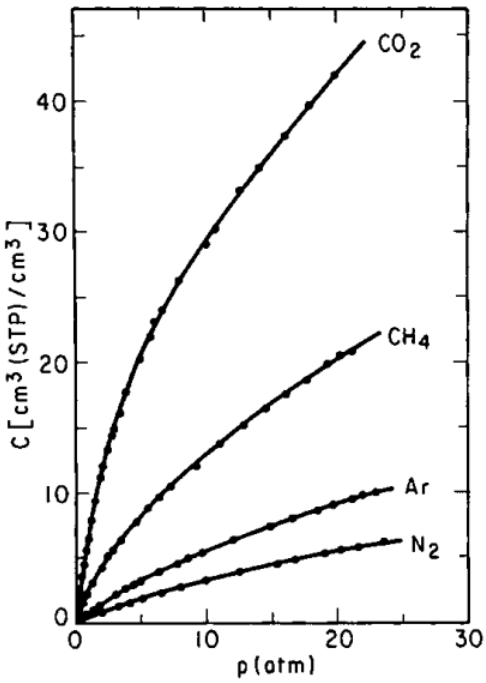

Figure 2.19: Gas sorption isotherms (35°C) in poly(phenylene oxide) following a direct relationship to critical temperature [50]

2.4 Diffusion

The kinetic limitations of membrane transport are related to the diffusion of penetrant molecules into the polymer matrix. It is affected by the ability of the matrix to transfer permeant molecules. Factors that are most dominant are the concentration dependence of diffusion, polymer rigidity (related to T_g), size and shape of diffusing gases, and temperature.

2.4.1 Concentration

Strong polymer-penetrant interactions result in swelling or plasticization of the material. In particular, glassy polymers are more susceptible to this phenomenon, due to the reduction of the interactions between adjacent polymer segments. [51] Plasticization can substantially reduce polymer performance due to the increase in diffusivity of both penetrants. Chemical crosslinking[52], thermal treatment[53], interpenetrating polymer networks[54], low molecular weight additives[54] and several other techniques have been used to reduce this effect.

2.4.2 Phase of Material

Van der Waals volumes are used for the estimation of intrinsic permeate molecular size, which is related to diffusion. Figure 2.20 shows the dependence of diffusion on molecular size dependence for natural rubber and poly(vinyl chloride) (glassy state) at 25 °C and 30 °C respectively. Although rubbery materials exhibit enhanced diffusive kinetics compared to that of glassy material, their size discrimination is significantly lower. This makes glassy polymers more industrially favorable for size separation transport processes.

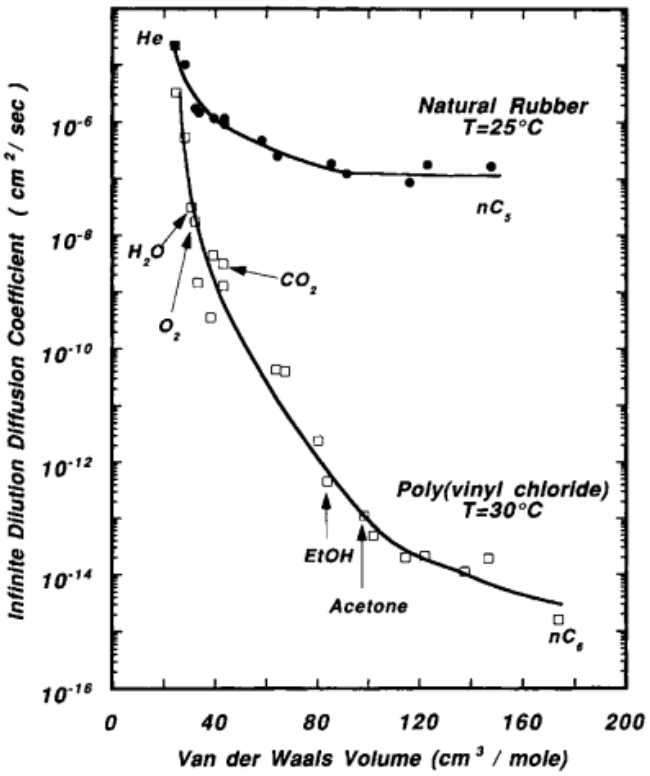

Figure 2.20: Infinite Diffusion Coefficient dependence on mean penetrant size for natural rubber at 25 °C and poly(vinyl chloride) at 30 °C.[55]

2.4.3 Temperature

The Arrhenius equation can be used to successfully model the temperature dependence of diffusivity, as diffusivity is an activated process.

$$D = D_o exp\left(\frac{-E_D}{RT}\right) \qquad (2.21)$$

E_D is the activation energy of diffusion, R is the ideal gas constant, T is temperature, and D_o is a constant. Amerongen investigated the permeability and diffusivity of different rubbers. [56] It was concluded that diffusivity is exponentially dependent on temperature and follows a linear relationship between ln(D) and 1/T (Figure 2:21).

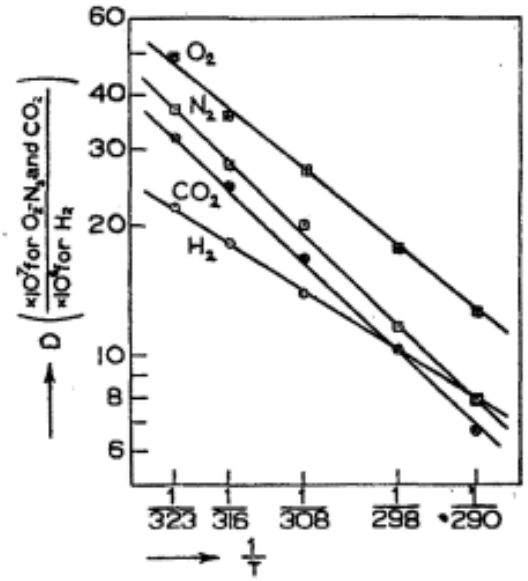

Figure 2.21: Relation between the diffusivity in natural rubber and temperatures for several gases.[56]

2.4.4 Kinetic Diameter

Diffusivity values decrease with increasing molecular diameter of gases. Higashimura, et al. investigated the diffusivity dependence of several gases on several substituted polyacrylates (Figure 2.22). D values have the greatest dependence on poly(1-phenyl-1-propyne), which also has the lowest diffusivities of gases tested.

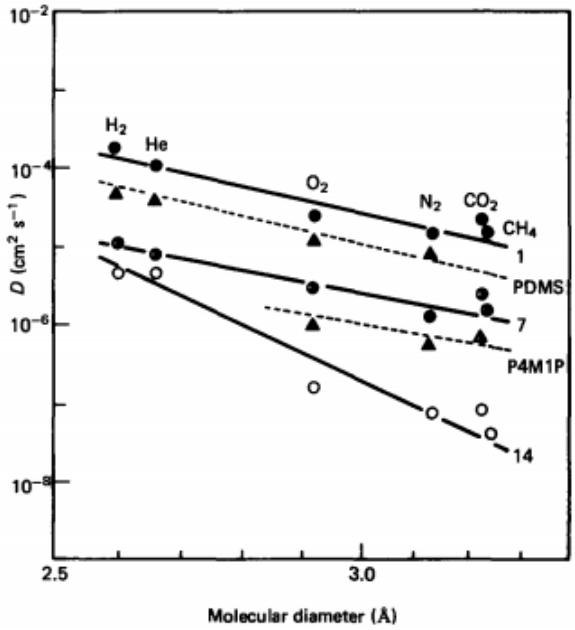

Figure 2.22: Diffusivity values as a function of molecular penetrant diameter for various substituted acrylate polymers[57]

2.5 Membrane Separation Using Liquid Crystals

Due to the anisotropic nature and birefringence of liquid crystals, most studies have been focused on electro-optical applications and only a limited amount of research is concerned with their liquid or gas transport behavior. The effect of liquid crystal phase transition on gas sorption was studied by Chen, et al.[58] The focus was on the temperature dependence on sorption of small chain thermotropic liquid crystals, methoxybenzilidene-butylanaline (MBBA), 4-(trans-4-pentylcyclohexyl)benzonitrile (PCH5), and 1-isothiocyanato-4-(trans-4-octylcyclohexyl)benzne (PCH8-CNs) (Figure 2.23).

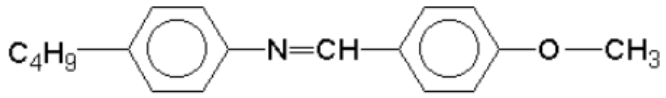

(a) MBBA (Cryst – 21 °C – N – 45 °C -- Iso)

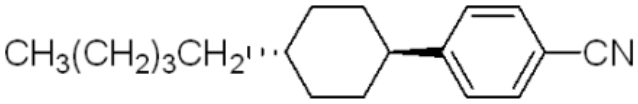

(b) PCH5 (Cryst – 30 °C – N – 55.2 °C -- Iso)

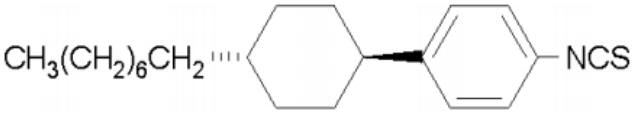

(c) PCH8-CNS

Figure 2.23: Low molecular weight liquid crystals employed for temperature dependent sorption studies[58]

The liquid crystals were placed on a cylindrical quartz pan and the gas of interest was introduced into the chamber after degassing the sample in the crystalline state.

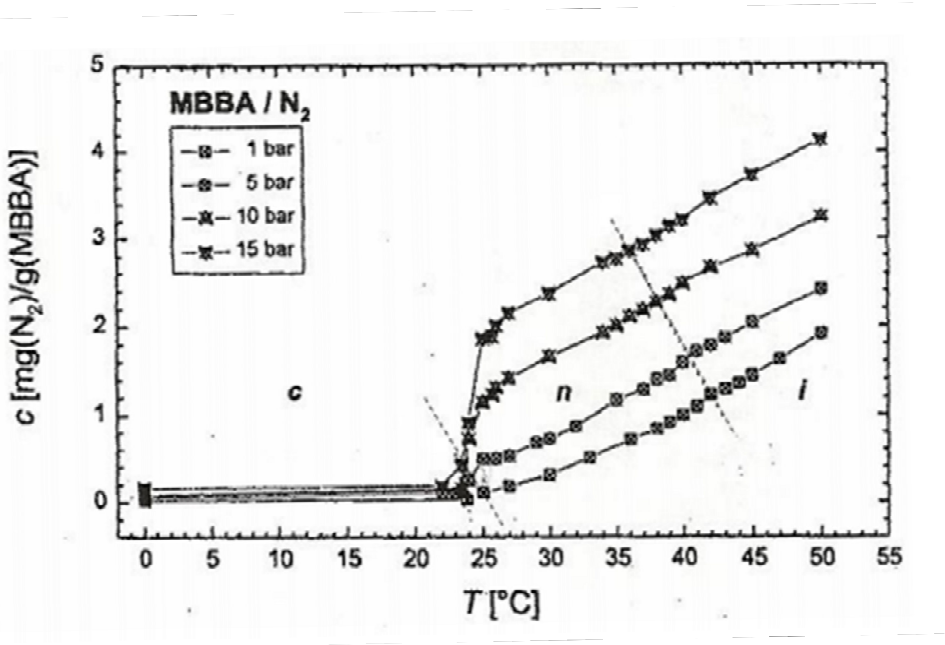

Figure 2.24: N_2 gas sorption for LC MBBA at several isobars[58]

MBBA sorption isobars for N_2 are shown by Figure 2.24. For temperatures under 21°C, the sorbed gas was extremely low due to a low free volume of the material. As the crystalline-mesomorphic transition

temperature was passed, the free volume of the material increased and a 'jump' in sorbed gas was observed due to the increase in material free volume. It was demonstrated that the transition temperatures are dependent on the amount of sorbed solute. The transition temperature decreasing as sorbed concentration or gas pressure increased, possibly disrupting the ordering of the material. With the time-dependent gas sorption data, Crank's method of calculating diffusivity was used, assuming an infinitely large pan diameter (no wall interactions) with an equilibrium solute concentration at time approaching infinity by using,

$$\frac{M_t}{M_\infty} = 1 - \sum_{n=0}^{n=\infty} \frac{8}{(2n+1)^2 \pi^2} \exp\left[\frac{-D(2n+1)^2 \pi^2 t}{4l^2}\right], (n = 0,1,2,...) \quad (2.19)$$

Where, M_t is the amount of sorbed gas at time, t and M_∞ is the amount of sorbed gas approaching equilibrium, at time infinity, l is the liquid crystal thickness, and D is the effective diffusivity. Among the gases tested (N_2, CO_2, Ar, and He) CO_2 showed the highest solubility, which is due to the enhanced interactions between the more polar CO_2 gas and liquid crystals.

Liquid crystals have been used as an additive to blend with polymers for enhancing oxygen selective membrane materials.[59] Tsuchida, et al. fabricated composite membranes of poly(methyl-methacrylate), as the support, and liquid crystalline (N-methoxybenzylidene)-4-butylaniline/α,α,α,α-tetrakis(o-pivalamidophenyl)-porphinato-cobalt(II) (CoP) blend as an oxygen carrier. [60] It was realized that the addition of liquid crystals increased permeability, without reducing selectivity at low temperatures. Also, the addition of CoP further increased permeability but reduced selectivity within the mesophase. The reduction of selectivity could possibly be attributed to micro-voids within the carrier/liquid crystal boundary.

Furthermore, Lin, et al. fabricated an ethyl cellulose base membrane blended with trihyptyl cellulose liquid crystal.[61] The addition of the liquid crystal improved both the permeability and selectivity of oxygen over nitrogen. It was observed that with an increase in temperature, both permeability as well as selectivity increased. This concurrent increase was attributed to the liquid crystal's super-molecular arrangement. This study resulted in the motivation to investigate the permeation properties of several cellulose based polymers blended with various liquid crystals. [62] The effect of permeation and selectivity on the polymer composite material, LC/polymer ratio, and operating temperatures and pressures was investigated. Permeability increased with increasing LC concentration, with selectivity either increasing or remaining constant. There was no noticeable impact on the cellulose based polymer chosen.

Polymer dispersed liquid crystal (PDLC) films have been studied for membrane separation applications using liquid crystal N-(4-ethoxybenzylidene-4'-n-butylaniline).[63] A solution casting method was used to prepare a 60/40 wt% polycarbonate (PC)/EBBA membrane. A concentration above 45wt% and slow evaporation of the solvent encouraged the growth of liquid crystal domains, which was confirmed by differential scattering calorimetry. Liquid crystal domains increased water transport by several orders of magnitude. In the crystalline state, an increase in permeability was found as the number of carbon atoms in the permeate molecules decreased. In the isotropic state, the reverse trend was observed. The authors stated that a diffusion controlled process was present at temperatures below the liquid crystal phase and the permeation is governed by a solubility process above the crystalline transition temperature, Figure 2.25.

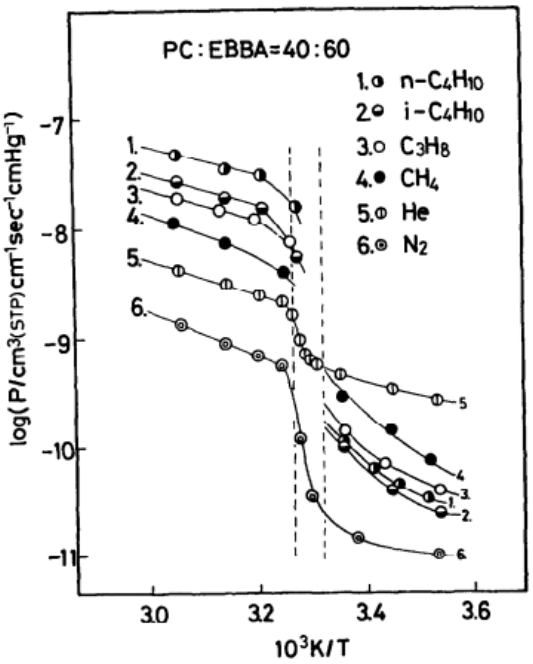

Figure 2.25: Permeability dependence on temperature for polycarbonate:EBBA (40:60) with several gases[63]

Photo switchable gas permeation membranes were investigated using azobenzene based liquid crystals.[64] Figure 2.26 demonstrates the isomerization mechanism for an azobenzene molecule.

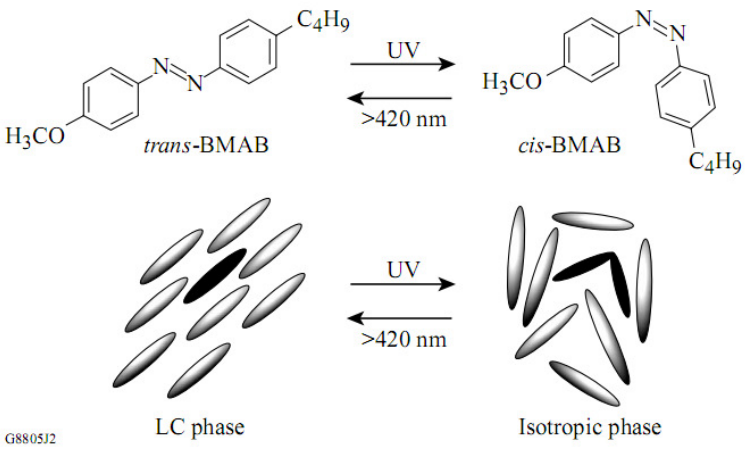

Figure 2.26: Demonstration of uv induced cis to trans isomerization for an azobenzene molecule[64]

The azobenzene derivatives convert incident light into mechanical energy through the process of trans-cis isomerization. The introduction of UV light converts the trans isomer to the cis isomer. The liquid crystal acquires a bent shape and disrupts the LC ordering, thus making the material isotropic. A response time of 5 seconds was observed for this particular liquid crystal. Applications of membranes where permeability can be controlled during operation to respond to changes in the environment can be realized.

Pervaporation is an effective membrane separation technique for organic liquid mixtures with azeotropic or close-boiling point mixtures.[65] The selective transport of organic mixtures is based on the solution-diffusion theory, where the separation is dominated by the difference in sorption. Separation of benzene/cyclohexane mixtures were studied using several side-chain liquid crystal polymers (Figure 2.27).

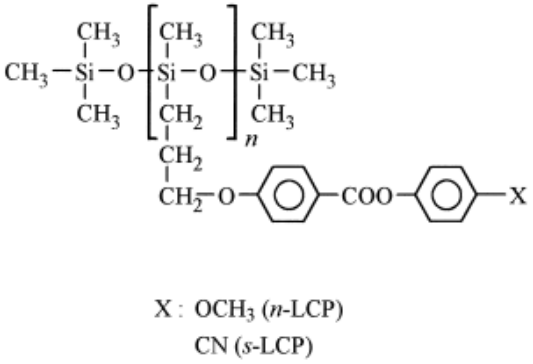

Figure 2.27: Siloxane based SCLC with various functional groups. x = OCH_3 (n-LCP) and x=CN (s-LCP)[65]

The n-LCP had a diffusion dominant transport in the glassy state and a sorption dominated transport in both the liquid crystal and isotropic state, while the s-LCP had diffusion dominant transport regardless of the phase. The change in n-LCP behavior was caused by a reduction of the diffusion selectivity, rather than an increase of sorption selectivity. This can be attributed to an increase in the thermal mobility of the side chains. Figure 2.28 shows the size selective diffusion mechanism in different phases of a polymer liquid crystal membrane for two solutes with different molar volumes: benzene (89.4 cm^3/mol) and cyclohexane (108.7 cm^3/mol).[66] The separation was diffusion dominated due to the two solutes permeating between ordered domains. The separation decreased with the transition from glassy to liquid crystalline to isotropic due to the domains becoming more randomized and flexible.

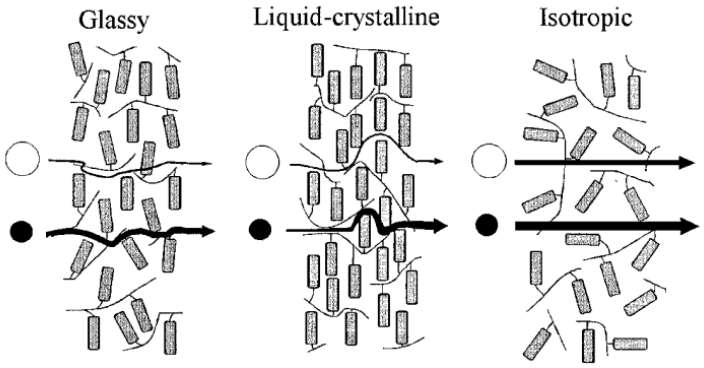

Figure 2.28: Simplified schematic of proposed diffusion mechanism for the transition from glassy to isotropic LC material[65]

Several groups have studied the effects of temperature, material phases and material microstructure on the gas transport properties of side-chain LCPs.[67-73] The isobaric sorption properties of CO_2 in several side-chain LCPs have been investigated.[67] Figure 2.29 contains sorption of CO_2 with respect to the change in enthalpies across phase trasitions. The magnitude of change of CO_2 sorption had a direct correlation to the change of enthalpies. A discontinuous change of CO_2 solubilities were found at several first order phase transitions. Gas sorption in the LCP semi-crystalline phase only occurs in the amorphous region as the gases are insoluble in the crystalline mesogen region, following a biphasic model. A large increase in sorption across the crystalline to LC transition supports the conclusion that gas sorption in the mesophase does not follow a simple biphasic model.

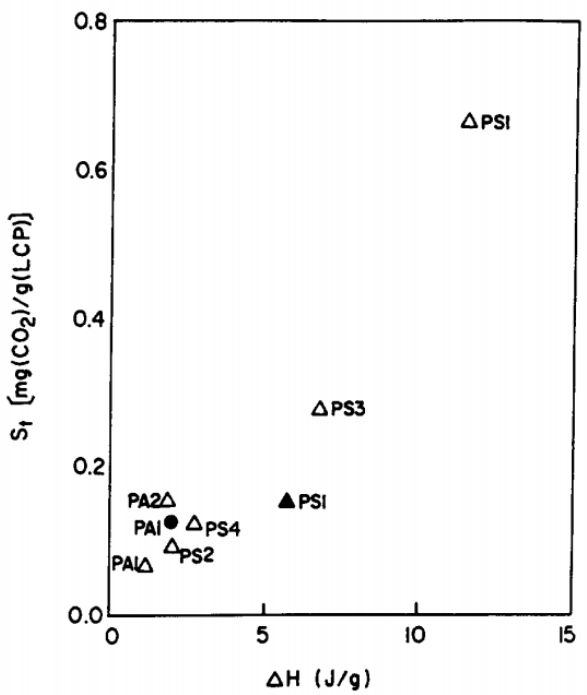

Figure 2.29: Correlation between transition sorption (S) and enthalpies of the transitions (ΔH). (▲) crystalline-smectic transition; (•) smectic-nematic transition; (Δ) LC-isotropic transition[67]

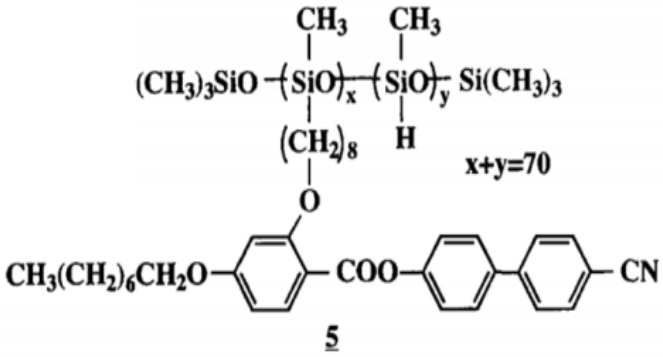

5

Figure 2:30: Laterally attached side chain liquid crystals. [72]

A polysiloxane based PLC membrane, fabricated using a spin coating technique, was synthesized with the side chain laterally attached, Figure 2.30.[72] Figure 2.31 contains activation energies for both permeation and diffusion at various temperatures and for different gases. It is shown that activation energies, for temperatures below the Tg, showed similar results to other reported polymers. Activation energies above the Tg were larger than typically reported. Diffusivity and solubility selectivity were both

reported to be larger than that of a bare PDMS membrane. In addition, permeability selectivities were a result of solubility differences of the gases, particularly with highly condensable gases.

Table 2
Activation energies for gas permeation (E_P), diffusion (E_D), and solubility (ΔH_S) in polymer membrane

Polymer	Gas	Temp. range (°C)	E_P (kcal/mol)	E_D (kcal/mol)	ΔH_S (kcal/mol)
LCPS	O_2	3–8	4.6	10	−5.6
		18–38	11	8.1	2.7
	CO_2	3–8	5.8	13	−7.0
		18–38	12	8.8	2.5
PDMS	O_2	18–38	1.6	2.8	−1.2
	CO_2	18–38	−0.6	3.4	−4.1

Figure 2.31: Reported activation energies for LCPS and PDMS below and above glass transition temperatures. E_p=activation energies for gas permeation; E_D=for diffusion. [72]

Chen et. al. synthesized two polysiloxane based side-chain liquid crystals with varying pendant groups (cyano and methoxy) for gas transport measurements. [70] As the system temperature is increased and approaching the LC to isotropic phase transition, a simultaneous increase in O_2/N_2 selectivity and O_2 permeability was observed for both polysiloxane based membranes. The same LC mesogens were reacted to an acrylate polymer backbone. [69] Similar trends were observed. A simultaneous increase in O_2/N_2 permeability selectivity and O_2 permeability occurred. In addition, the activation energy for permeation exhibited an abrupt change in slope at the phase transition.

Kawakami et. al. have shown that the overall permeability of a LC polysiloxane with side chain mesogenic groups was governed by an activated diffusion mechanism as has been observed in other glassy polymers.[72] In this particular case, the transport properties were dominated by the polysiloxane main chain, which has higher flexibility and free volume. On the other hand, the solubility increased with increasing temperature above the T_g apparently due to the increased sorption of the penetrant gas in the increasingly disordered liquid crystalline domains.

Main chain LCPs are different than side chain LCPs, due to the placement of their rigid mesogenic groups. The mesogens are incorporated in the main chain polymer backbone rather than attached perpendicular to the polymer backbone. Much of the focus of research has been on their low permeability or barrier properties, due to their intrinsic nature to pack tightly. This is most easily shown by their low molar volume compared to other conventional polymers[74] Figure 2.32 shows a drawing of the ordering of both isotropic and mesomorphic phases of MCLCPs.

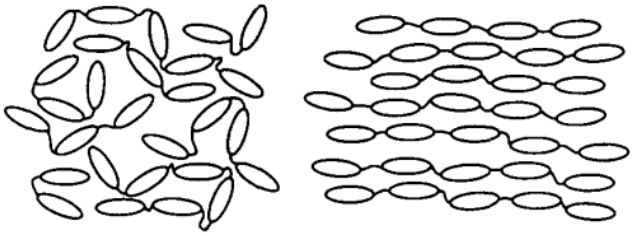

Figure 2.32: Schematic illustration of polymer chains in isotropic and mesomorphic arrangements[56]

In a preliminary study, a main chain thermotropic liquid crystalline copolyester was found to have low gas permeability, similar to high-barrier polymer membranes.[75] The low gas permeability of main chain PLCs appears to be due to the very low solubility, rather than low mobility for penetrant diffusion. This was due to gas molecules only being soluble in a small portion of the polymer (defects and boundaries between domains). It was determined that by increasing the volume fraction of the regions of anisotropic character, the solubility of the material decreased, while the apparent diffusivity was affected to a lesser extent.[76] This leads to the conclusion that gas molecules are relatively insoluble in the ordered region, similar to that of crystalline polymers.

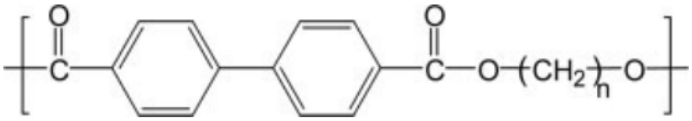

Figure 2.33: n=3 (PP3BB), 4 (PBBB), 5 (PP5BB) and 6 (PHBB)[77]

Figure 2.33 depicts s series of polyesters based on 4,4'-bibenzoic acid were synthesized and tested for their oxygen transport properties.[77] An odd even effect was observed when changing the aliphatic spacer length. Comparing odd and even chain length independently, as the chain length increased, diffusivity increased while keeping solubility relatively constant. This is shown in Figure 2.34. The low solubility was said to be caused by the presence of relatively small free volume hole sizes in the liquid crystal state, which is independent of spacer length.

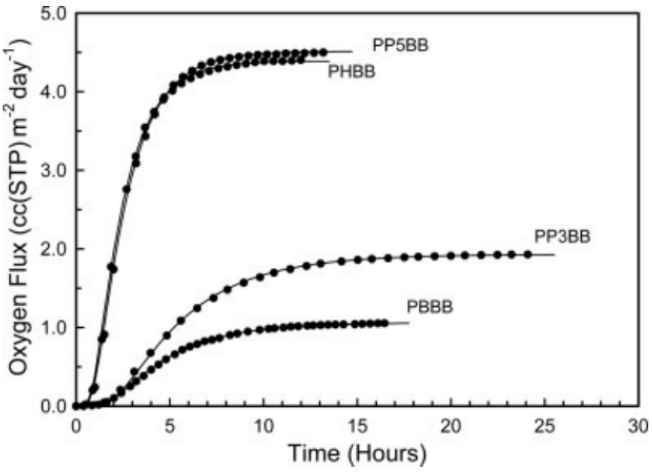

Figure 2.34: Flux vs time data for quenched copolyester films at 23 ˚C[77]

It was determined by AFM, for Poly(pentamethylene 4,4'-bibenzoate) (P5BB), that the smectic PLC was ordered with the characteristic wavy lamellae layer. [78] The permeability data of oxygen in the crystalline phase support a two-phase model of impermeable crystallites dispersed in more permeable smectic regions.

Furthermore Poly(hexamethylene 4,4'-bibenzoate) (PHBB) was copolymerized with a non-liquid crystalline poly(hexamethylene isophthalate) (PHI) and studied for oxygen transport properties.[79] An increase in comonomer PHI was accompanied with an increase in oxygen flux but PHBB-75I had a higher oxygen flux compared to PHI (Figure 2.36). It was concluded that PHI was more crystalline than PHBB-75I and verified by SAXS. The small mole fraction of the LC could have disrupted the inherent crystallinity of PHI.

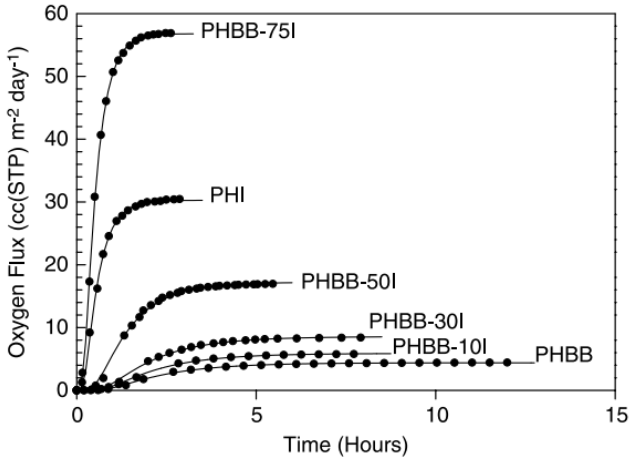

Figure 2.36: Oxygen flux at 23 °C for varying co-monomer ratios[79]

Chapter 3: Single and Mixed Gas Permeation Apparatus

3.1 Introduction

A constant volume-variable pressure (single gas) and constant pressure-variable volume (mixed gas) apparatus was built and integrated with a LabView based computer control and data acquisition system. Purchasing a membrane permeation instrument is very expensive and often has limitations on operation and measurement conditions. The instrument described here gives the user the freedom to change several conditions: feed pressure and composition, system temperature, permeation time, degassing time and permeate volume (for low and high transport runs). The system was designed to have the ability to measure both single and mixed gas permeation. The single gas permeation apparatus is based on a pressure-rise technique, and allows the measurement of diffusivity and permeability, from which the solubility values can be calculated. The mixed gas permeation apparatus relies on a downstream sweep gas that is then fed into a gas chromatograph, thus allowing true permeabilities to be measured.

3.2 Materials and Apparatus

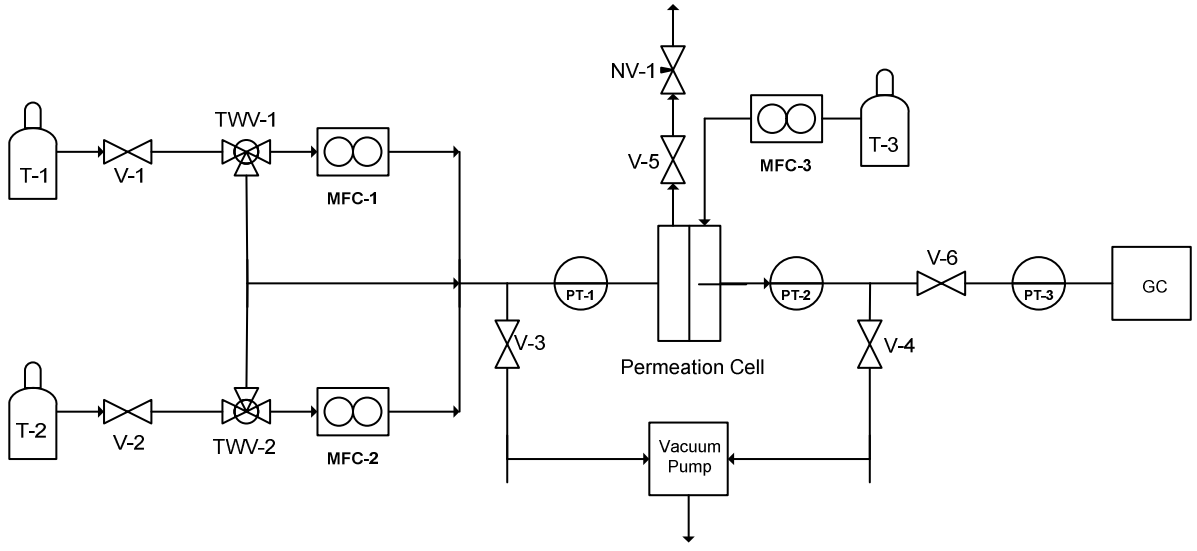

Acronym	Name
T	Gas Tank
V	Shut-Off Valve
TWV	Three Way Valve
MFC	Mass Flow Controller
PT	Pressure Transducer
NV	Needle Valve
GC	Gas Chromatography

Figure 3.1: Permeation apparatus for mixed and single gas transport runs

A schematic of the permeation apparatus is depicted in Figure 3.1. All pipes and fittings are constructed from 304 stainless steel and were purchased from Swagelok. Six Swagelok shut-off valves were used in conjunction with six SMC solenoid valves. The solenoid valves were connected to a filtered in-house air source for air actuation. In addition, the solenoid valves were connected to a National Instrument digital I/O device for automated control. Two manual 3-way valves were used for switching between single and mixed gas runs. A total of three MKS pressure transducers (PTs) were used for feed side and permeate side pressure readings, respectively. A pressure transducer was used to measure feed side pressures between 0.5 and 10 bar. A low pressure transducer was used for permeate side pressure measurements and can measure pressure between 0.0 and 10 torr. This pressure transducer was used for single gas runs. A second pressure transducer placed in the permeate side of the apparatus could measure between 0.5 and 10 bar and was used for single gas runs of high throughput membranes and mixed gas runs to measure the sweep gas pressure. The pressure transducers had errors below 2%. Two MKS mass flow controllers (MFCs) were used for automated control of feed gas flow rates, respectively. Feed gas flow rates could be varied from 0 to 500 standard cubic centimeters per minute (sccm) of helium and had errors below 2%. An MKS mass flow meter (MFM), with a range from 0 to 20 sccm N_2, was used to record sweep gas flow rates. Errors in the unit were less than 2%. The MFM and MFCs were calibrated using a bubble flow meter and stop watch. Long calibration times were used to ensure minimal operator error. The average of three volumetric flow rates had values deviating between 1% and 3%. A Swagelok needle valve was used to maintain mixed gas feed pressures. All pressure transducers, mass flow controllers and mass flow meters were connected to a national instruments USB-6009 controller for data acquisition and control. A 53 liter BINDER forced air convection oven with temperature control between 5 ^{o}C above ambient to 300^{o}C was used. The resolution was 0.3 ^{o}C. Three Omega thermocouples were used to monitor the temperature inside the membrane cell and inside the feed and permeate pipes,

respectivley. The Omega thermocouples were connected via an 8 Channel thermocouple USB data acquisition module. This ensured that system startup was initiated only after all temperatures were at equilibrium. In addition, temperatures of the steady-state mixed gas and sweep gas were monitored throughout the experiment.

3.2.1 Membrane Cell

The permeation cell is shown in Figure 3.2. The membrane is placed between two stainless steel cylindrical disks and bolted using six stainless steel screws. The three Viton o-rings were used to minimize gas leaks in the system. Viton material has good chemical and thermal resistance, low permeability and good compression. The multiple o-rings worked to seal the permeate side from the feed gas and the permeate side from the atmosphere. Two porous metallic discs are used to support the membrane on each side of the cell. Figure 3.2a represents the top view of the permeation cell and Figure 3.2b represents the side view of the permeation cell.

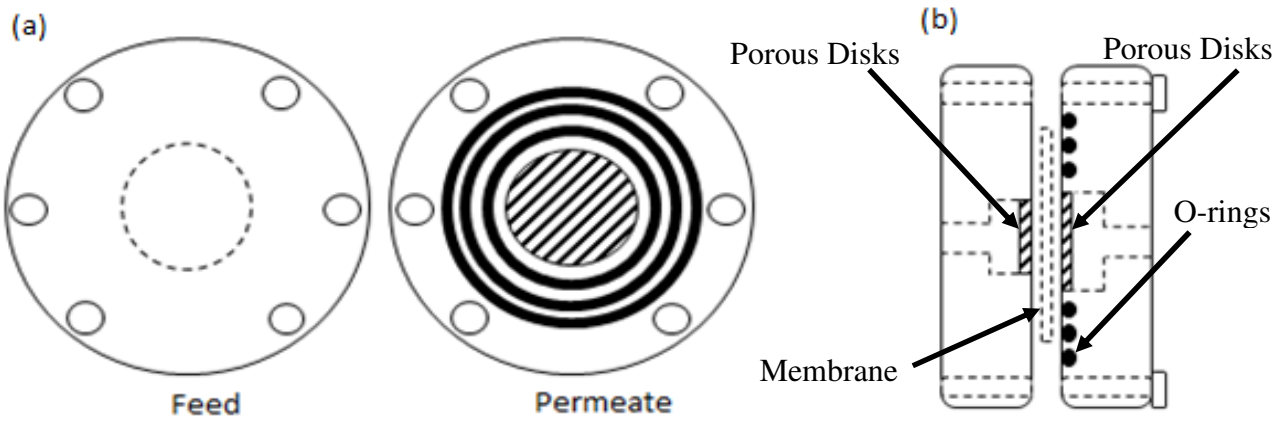

Figure 3.2: Membrane cell holder used for permeation experiments. (a) Top-view. (b) Side-view

3.2.2 Six-Port Sample Loop

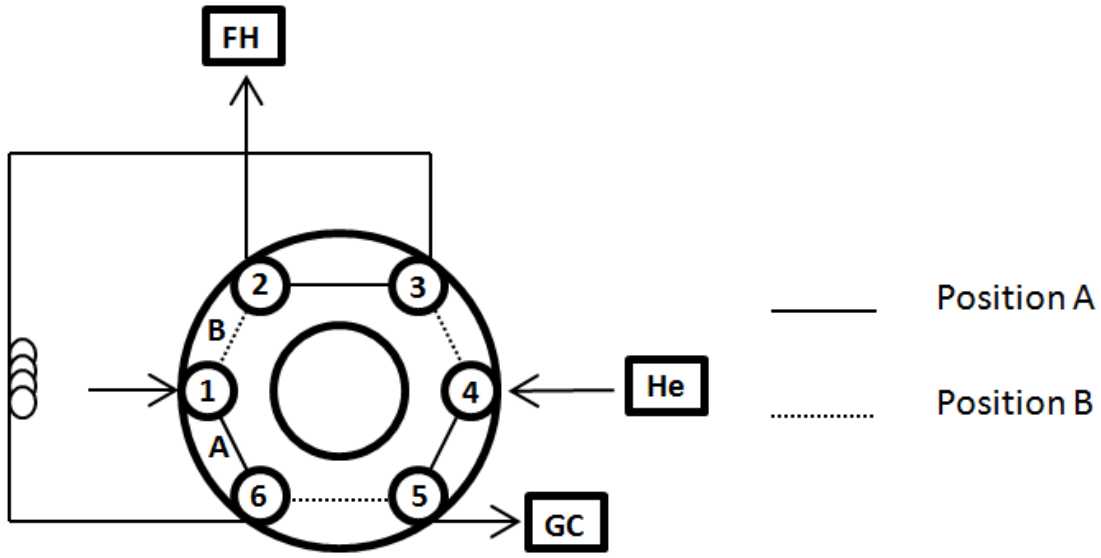

Figure 3.3: 6-port automated valve for permeate composition analysis

Mixed gas streams were controlled and analyzed using a Shimadzu GC-2014 equipped with a 6-port sampling valve, depicted in Figure 3.3. In position A, the permeate gas is swept into port 1 to fill the sample loop and exits port 2 into a fume hood (FH). The sample loop volumes used were from 50 ul to 2ml. The smaller sample loops were used for runs with higher gas transport, preventing saturation of the FID detector. The larger sample loops were used for runs with lower gas transport, to minimize error. At pre-determined time intervals, the valve is switched to position B. The gas mixture inside the sample loop is carried by the sweep gas to the GC injection port. The sample then passes through the GC column, for separation. Finally, a flame ionization detector (FID) detects the ions formed during combustion of the organic compounds. Samples were taken at intervals of ten minutes until steady state was attained, indicated by a constant peak area. The time to reach steady-state varied between membranes from one hour to several hours. The 6-port valve and GC is controlled using Shimadzu software.

3.3 LabView Program

National Instrument's Labview was used to devlop code for the automated control of the permeation equipment. Two mass flow controllers, three pressure transducers, six solenoid valves, one

mass flow reader, and three temperature transducers were independently and simultaneously controlled. The user interface is depicted in Figures 3.4-3.6.

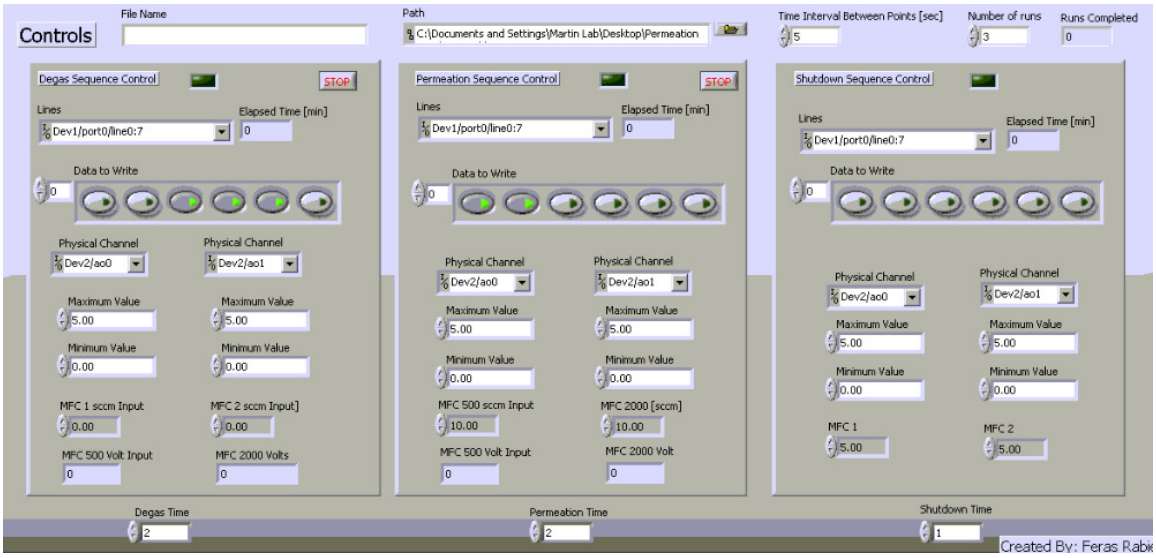

Figure 3.4: LabView Control Interface

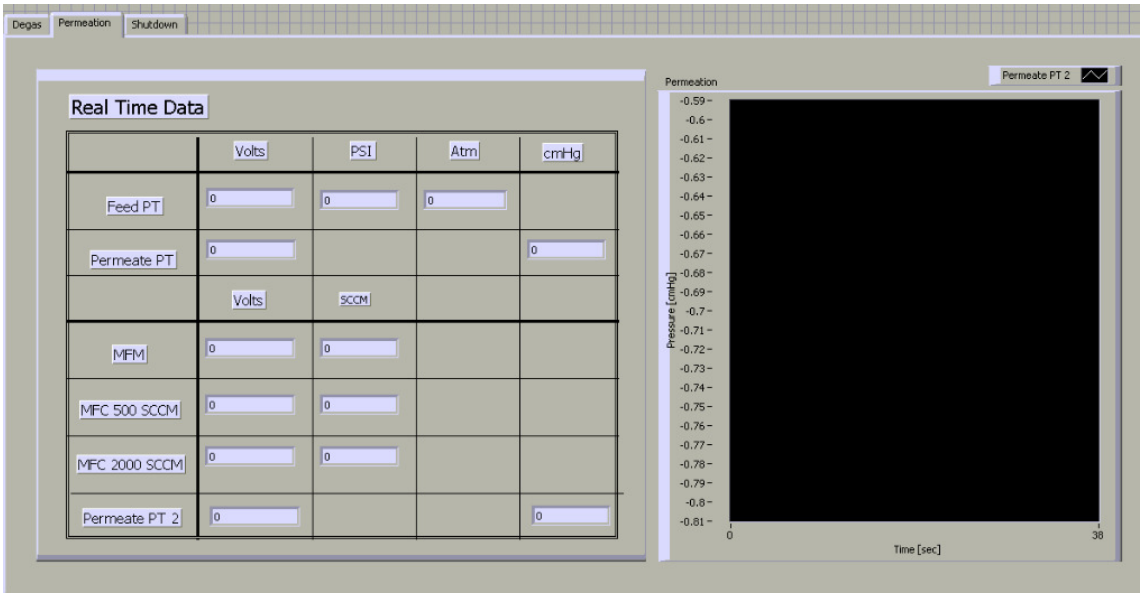

Figure 3.5: Display for measurement outputs.

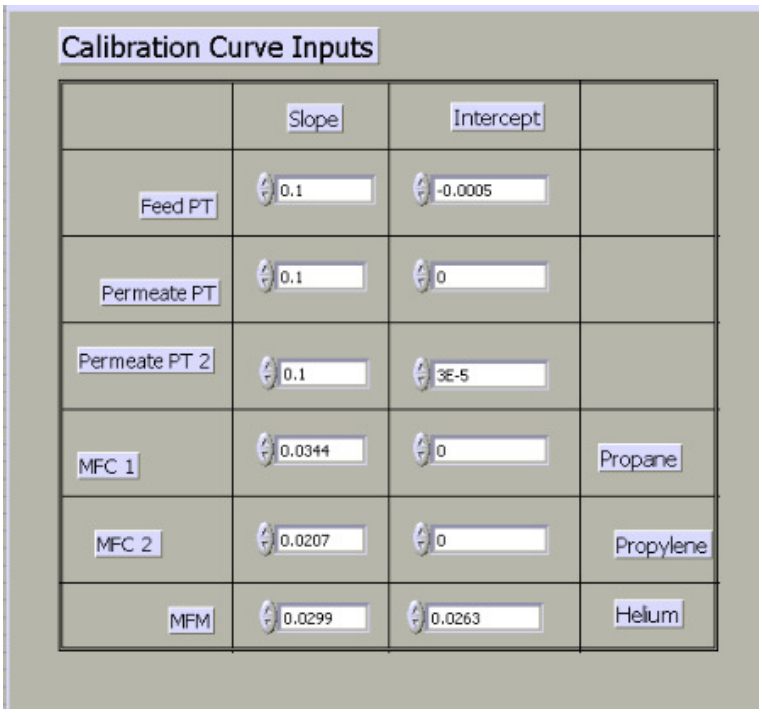

Figure 3.6: User input calibration data

The program was divided into three sequences: degas, permeation, and shutdown. The user has the ability to independently specify the time for each sequence. Once a sequence is complete, the system will advance to the next sequence or end the code. The user can also prematurely end the current sequence and start the next sequence. In addition, the code allows the user to input a maximum permeate pressure. If the maximum pressure is reached, the program will close all valves and evacuate the system. This protects the low pressure transducer from damage.

After a permeation sequence, a file is created and all measurements are saved. Recorded data consists of feed and permeate pressures, feed and sweep gas flow rates, testing time, and system temperatures. User controlled variables are feed pressure, two feed gas flow rates, the sweep gas flow rate, and temperature. The frequency of data points measured is constant at 1 Hz and the frequency of points being saved can be varied by the user. The system will cycle between degasing and permeation sequences for the number of cycles specified by the user. Once the cycles are completed, the system will go into the shutdown sequence. The system will shut feed gas valves and evacuate all gas to the fume hood.

Calibration of instruments was performed on a regular basis. The calibration data (slopes and intercepts) were input into the user interface (Figure 3.6).

3.4 Mixed Gas Experiments

Retention time of each gas through the GC column is used to identify the permeating gases. This is dictated by the gas, column material, and column length. The voltage generated from the FID detector is directly proportional to the amount of sample passing through the detector at any given time. Shimadzu software integrates the voltage vs time data to obtain the area for a sample. The area of a peak is proportional to the amount of gas that is present in the sample loop and is used for calibrations. Conditions held constant between the calibration and permeation runs are the pre-heater temperature, individual FID detectors, oven temperatures, split ratio and flow rates, and column type, diameter, and length. The amount of tested gas was plotted against peak area was used for to calibrate for future permeability runs.

Gas standards were prepared using tedlar bags, acquired from Restek. Tedlar bags were filled (at 1 atm) with helium (2 bags), propane, and propylene respectively. A gas tight syringe was used to inject a known volume of testing gas into the helium filled tedlar bag. A sample was then extracted and inserted into the injection port for analysis. Several samples per concentration were tested and the average was taken. This process was repeated for each gas until an adequate range of concentration was acquired. Figure 3.7 is an example of propane and propylene calibrations using this method.

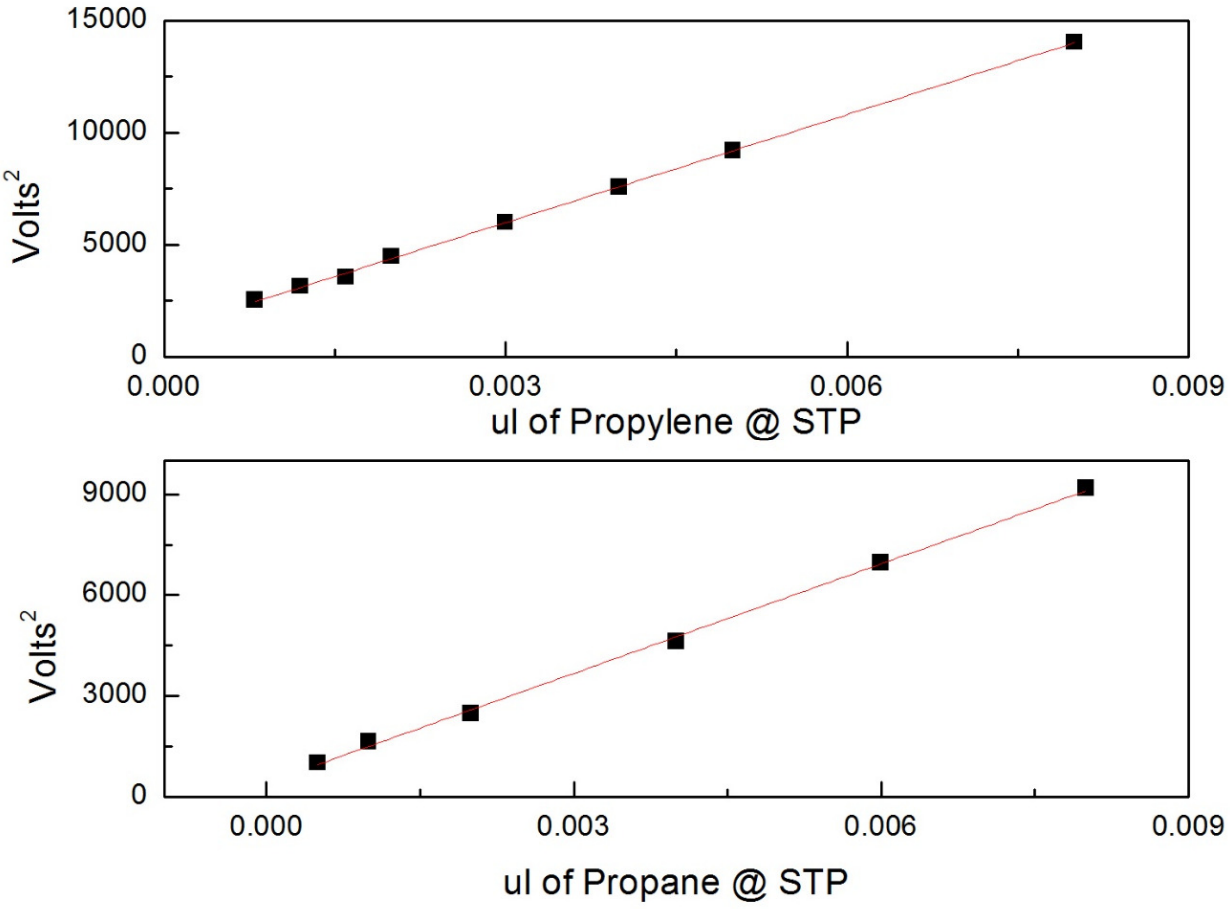

Figure 3.7: Calibration curves constructed for propylene (top) and propane (bottom).

For the testing of mixed gases, the constant pressure-variable volume method was used. An initial degas period of two hours was used to remove any sorbed gas from the membrane. A leak test was not necessary, as low pressures were not required. The two feed gases were fed with a flow rate of, at minimum, 100 times greater than the flux across the membrane. This was to ensure a constant composition at the interface of the membrane. During mixed gas permeation experiments, Valves 1 and 2 (Figure 3.1) were open and the gas was sent to the mass flow controllers. In addition, Valve 5 was open to allow for a steady flow of mixed gas across the membrane cell. Valve 6 was also open and helium swept the permeate gases to the GC. The permeate stream was maintained at a pressure of 1 atm (or slightly above), which was measured by a second MKS pressure transducer.

An Rt-QS-BOND PLOT Column (Restek) was used in order to separate gases for analysis. The column length was 30 meters long and had an inner diameter of 0.32 mm. The retention time of compounds in PLOT columns depends on diffusion of the gas into a porous layer as well as interactions of the compound and the column. The retentive stationary phase makes it ideal for low molecular weight hydrocarbons and other volatile gases to be separated. Propane and propylene separation was of particular interest. Retention time was shorter for propylene, allowing for good peak separation. Figure 3.8 is an example of data attained from the Shimadzu GC program. Propylene, with a retention time of about 4.8 minutes, was successfully separated from propane, with retention time of 5 minutes. If greater separation is required several variables can be changed, including split ratio, flow rate, temperature, and column length.

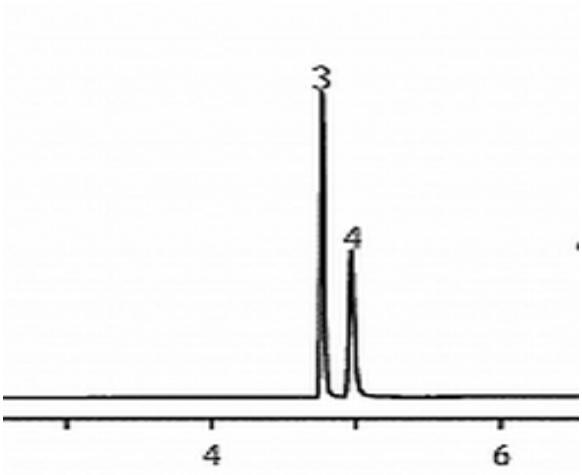

Figure 3.8: Example of peak separation for propane/propylene gas mixture when running a mixed gas experiment and GC simultaneously

The following equation was used to calculate the permeability of gases when testing under mixed gas conditions.

$$PC_3H_i = \frac{x_{1,C3Hi} S_F l}{x_S^p A(P_2 x_{2,C3Hi} - P_1 x_{1,C3Hi})} \qquad (3.1)$$

PC_3H_i are the permeation for propane and propylene. Subscripts of 2 correlate to the feed side of the membrane and subscripts of 1 correlate to the permeate side. P is the partial pressure of propane and propylene, *x* is the mole fraction of the streams, S_F is the sweep flow rate in the permeate stream, A is the active separation area, and l is the thickness of the membrane.

3.5 Single Gas Experiments

For single gas runs, errors in permeability values are proportional to errors in the permeate side volume determination. Thus, it is important to minimize the error of the permeate volume measurement. Many teams either manually fill the permeate side with a liquid or purchase a membrane cell with known permeability characteristics and back calculate volume. Filling the permeate side with a liquid is very inaccurate, as there will be air bubbles trapped and many regions cannot be filled, such as the inside of a pressure transducers and small diameter pipes. Purchasing a membrane with known permeation values has proven to be accurate, but the cost of such membranes can be up to $1000. As a result, an in-house method was designed to accurately and cost effectively obtain the volume in the permeate side. A known volume container was purchased from Swagelok, V_1, with an error of less than 2% and attached to the membrane cell, shown in Figure 3.9. Impermeable aluminum tape was used in place of a membrane, isolating the feed side from the permeate side. The entire permeate side of the system (including the connected container, V_1) was filled with hydrogen, with several cycles of vacuum and filling back with hydrogen to 1 atm. Then the system was placed under vacuum to a pressure of 5 torr and valve V_{1b} was closed. Subsequent to this, the remaining system, with volume V_P, was placed under vacuum at a pressure of 0.1 torr. Valve, V_{2b}, was shut off and the system was isolated from the vacuum. Valve, V_{1b}, was then opened and the pressure in the entire system was allowed to equilibrate to a measured pressure P_{Final}. From a simple mole balance, V_p (permeate volume) is easily and accurately calculated (3.2). The calculated volume will be slightly higher than the actual volume because of the pipe connecting valve V_1B to the system. A Swagelok pipe with a known inner diameter was used and the calculated volume (less than 1% of the system volume) was subtracted.

$$P(5torr) * V_1 + P(0.1torr) * V_P = P(final) * (V_1 + V_P) \qquad (3.2)$$

Ideal gas behavior was assumed based on the low pressures and the use of hydrogen as the gas for testing.

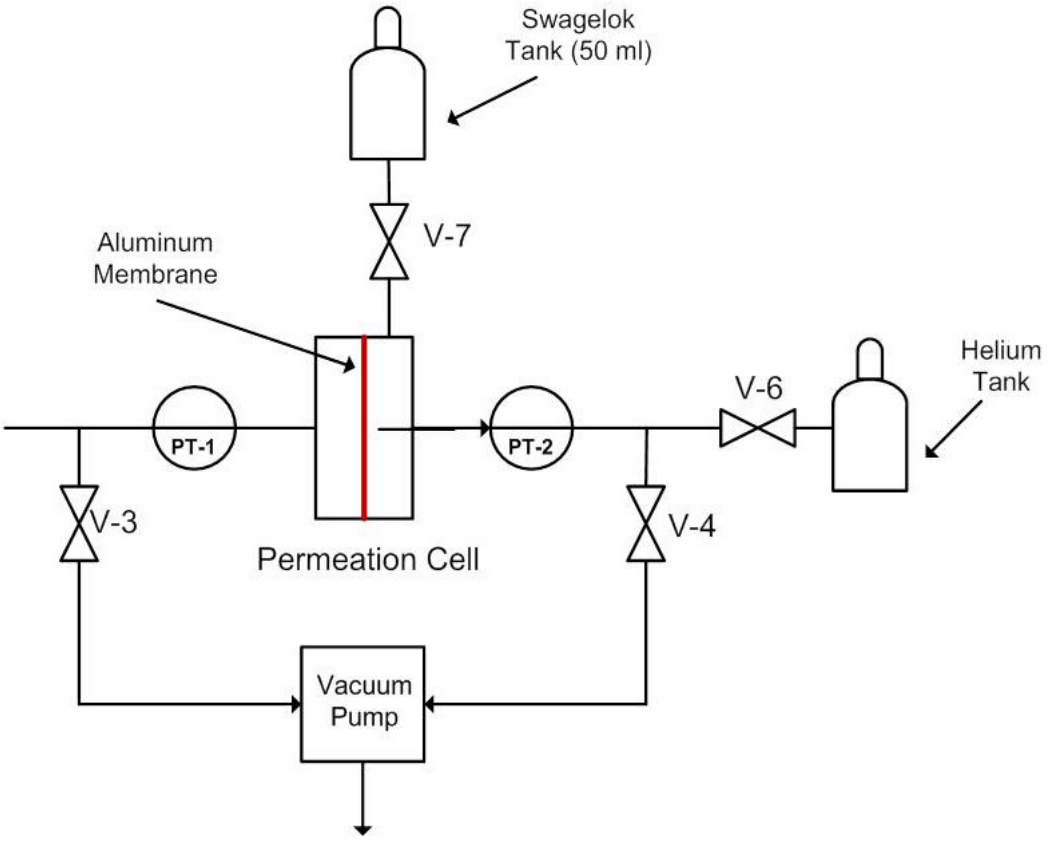

Figure 3.9: In-house configuration for determining the permeate volume

It is then necessary to check for system leaks. After the membrane is placed in the permeation cell, a quick degassing of the system (30 minutes) is followed by all valves being deactivated and allowing the system to idle for a minimum of one hour. If a large leak is detected (greater than 5% of the predicted flux) the system is resealed and retested for proper isolation. Once the desired seal is acquired, the slope of pressure vs time is attained and subtracted from permeation runs prior to data analysis.

During the degas sequence, valves 3 and 4 (Figure 3.1) are open, allowing the system to be evacuated. Valve 6 was employed to protect the GC unit from low system pressures, which can cause complications with the unit and column. Typical degassing time was set to 3 hours.

During single gas runs, MFC1 and MFC2 are set to zero, and the feed gas is bypassed around the mass flow controllers. Flowing the gas through the mass flow controller will result in a longer time to reach desired feed pressures. This will result in time lag values, which are to calculate solubility and diffusivity calculations, to be unattainable or inaccurate

In addition, valve 1 or 2 is activated and a gas at a constant pressure is applied to the feed side of the membrane. The permeate gas is accumulated in a known volume confined by valve 6. The experiment

is active until a steady state is reached. Experiment times depend on the membrane material and thickness, gas and system temperature. Pressure vs time is plotted in real time to give the user an indication of the progress of the run, as depicted in Figure 3.10.

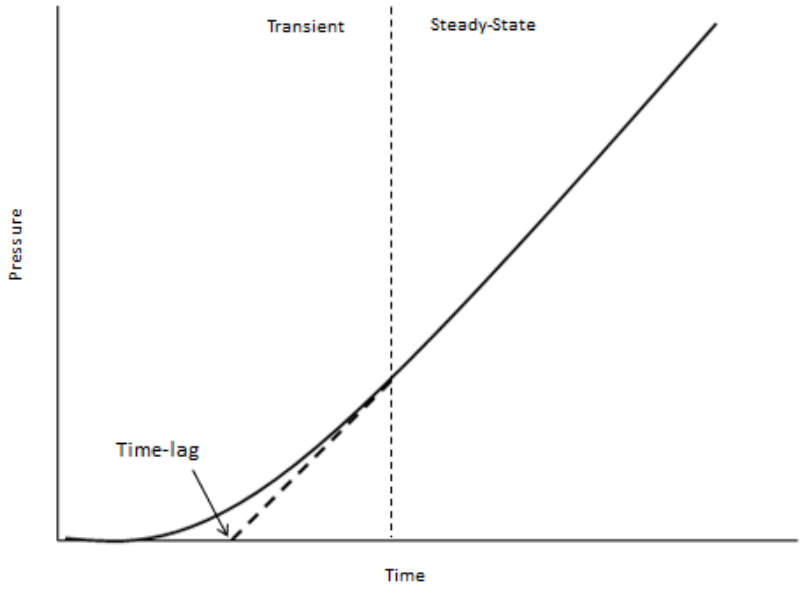

Figure 3.10: A schematic of the pressure vs time data attained through a single gas permeation run

The following equation is used to calculate permeation through the membrane:

$$P\ [Barrer] = \frac{(\left[\frac{dP}{dt}\right]_P - \left[\frac{dP}{dt}\right]_{leak})*V}{RT} * \frac{lM_V}{A\Delta P} \qquad (3.3)$$

where V is the permeate volume, R is the ideal gas constant, T is system temperature, dP/dt is the steady-state pressure increase due to permeation and to the system leak, l is the membrane thickness, M_V is the molar volume of the gas, A is the active permeation area of the membrane, and ΔP is the pressure difference between the feed and permeate side, which is assumed to be equal to the feed pressure. The diffusivity is then calculated using the following equation:

$$\mathrm{D} = \frac{l^2}{6\Theta} \qquad (3.4)$$

Θ is the time lag obtained by extrapolating the steady state pressure vs. time data (Figure 3.10) and l is the thickness of the membrane. Solubility can be found using:

$$S = \frac{P}{D} \quad (3.5)$$

Single gas and mixed gas values measured using the above methods are comparable.

Chapter 4: Polymer Dispersed Liquid Crystals for Vapor Phase Transport

4.1 Abstract

Novel polymer dispersed liquid crystal (PDLC) membranes were fabricated using a solvent induced phase separation technique (SIPS) followed by a thermally induced phase separation technique (TIPS). The thermal phase behavior of the PDLC membranes and the liquid crystal (LC) domain dispersities and sizes were characterized using FE-SEM, DSC and POM techniques. Diffusion, Sorption, and permeation characteristics of the membranes were measured. Single gas sorption selectivities were low but an increase in permeability selectivity was observed in mixed gas permeation experiments due to competitive sorption of different gases. Permeability and selectivity increased with increasing LC concentration in the membrane. In addition, an increase in temperature enhanced interactions of the polymer/8CB blend with propylene and resulted in an increase in permeability and selectivity.

4.2 Introduction

Due to the low relative volatilities and similar boiling points of olefins and paraffins, low temperature distillation is usually required for their separation and has been used for the past 60 years.[80] Cryogenic distillation systems are expensive to build and operate and are currently only economically viable for streams containing high quantities of olefins.[81] The large energy and capital investment of classical separation techniques provides an incentive for research on new separation technologies.

There has been great interest in membrane separation technologies for their low energy consumption, low capital cost, as well as minimal maintenance. Liquid crystalline materials have not yet been investigated for applications related to paraffin/olefin separations. Liquid crystals have fluid like physical characteristics as well as anisotropic structural features, at a microscopic level. Thermotropic liquid crystals have unique phase behavior, ordering and rheological properties make them potentially useful for several separation applications. [66, 71, 82]

In this work, polymer dispersed liquid crystal (PDLC) membranes were fabricated using a solvent-induced phase separation method (SIPS) followed by thermally-induced phase separation (TIPS)[83] in order

to prodcue well dispersed domains of liquid crystals. The phase behavior and gas transport properties of the PDLC membranes were then studied.

4.3 Experimental

4.3.1 Materials.

4-cyano-4-octyliphenyl (8CB) and N-(4-Methoxybenzylidene)-4-butylaniline (MBBA) were used as received from Wako Chemicals USA Inc. (Richmond, VA, USA). Structures of these liquid crystalline molecules are depicted in Figure 4.1. Polysulfone (M_n=22,000) was purchased from Sigma Aldrich (St. Louis, MO, USA) and used without further purification.

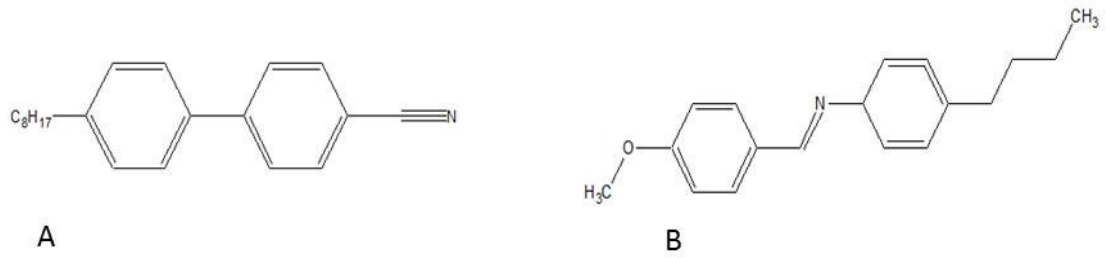

Figure 4.1: Liquid crystal structure of 8CB (a) and MBBA (b)

4.3.2 Preparation of PDLC Films:

The polymer and mesogen (Table 4.1) were dissolved in chloroform at a ratio of 0.1 grams of solute (polymer and mesogen) to 1 ml of solvent. The mesogen content was varied between 0 and 60 wt%. The solution was sonicated at 40 ^{o}C for two hours and cast on a clean glass substrate

Table 4.1: Membranes fabricated for studies

Membrane	LC wt%
20_8CB	20
35_8CB	35
55_8CB	55
40_MBBA	40

60_MBBA	60
PSf	0

4.3.2.1 Solvent Induced Phase Separation (SIPS)

The solvent evaporation rate was controlled using a weighted glass cover to create a seal. The complete evaporation of solvent (chloroform) took approximately 36 hours. The final films had a uniform thickness ranging from 40 um to 60 um. The films were dried under vacuum at 60 ^{o}C for several hours, until the total weight of the membrane no longer changed. The cast film was immersed in de-ionized water overnight to help facilitate removal from the glass substrate. The membranes were weighed before and after water immersion to insure that there was no water uptake.

4.3.2.2 Thermally Induced Phase Separation (TIPS)

The films were cast using an identical procedure as described in the SIPS method. The resulting films were heated 175 ^{o}C, resulting in the dissolution of any LC domains. The temperature was helod for 30 minutes and then cooled at a rate of 2 ^{o}C/min to room temperature. The slow cooling rate resulted in the controlled nucleation and growth of uniformly dispersed LC domains.

4.3.3 Characterization.

Differential Scanning Calorimetry (DSC) measurements were performed using a Perkin Elmer DSC-2 instrument**.** The samples were cooled to 0^{o}C and heated at a rate of 10 ^{o}C/min. Cooling rates were maintained at 2 ^{o}C/min. Equilibrium times were 20 minutes.

An Olympus BX51 polarized optical microscope equipped (POM) with a Linkam LTS 350 hot stage and a Linkam TMS 94 temperature programmer was used to investigate the temperature dependent textures of the PDLC membranes. The birefringence of the membranes were observed at several temperatures and concentrations.

Field Emission Scanning Electron Microscopy (FE-SEM) was employed for the characterization of domain dispersion, size and regularity. A freeze fracture technique using liquid nitrogen to explore the liquid crystal domains in the cross-section of the membranes was used. The PDLCs were immersed in acetone in order to remove the liquid crystals and simultaneously keep the polymer matrix intact.

Sorption and diffusion measurements were performed using an Intelligent Gravimetric Analyzer (IGA, Hiden-Isochema). Single gas sorption experiments using both propane and propylene were run in the nematic and isotropic phases. Values of the ideal sorption and ideal sorption selectivity were measured. Diffusion and ideal diffusion selectivity were determined using Crank-Nicolson method to model the gas uptake with time.

A constant pressure/variable volume apparatus was used for mixed gas permeability measurements. LabView was employed in order to measure, control, and record all instrument activity and parameter values For mixed gas permeability experiments, the following equation was used to calculate both the propane and the propylene permeability[84], as well as their respective selectivity.

$$PC_3H_i = \frac{x_{1,C3Hi} S_F l}{x_S^P A(P_2 x_{2,C3Hi} - P_1 x_{1,C3Hi})} \qquad (4.1)$$

Subscripts of 2 correspond to the feed side of the membrane and subscripts of 1 correlate to the permeate side. P is the partial pressures of propane and propylene, x is the molar fraction of the feed or permeate, S_F is the sweep flowrate in the permeate gas (N_2 or He), A is the active separation area, and L is the thickness of the membrane. Prior to a permeability run, membranes were degassed at room temperature until minimum system pressure was reached and held constant, for several hours.

4.4 Results and Discussion

4.4.1 Morphological Properties of 8CB/PSf Membranes

Optical Microscopy was used to characterize PDLC membranes for both the SIPS and TIPS processes. This helped characterize the presence of ordered domains of liquid crystal within the polymer matrix. In addition, the mechanism of the thermally induced phase separation (TIPS) process was investigated. Figure 4.2 shows polarized optical micrographs of films containing 35wt% and 55wt% 8CB in Polysulfone (35_8CB and 55_8CB respectively,) using the SIPS membrane fabrication process. Liquid crystal domain formation for 35_8CB was not clear. In addition, no birefringence is present under cross polarizers. The 55 wt% film exhibits birefringent and well defined liquid crystal domains indicating material anisotropy.

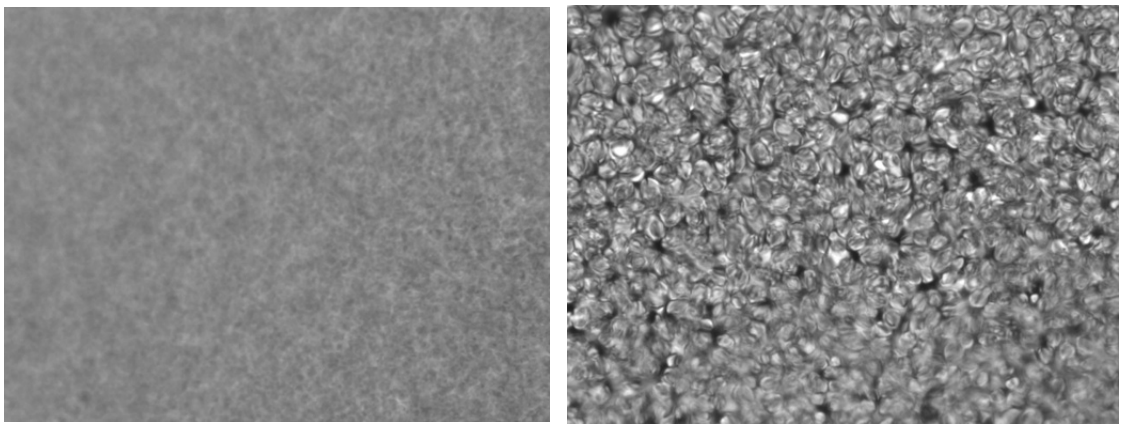

Figure 4.2: Optical Microscopy images of 35_8CB (left) and 55_8CB (right) in Polysulfone at 21°C and placed between cross polarizers.

The phase separation is dependent on the concentration of LC in the polymer. Assuming sufficient time is given to reach equilibrium, LC domains are formed at concentrations higher than the saturation limit of the LC in the polymer.[85] 35_8CB had relatively small domains compared to that of 55wt%. Boundaries were not as well defined and no apparent birefringence was present. The loading of 35_8CB was just above the solubility limit resulting in the formation of small domains. At 35wt%, LC was largely dissolved in PSf. 55wt% 8CB in PSf, exhibited large and clearly visible domains. The liquid crystal droplets were uniformly dispersed with a homogeneous pore diameter with isolated boundaries and birefringence.

4.4.2 LC Domain Formation via TIPS

In practice, it is difficult to control the solvent evaporation rate, and thus it is difficult to control domain size, in particular for large scale fabrication. For this reason, after the membranes were fabricated by the SIPS process, the PDLC film was heated until the LC molecules fully dissolved in the thermoplastic polymer matrix. A TIPS process subsequent to a SIPS process ensured a more controlled fabrication process resulting in uniform liquid crystal dispersion and more controllable domain diameters. The PDLC film was subjected to a temperature of 175 °C then cooled to room temperature at a rate of 2 °C/min. At 175°C the liquid crystal (8CB) was completely dissolved in the polymer (Figure 4).

Figure 4.4: 55% 8CB fully dissolved in polysulfone, 175 ^{o}C

The coalescence of the liquid crystals began at a temperature of 158^{o}C. A progression in domain growth with the LC becoming more uniform in size and shape was observed as the temperature continued to decrease. This was due to the solubility of the LC decreasing with decreasing temperature. Ordering took place at 37 ^{o}C (initial birefringence observed), which was consistent with the nematic/isotropic transition of 8CB as determined using DSC.

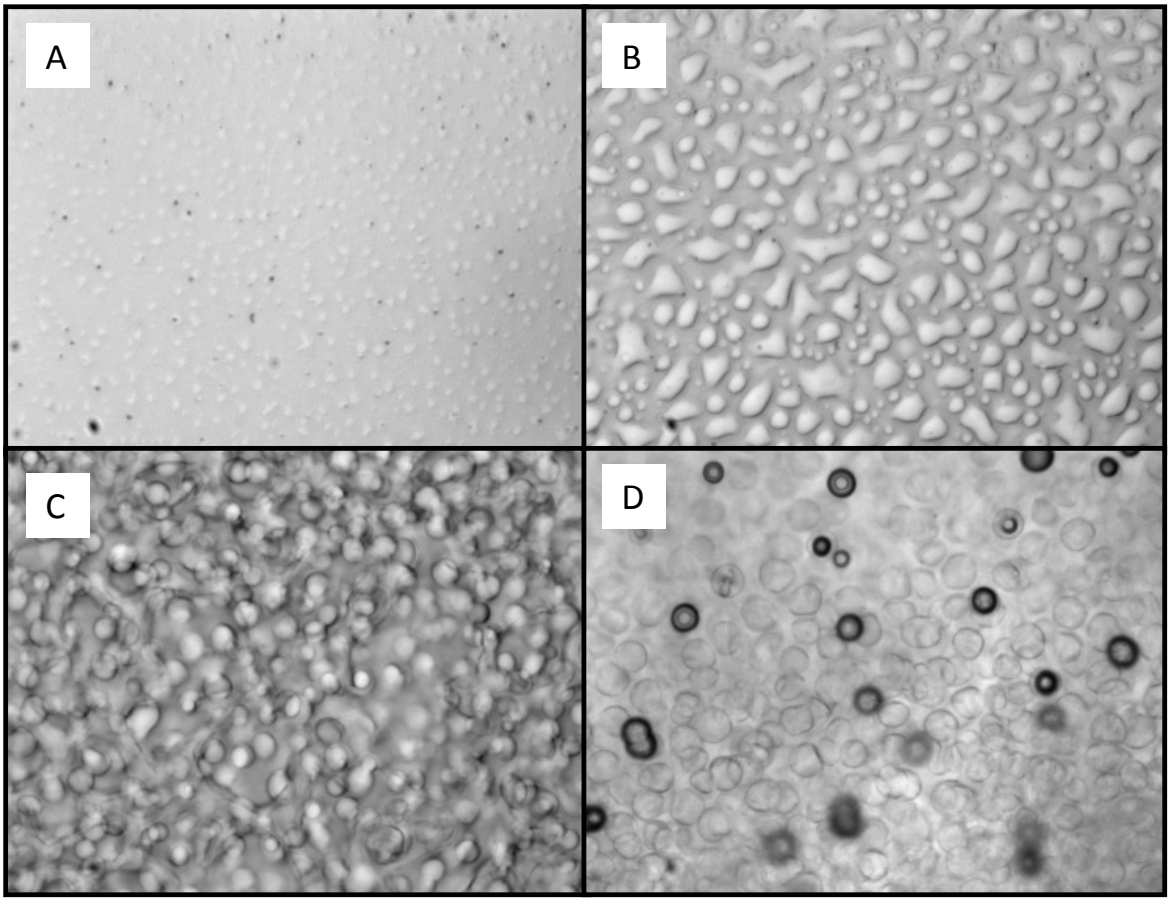

Figure 4.5: Optical microscopy on 55%8CB in polysulfone. (a) 158 °C, (b) 151 °C, (c) 115 °C, (d) 21 °C.

4.4.3 Thermal Phase Transitions

Figure 4.6 contains DSC measurements for the 8CB/PSf membranes with varying concentrations. This was done to ensure that the thermotropic liquid crystal phase behavior was preserved within the polymer membrane and to identify the associated temperatures of phase change with the respective LC concentration or domain size. Membranes were fabricated using the SIPS method and followed by the TIPS method. DSC thermographs were performed for several isobar cycles. The T_g for polysulfone was measured to be 182.7 °C (ΔC_p=0.18 J/gx°C). The addition of 8CB at concentrations below phase separation results only in the plasticization of PSf. The T_g for membrane 20_8CB decreased to 75.3 °C (ΔC_p=0.23 J/gx°C) and no additional peaks were present. 35_8CB exhibited a lower polymer T_g of 38.1 °C (ΔC_p=0.32 J/gx°C). The large shift from 20 wt% to 35 wt% 8CB indicates the saturation limit of LCs in the PSf is close to 35 wt%. Similar phenomena were also reported for a polycarbonate/dibutylsuccinate system, where the T_g was depressed from approximately 150 °C to 40 °C with a diluent concentration of 25 wt%.[86] In

addition, an increase in the change of specific heat across the transition temperature was observed with increased 8CB concentration, suggesting large changes in polymer morphology across the T_g for the 8CB/PSf systems. 55_8CB (55 wt%) exhibited a T_g of 38.6 °C, very similar to that of 35_8CB, indicating that the saturation limit of PSf is below 35 wt% and the addition of LC above this limit resulted in the formation of larger domains.[87]. LC domain phase transitions overlapped with the T_g and accurate ΔC_p values could not be measured. In contrast, 35_MBBA and 60_MBBA (35 wt% and 60 wt% MBBA in Psf) had no LC phase transitions detectable by DSC and no birefringence was observed via POM.

55_8CB had two phase transition temperatures corresponding to the LC domains. The first peak was at 31.2 °C (ΔH=0.12 J/g) and a second larger peak was at 38.6 °C (ΔH=0.77 J/g. The 8CB smectic to nematic transition temperature is 32.6 °C (ΔH=0.32 J/g) and the nematic to isotropic transition temperature is 39.8 (ΔH=2.3 J/g). Although, 55_8CB had no detectible crystalline to smectic transition, smectic/nematic and nematic/isotropic phase transition temperatures of the LC droplets agree well with pure 8CB. 35_8CB exhibits only a very small, almost undetectable, peak at the expected temperature for the nematic/isotropic transition. This supports the conclusion that only a small fraction of the 8CB is present in LC domains, with the majority being dissolved in the polymer.

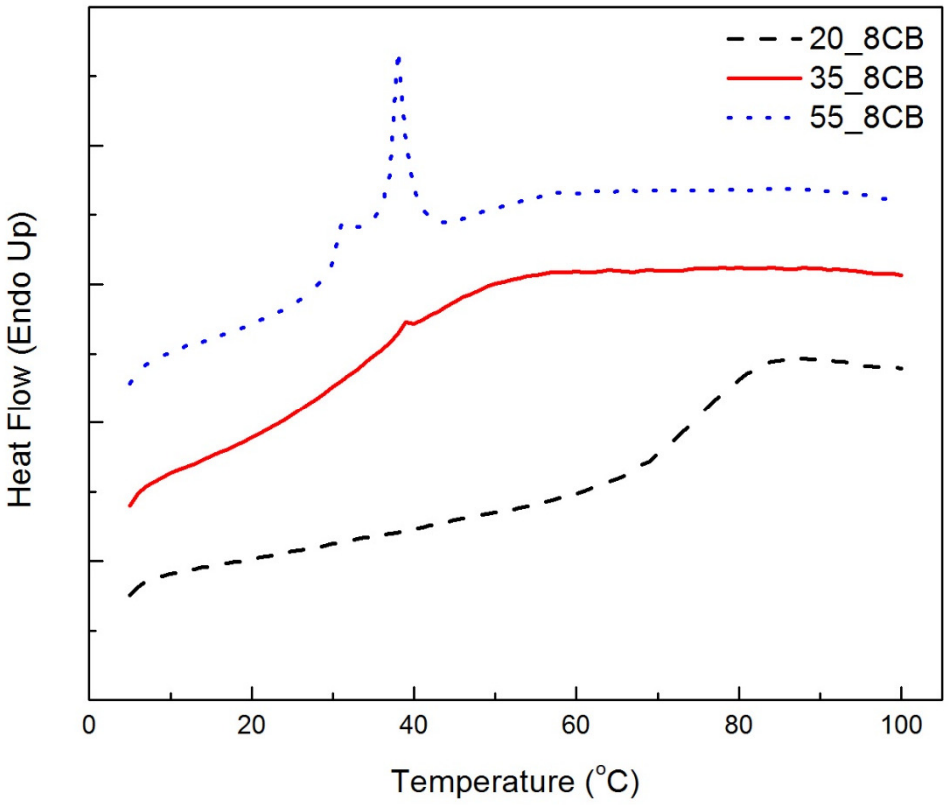

Figure 4.6: DSC isobars of polysulfone with 8CB

Table 4.2: DSC-data for pure 8CB and 55_8CB membrane.

Sample	T_{C-S} (°C)	ΔH (J/g)	T_{S-N} (°C)	ΔH (J/g)	T_{N-I} (°C)	ΔH (J/g)
8CB	21.3	87.09	32.6	0.32	39.8	2.30
55_8CB			31.2	0.12	38.6	0.77

Table 4.3: DSC-data for pure polysulfone and membranes containe 8CB LCs

Sample	T_g (°C)	ΔC_p (J/gx°C)
PSf	182.7	0.18
20_8CB	75.3	0.23
35_8CB	38.1	0.32
55_8CB	38.5	a

[a] not determined

4.4.4 LC Domain Sizes and Regularity

FE-SEM was employed to observe the cross section of the PDLC membrane and to characterize the regularity, size, and dispersion of the liquid crystal domains. Figure 4.7 shows the cross-section of a pure PSf membrane following an acetone wash. No noticeable defects in the matrix were observed.

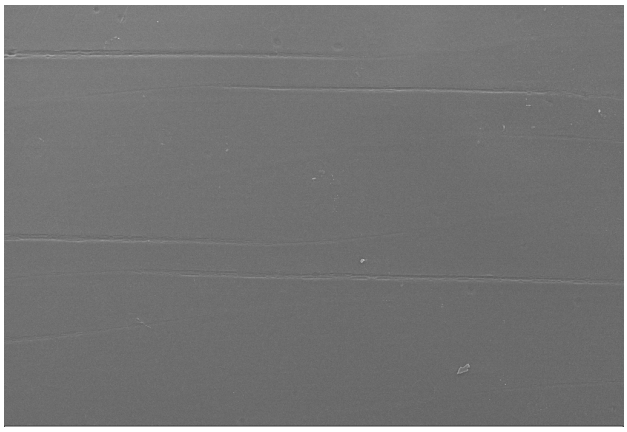

Figure 4.7: Pure polysulfone immersed in acetone (cross section).

MBBA and 8CB were both used for the formation of liquid crystal domains. Figure 8 shows both 40 wt% and 60 wt% MBBA in polysulfone (40_MBBA and 60_MBBA respectively.) 40 wt% MBBA had a nominal pore diameter ranging from 0.5 and 4 microns. At this concentration the liquid crystals existed as individual domains. At 60 wt% MBBA, the density of the domains began to increase and form a co-continuous phase within the polymer matrix. As noted earlier, neither 40_MBBA or 60_MBBA exhibited LC transition peaks in the DSC or birefringence under crossed polarizers. The co-continous LC phase at 60 wt% MBBA leads to an undesirable film for membrane separation applications. Pressure gradients between the feed and permeate sides would physically remove the LC from its support. This would result in the permeating gases diffusing across the membrane unregulated or with minimum resistance, leading to very low selectivity and poor membrane stability.

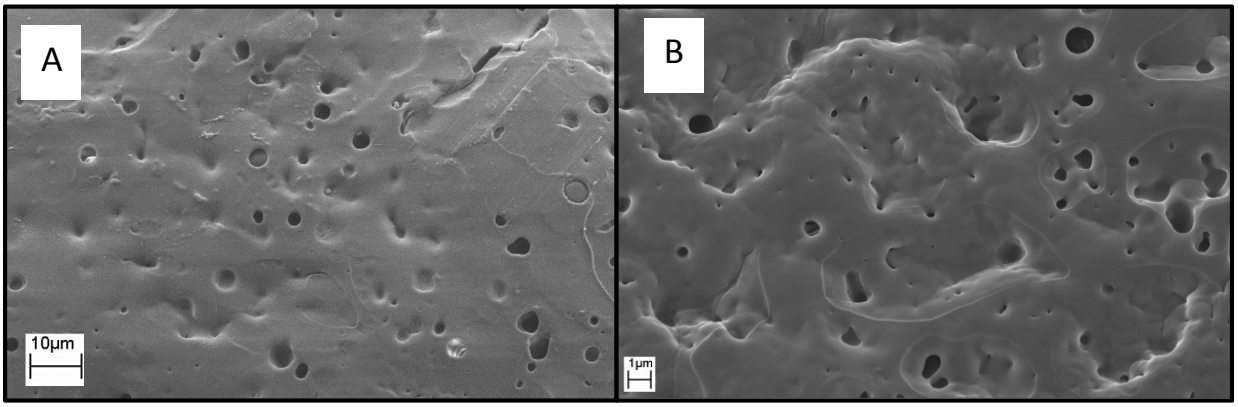

Figure 4.8: Liquid crystal MMBA in a PSf matrix (a) 40_MBBA and (b) 60_MBBA

Figure 4.9 depicts FE-SEM images of 8CB in polysulfone at different 35 and 55 wt%. 35_8CB sample clearly shows LC domains in the Psf matrix, confirming that 35 wt% is above the equilibrium saturation limit for 8CB in PSf. The LC domain size increased with increasing 8CB content, from ~1-3 µm in 35_8CB to ~6-12 µm in 55_8CB. A well dispersed film is created with very little or no connectivity between LC domains for both 35_8CB and 55_8CB.

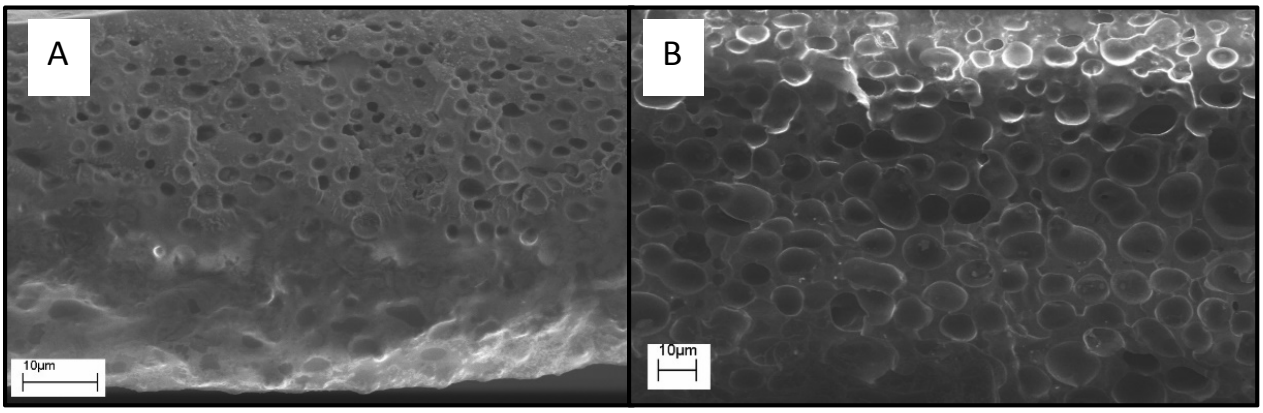

Figure 4.9: Liquid crystal 8CB in a PSf matrix (A) 35_8CB and (B) 55_8CB

4.4.5 Gas Sorption and Diffusion in 8CB

Single gas propylene and propane sorption isotherms for pure 8CB were collected in both the liquid crystal mesophase (35 °C) and isotropic phase (45 °C) at pressure increments between 0 mbar and 5000 mbar. Propylene exhibited a higher sorption than propane at all pressure. The higher solubility of propylene can be attributed to stronger interactions between the polar propylene molecules and the polar 8CB molecules. Solubility selectivities of approximately 1.2 were observed for both the LC and isotropic phase. Previous studies on liquid crystal sorption reported that solubility depended on the phase behavior of the LC material.[67, 88] Sorption of light gases significantly increased across the crystalline/LC and LC/isotropic transitions, which was attributed to an increase in free volume and mesogenic mobility. In this study, at pressures below 1.5 bar propane and propylene showed an increase in sorption in 8CB when going from the nematic to the isotropic phase. At 5 bar, propane and propylene exhibited a 26 % and 24 % decrease in sorption respectively. The increased sorption of propane and propylene in the nematic phase indicate enhanced interactions between the permeant gases and ordered liquid crystal

mesogens. This is likely due the affinity between the rod-like shape of the molecules and the oriented nematic LC phase. A similar phenomena was previously reported by our research group.[82] Supported liquid crystal membranes were fabricated to study the transport of substituted aromatic solutes. Para isomers exhibited a solubility decrease across the nematic to isotropic phase, while the ortho and meta isomers exhibited no change in solubility. This was attributed to the affinity of the rod-like para isomers with the unidirectional orientation of the LC material in the nematic phase.

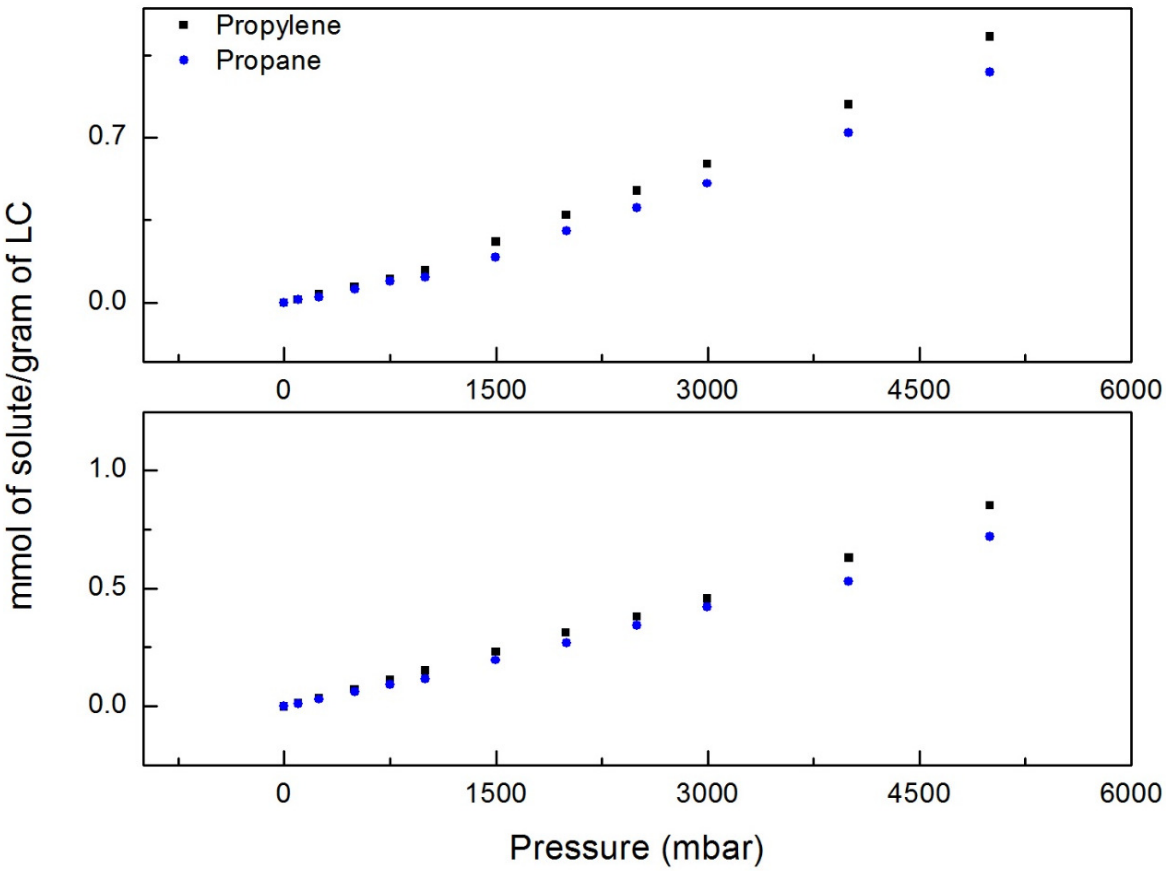

Figure 4.10: Sorption of propane and propylene in 8CB (top) 35°C (bottom) 45°C

Crank's method for diffusivity was employed to model the diffusion properties of pure 8CB. Assuming a flat sheet with infinite diameter and thickness, l, the final equation is:

$$\frac{M_t}{M_\infty} = 1 - \sum_{n=0}^{n=\infty}\left[\frac{8}{(2n+1)^2} exp\left(\frac{-D(2n+1)^2\pi^2 t}{4l^2}\right)\right], (n = 0,1,2 \dots) \qquad (4.6)$$

M_t is the total sorbed mass of gas at time t, M_∞ is the total sorbed gas once the material reached equilibrium, l is the thickness of the flat sheet, t is time, and D is the effective diffusion.

Figure 4.11 contains plots of the the model (equation 4.6) for the ratio of sorbed gas to the total possible sorbed gas with time fitted to experimental data. A one step pressure increase from 0 to 1 bar for both propane and propylene was used. Table 4.2 summarizes the calculated diffusivity values. Diffusivities of all gases increased as the temperature increased. In addition, diffusivity selectivity was higher in the nematic state compared to the isotropic state. Nematic 8CB ordering resulted in a more controlled spacing between the mesogens, compared to the randomized spacing in an isotropic state.[89] This selective size discrimination resulted in a higher selectivity.[82]

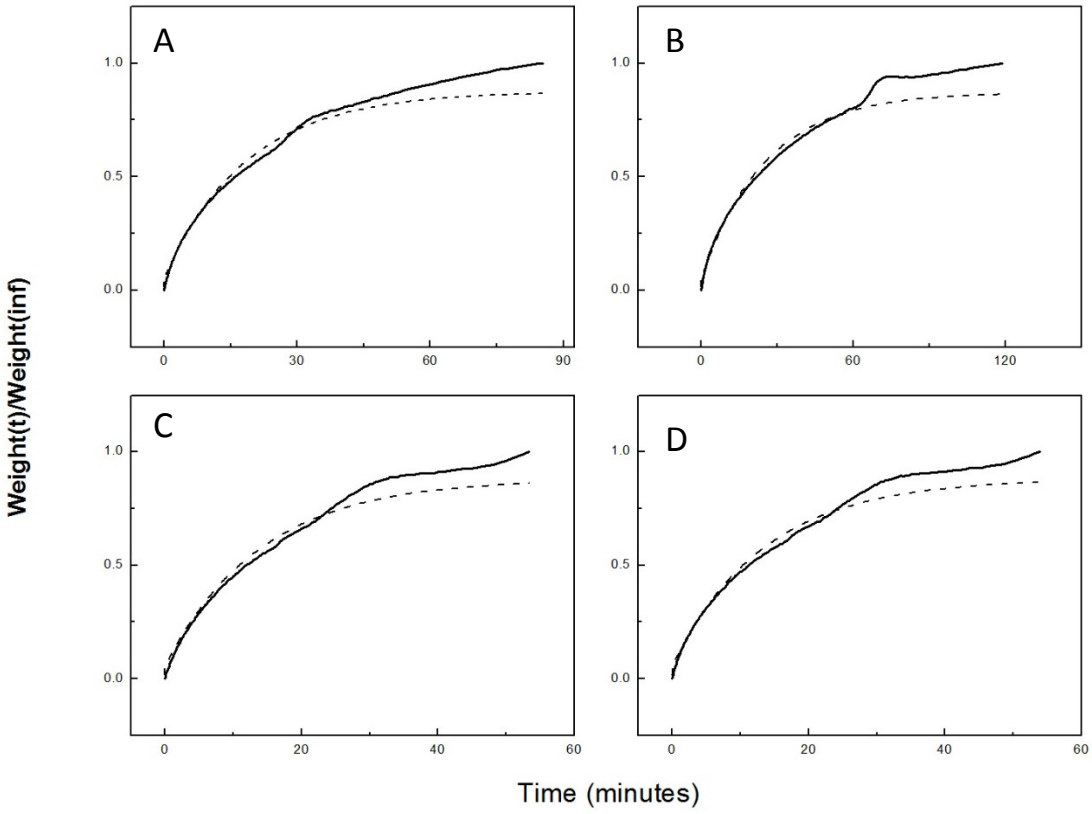

Figure 4.11: Diffusivity of 8CB in PSf for propane and propylene at several temperatures (a) C3H6 mesophase, 35 °C (b) C_3H_8 mesophase 35 °C (c) C_3H_6 isotropic 45 °C (d) C_3H_8 isotropic 45 °C. Calculated (- - -) and Experimental (▬)

Table 4.4: Diffusivity values for 8CB at different temperatures

8CB	Diff x10^4 (cm^2/sec)	Diffusion Selectivity
Propylene (35^{o}C)	1.45	1.34
Propane (35^{o}C)	1.08	
Propylene (45^{o}C)	1.92	0.95
Propane (45^{o}C)	2.01	

4.4.6 Mixed Gas Transport in 8CB/PSf Membranes

Mixed gas permeability measurements were performed for pure PSf, 35_8CB, and 55_8CB membranes. Room temperature permeabilities and selectivities of membranes with increasing 8CB concentration are plotted in Figure 4.12. The lowest permeability (1.5 barrer) and selectivity (1.3) was measured for pure PSf. The addition of 35 wt% 8CB increased the permeability by about 25% to 1.9 barrer. In addition, selectivity was increased to 1.6. The LC domains present in 35_8CB showed no thermal phase transition characteristics, which implies LC domains present in the polymer matrix were isotropic or the domain fraction was too small for the transitions to be observed. The increase to 55 wt% 8CB gave both the highest permeability (3.4 barrer) and selectivity (5.9). At this concentration, the presence of ordered LC domains was confirmed by POM, DSC and FE-SEM. The ordering and larger volume fraction of these domains resulted in an increase of both selectivity and permeability. Although sorption and diffusion selectivity for single gases in pure 8CB were below 2, a mixed gas selectivity of 5.9 was achieved using PDLC membranes. The competitive sorption behavior preferentially sorbs the more polar propylene gas over propane.

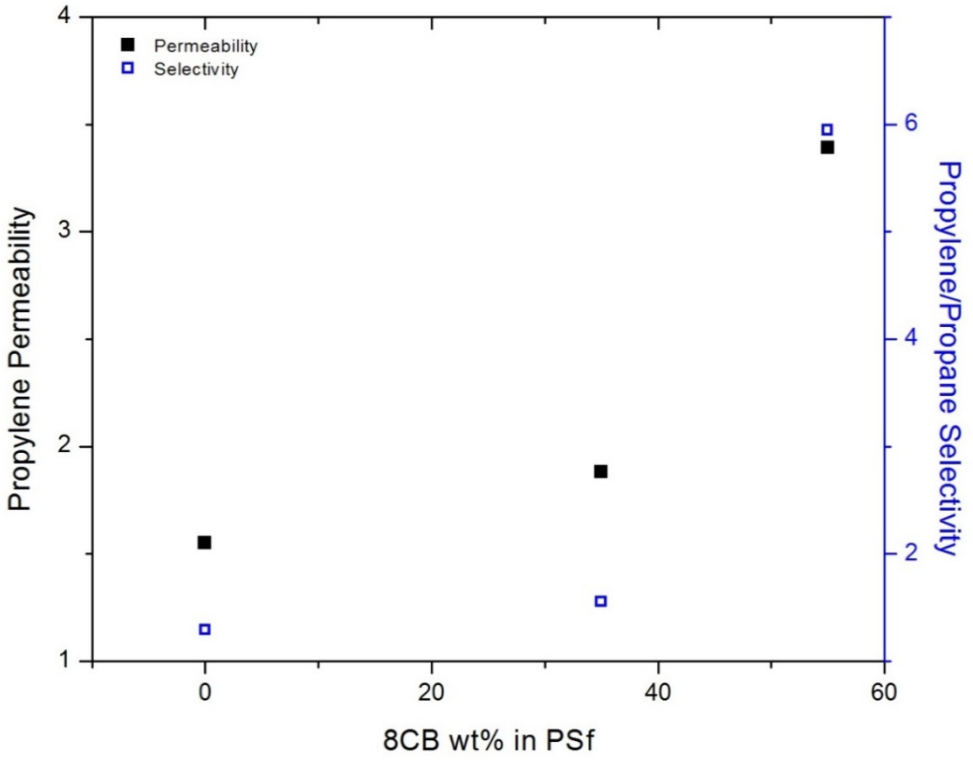

Figure 4.12: Permeability and selectivity values obtained by varying 8CB concentration at room temperature.

The temperature dependence of permeation and selectivity for both 35_8CB and 55_8CB membranes was investigated. Figure 4.13 shows propylene permeabilities and selectivities of a 35_8CB membrane at different temperatures. An increase in permeability from 1.88 barrer (21 ^{o}C) to 2.98 barrer (37 ^{o}C) was found when approaching the glass transition temperature of the matrix. Propylene/propane selectivity goes through a maximum, from 1.5 to 2.2, which falls in the temperature region of the liquid crystalline phase of pure 8CB. This indicates that the introduction of 8CB can enhance the interactions of PSf with polar gases. At temperatures above the glass transition of the 8CB/PSf blend, increases in segmental mobility of the polymer matrix and 8CB resulted in a dramatic increase of propylene permeability (253 barrer) and a decrease in selectivity (1.1). Crossing the T_g of 35_8CB resulted in large morphological changes of the polymer blend, which was confirmed from DSC results showing large increases in ΔC_p values with increasing 8CB content.

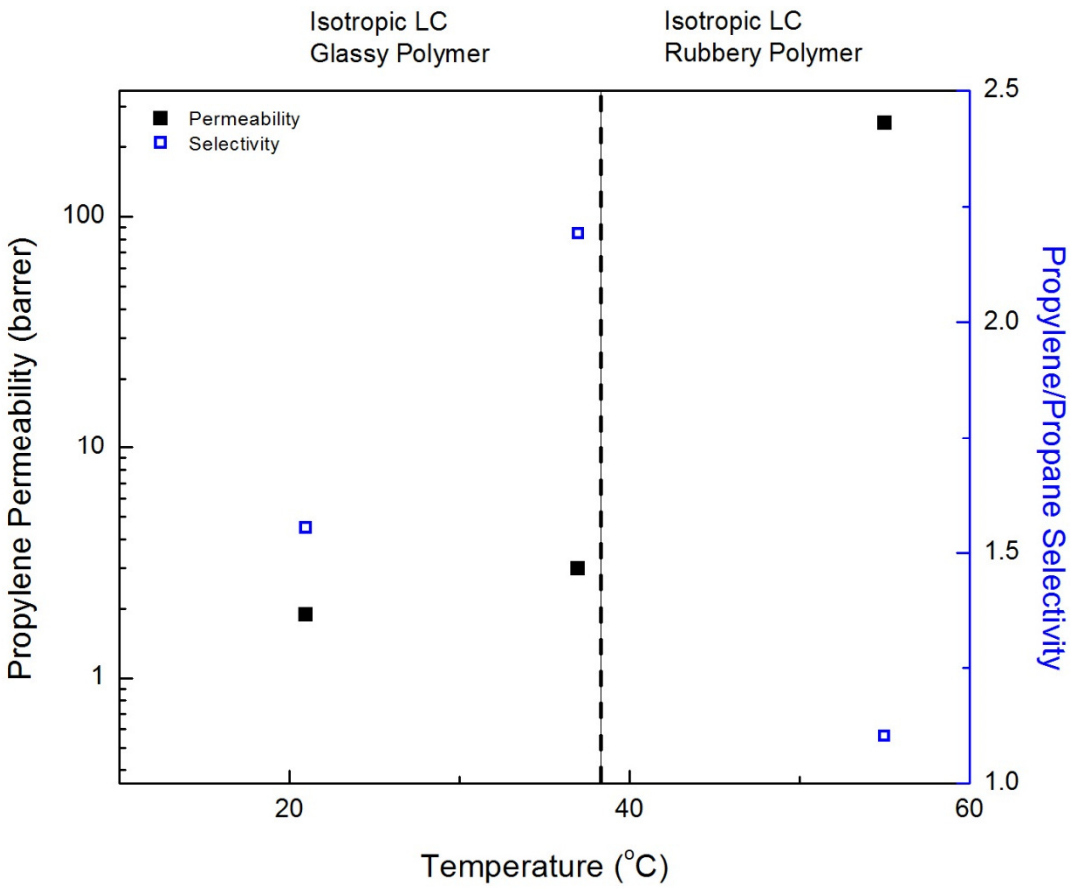

Figure 4.13: Temperature dependent permeability and selectivity for 35_8CB membrane

Figure 4.14 shows the permeability and selectivity values for a 55_8CB membrane at different temperatures. Smectic LC domains within the PSf/8CB blend in the glassy state resulted in the highest selectivity and permeability. In the nematic state the permeability increased to 4.0 barrers and the selectivity decreased to 5.5. The decreased selectivity of propylene over propane is attributed to a decrease in the LC mesogenic ordering from the smectic to the nematic LC phase. The glass transition temperature of the PSf/8CB blend and the isotropization of LC domains both occur at ~38 °C. Crossing this transition resulted in a large increase in permeability (443 barrer at 55 °C) and a reduction in selectivity (4.2 at 55 °C). This behavior is similar to that observed for the 35_8CB membrane. At 55 °C, 55_8CB and 33_8CB have a rubbery polymer matrix with a constant 8CB/PSf ratio. At these conditions, the permeability selectivity of the 55_8CB membrane (4.2) was significantly higher than the 35_8CB membrane (1.1). This indicates that the LC domains, regardless of ordering, also enhance the selectivity of propylene over propane.

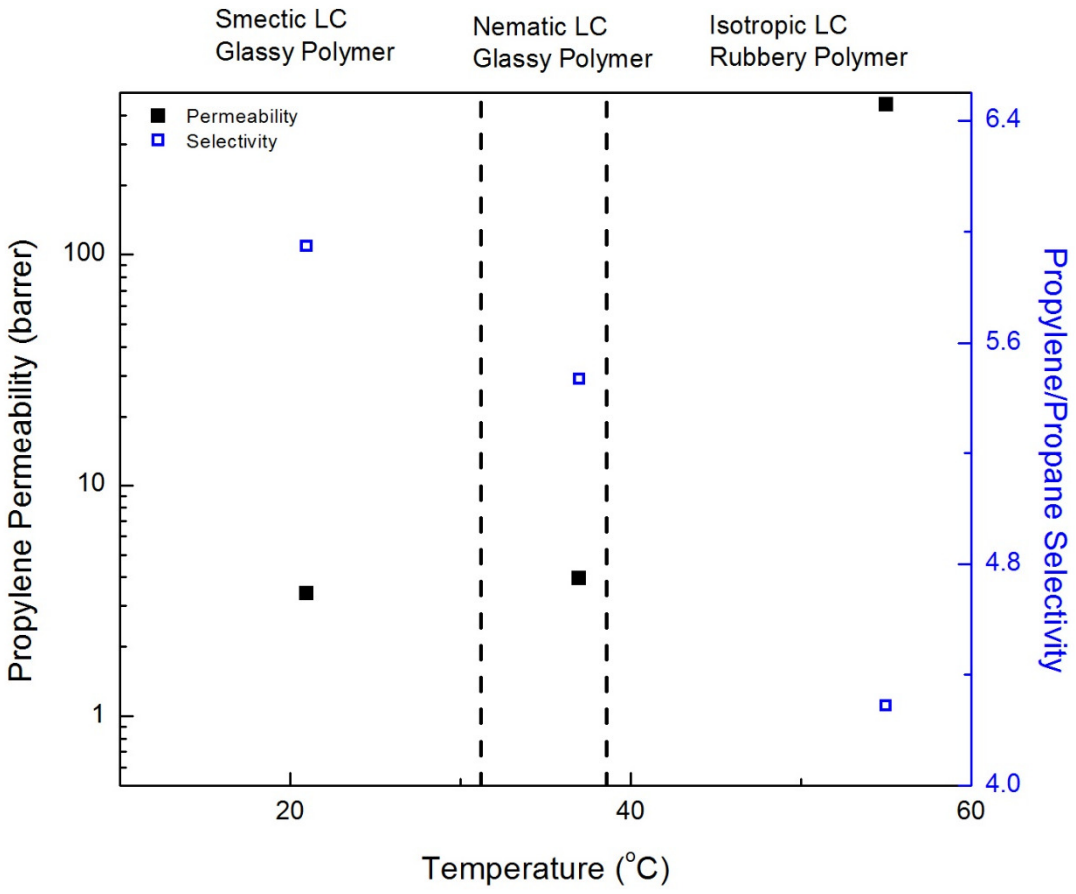

Figure 4.14: Temperature dependent permeability and selectivity for 55_8CB membrane

Figure 4.15 reports propane permeability values of membranes 35_8CB and 55_8CB at several temperatures. Although total propane and propylene permeability is highest for 55_8CB, propane permeability is consistently lower for 55_8CB. The addition of LC material enhanced the interactions of propylene with the membrane which led to the depression of propane permeability. This behavior is also confirmed from an increase of mixed gas permeability selectivities from ideal sorption and diffusion selectivities.

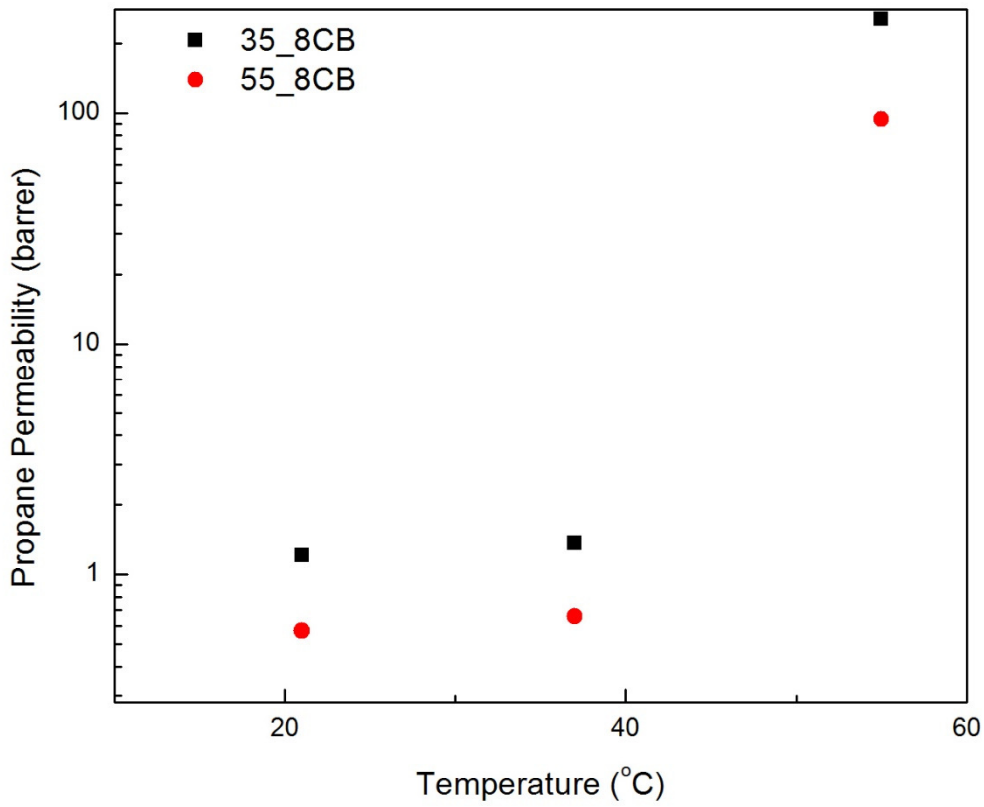

Figure 4.15: Temperature dependent propane permeability for 8CB/PSf membranes

4.5 Conclusions

A solvent induced phase separation technique combined with a thermally induced phase separation technique was used to fabricate polymer dispersed liquid crystal membranes using polysulfone and 8CB. LC domains with smectic/nematic and nematic/isotropic phase transitions occur for 55wt% 8CB in PSf (55_8CB). 55_8CB had a narrow pore size distribution, homogeneous dispersion and a regular spherical pore shapes without interconnections. Sorption of propane and propylene in 8CB decreased across the nematic/isotropic transition indicated the orientation of the LC material in the nematic phase has a higher affinity to rod-like gases. Single gas diffusion studies showed an increase in diffusion selectivity across the isotropic/nematic transition. The presence of propylene depressed the gas transport

of propane and led to an increase in selectivity for propylene over propane. An increase of both permeability and selectivity was observed for membranes with smectic and nematic phases. A temperature increase for 35_8CB membrane with a glassy polysulfone/8CB matrix resulted in higher permeability and selectivity. Lower selectivities were observed for permeation through a rubbery 8CB/PSf matrix. The amount of phase separated LC content, irrespective of ordering, also enhances interactions of propylene over propane.

Chapter 5: Gas Transport of Side-Chain Liquid Crystal Polymers

5.1 Abstract

A cyanobiphenyl based side-chain liquid crystal polymer (LCP) with a polybutadiene diol backbone was synthesized, and its gas transport properties were studied. The linear LCP, with comb-like attached mesogens, exhibited a stable liquid crystal smectic mesophase. The LCP was impregnated in a porous PTFE support for gas transport studies. Diffusion dominated transport was observed in the glassy state, and a selectivity of approximately 30 was observed for He/CH_4. Gas transport in the smectic phase was solubility dominated. Mesogenic mobility increased with an increase in temperature, and the segmental motional of the mesogenic units facilitated the solubility of propylene resulting in a solubility selectivity that also increased with temperature. As a result, the permeability selectivity had a local maxima in the smectic phase near the isotropic transition. In addition, permeability increased with temperature. Selectivity diminished when the clearing point temperature was exceeded. Increasing the feed pressure enhanced propylene selectivity by increasing propylene solubility and decreasing propane solubility. Mixed gas permeability measurements had slightly higher selectivities than single gas experiments due to preferential interactions of the LCP with the polar propylene molecules. LCP single gas sorption experiments agreed well with the results of membrane permeability and selectivity studies.

5.2 Introduction

Liquid crystal polymers (LCPs) are classified into two categories: main chain LCPs (MCLCPs) and side chain LCP (SCLCPs). MCLCPs incorporate the mesogenic unit in the polymer backbone, while SCLCPs incorporate the mesogenic unit laterally attached to the polymer.[43] Decoupling the motion of the mesogenic unit from the flexible polymer backbone is necessary to attain liquid crystal behavior; long alkane chains are used for this purpose.[90] This gives the liquid crystal mobility to form independent phases (crystalline, nematic, smectic, isotropic). Prior studies have focused on the improved mechanical properties and optical anisotropy for polymer processing, light modulators, photonic, ferroelectric and anti-ferroelectric applications.[16, 21-24] In contrast research focused on understanding the mechanism and performance of LCPs in gas transport applications has been limited.[67-70, 72] In this chapter, the transport

properties of several light gases and propane and propylene for a cyanobiphenyl based side-chain LCP based on a polybutadiene diol backbone will be investigated.

5.3 Experimental

Differential Scanning Calorimetry (DSC) measurements were performed using a Perkin Elmer DSC-2 instrument. The sample was cooled to 0 ^{o}C and heated at a rate of 5 ^{o}C/min until the isotropic transition temperature was passed. Equilibrium times were 20 minutes. Several cycles of heating and cooling were performed to ensure no hysteresis was present in the sample. Polarized Optical Microscopy (POM) using an Olympus BX51 optical microscope equipped with a Linkam LTS 350 hot stage and a Linkam TMS 94 temperature programmer was used to investigate the temperature dependent phase transitions of the PLC. Field Emission Scanning Electron Microscopy (FE-SEM) was utilized to qualitatively analyze the BDPLC impregnation efficiency in the 0.2 um, PTFE, porous support. A freeze fracture technique using liquid nitrogen was used to investigate the cross-section of the membranes. Sorption measurements were performed using an Intelligent Gravimetric Analyzer (IGA). Single sorption isothermal runs of both propane and propylene in the smectic phase were measured. Prior to progressing to another gas or temperature, the system was degassed for several hours. The weight change, accounting for buoyancy, was recorded and the concentration of sorbed penetrant gas was calculated. A constant volume/variable pressure and constant pressure/variable volume apparatus was used for single and mixed gas permeability measurements, respectively. A Shimadzu GC-2014 with a Restek Rt-Alumina PLOT column and an automated 6-port valve were used to separate and measure the concentration of membrane permeate stream (propane and propylene). LabView was employed in order to measure, control, and record all instrument activity and parameter values. 300 MHz NMR was used with $CDCl_3$ to quantify grafting densities and ensure proper synthesis and purification.

5.4 Synthesis

A liquid-crystalline thiol containing a 4-cyanobiphenyl as the mesogen and a mercapto-terminated hexamethylene spacer (monomer TH1) was prepared for grafting onto OH-terminated polybutadiene-

diols. The detailed synthetic procedure and characterization of the monomer has been previously reported.[91]

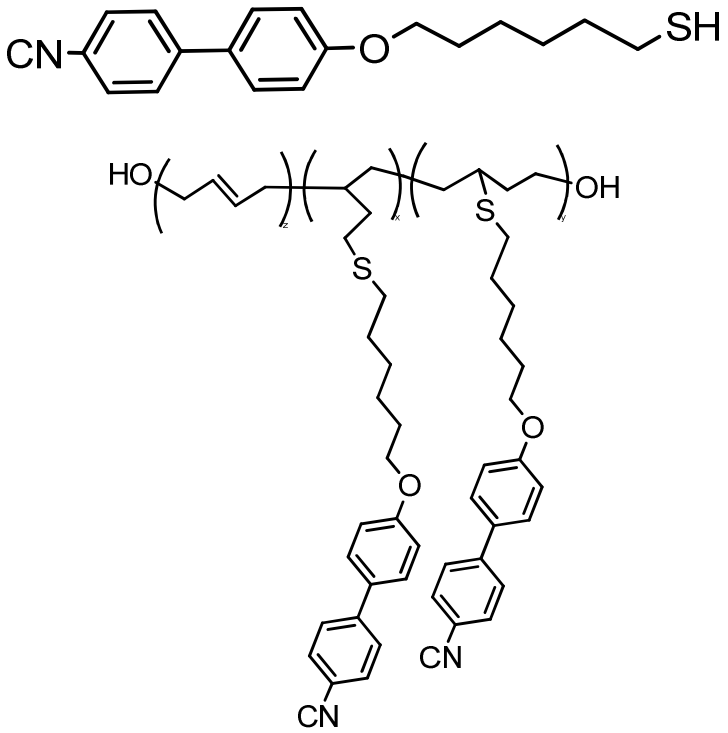

Figure 5.1: Liquid crystal thiol (TH1) (top). Liquid crystal thiol grafted onto a polybutadiene-diol (bottom).

A radical addition process was used to graft TH1 onto the double bonds of the telechelic poly(butadiene)diol (commercially available as Krasol LBH 3 000, M_n = 2,800 g/mol, M_w/M_n = 1.1, 65 mol.% of 1,2- and 35 mol.% of 1,4-butadiene units, content of hydroxyl groups of 2.0 per one polymer chain).

Molecular weights and molecular weight distributions of the LCP were estimated using size exclusion chromatography (SEC) (M_n = 17 990 g/mol, M_w/M_n = 1.34) and right angle light scattering (RALS) (M_n ~ 17 970 g/mol, M_w/M_n = 1.61). The structure of the grafted poly(butadiene)diol was confirmed by ^{1}H NMR spectroscopy. Using this method, the amount of mesogenic side-chains grafted (R_e) was calculated to be 88 mol.%. The pendant vinyl 1,2-units were completely modified by the radical addition.

5.5 Results and Discussion

5.5.1 LCP Characterization and Impregnation in a Porous Support

The thermal behavior of TH1 was determined by differential scanning calorimetry (DSC.) On the heating run, only one peak corresponding to melting of a liquid-crystalline smectic A phase was observed (T = 76.2 °C, ΔH = 2.36 J/g). The peak position was confirmed on cooling (T = 75.3 °C, ΔH = -2.25 J/g).

The thermal behavior of the LCP was also determined by DSC, although the glass temperature transition could not be detected under the experimental conditions. The thermal behavior of the LCP at several lower grafting densities was reported.[91] A simple extrapolation of T_g vs R_e data estimated the T_g at approximately 23 °C On heating and cooling, only one peak corresponding to a smectic/isotropic transition at T = 86.14 °C (ΔH = 3.92 J/g) and T = 80.93 °C(ΔH = -7.30 J/g) was observed, respectively.

Polarized optical microscopy (POM) was used to confirm the liquid crystal morphology. Figure 5.2 shows cross-polarized images of the LCP at 21 °C and 70 °C. At 21 °C the LCP exhibited a glassy smectic phase, which can be identified by the schlieren texture with s = ±1. 70 °C POM images show the BDPLC in a smectic mesophase. The clearing point during the heating run was approximately 85 °C.

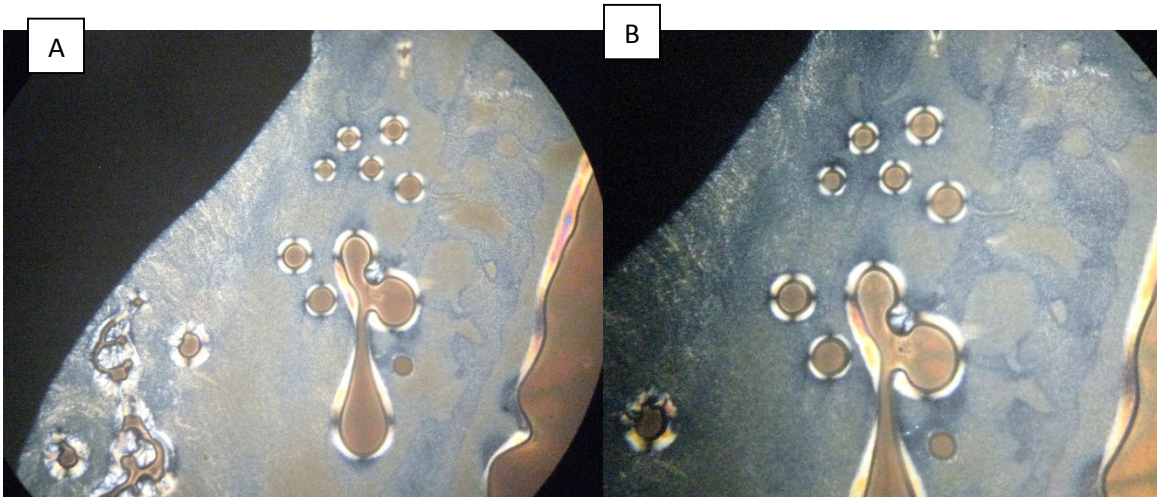

Figure 5.2: Glassy smectic LC under POM, 21 °C (A) and smectic, 70 °C (B)

Several techniques were attempted to fabricate a stable membrane that was free of pinholes or imperfections. The most effective way to obtain a stable film was to impregnate the liquid crystal polymers in a porous support. The LCP was dissolved in THF at 5 wt% and sonicated for 30 minutes. The solution was then poured onto a Teflon surface, into which the PTFE 0.2um support was immersed. The solvent was allowed to slowly evaporate overnight and the membrane was then placed in a vacuum oven above the isotropic transition temperature for thermal annealing and solvent removal.

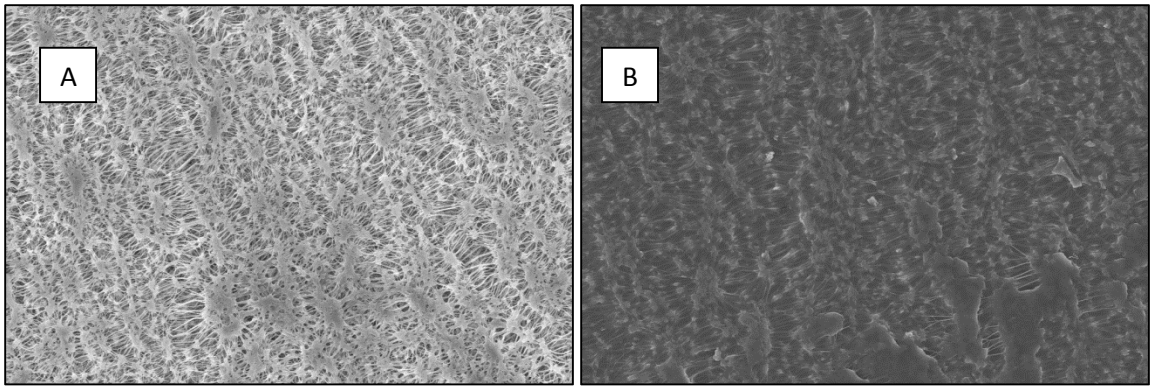

Figure 5.3: SEM images of support with and without BDPLC. Blank 0.2 um PTFE unlaminated support (A); PTFE support impregnated with BDPLC (B).

SEM images were taken of the cross-section of the blanked PTFE support and LC impregnated support (Figure 5.3.) Figure 5.3a shows the cross-section of the blank PTFE support with an average pore diameter of 0.2 um. After LCP impregnation, a homogenous membrane with no pinholes was created, shown in Figure 5.3b. During room temperature runs, the membrane was extremely robust, being able to routinely withstand a pressure of up to 6 bar. As the temperature approached the isotropic phase transition, membrane stability became an issue. Polymer viscosity decreased, due to the phase change, and pinholes were formed. Gas transport data in the isotropic state could only be obtained at a pressure of 1.5 atm. Due to the presence of the porous support, it was necessary to have a membrane thickness of 120 um.

5.5.2 Propane and Propylene Single Gas Sorption

Figure 5.4 and 5.5 contain propane and propylene single gas sorption isotherms for the pure PLC. The measurements were performed in the liquid crystalline phase at temperatures of 35 ^{o}C and 50 ^{o}C. Propane and propylene sorption increased with increasing pressure for both temperatures. In addition, an increase in propylene/propane sorption selectivity with increasing pressure is observed for both temperatures. In the 35 ^{o}C runs, the sorption selectivity increased from 0.9 at 250 mbar to 1.7 at 5000 mbar. At 50 ^{o}C, selectivities increased from 1.3 to 2.1. Propane sorption remained relatively constant between 35 ^{o}C and 50 ^{o}C. In contrast, propylene sorption increased with an increase in temperature resulting in a higher sorption selectivity at a higher temperatures in the LC phase.

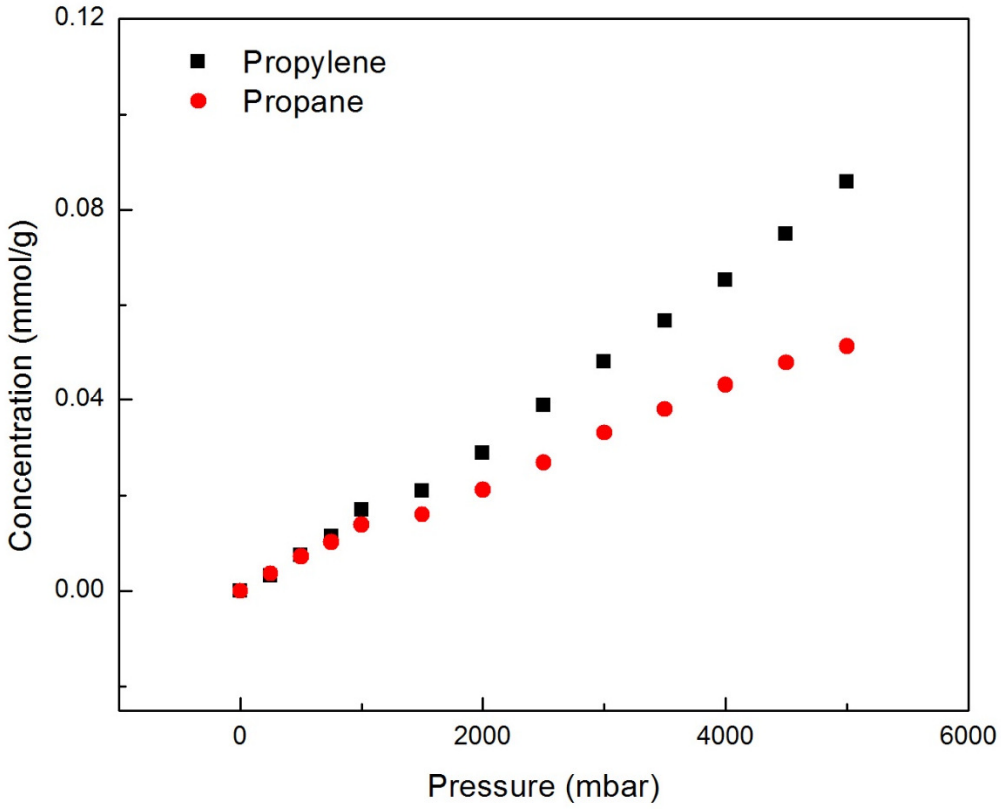

Figure 5.4: Propane and propylene sorption with BDLC in the smectic mesophase at 30 °C

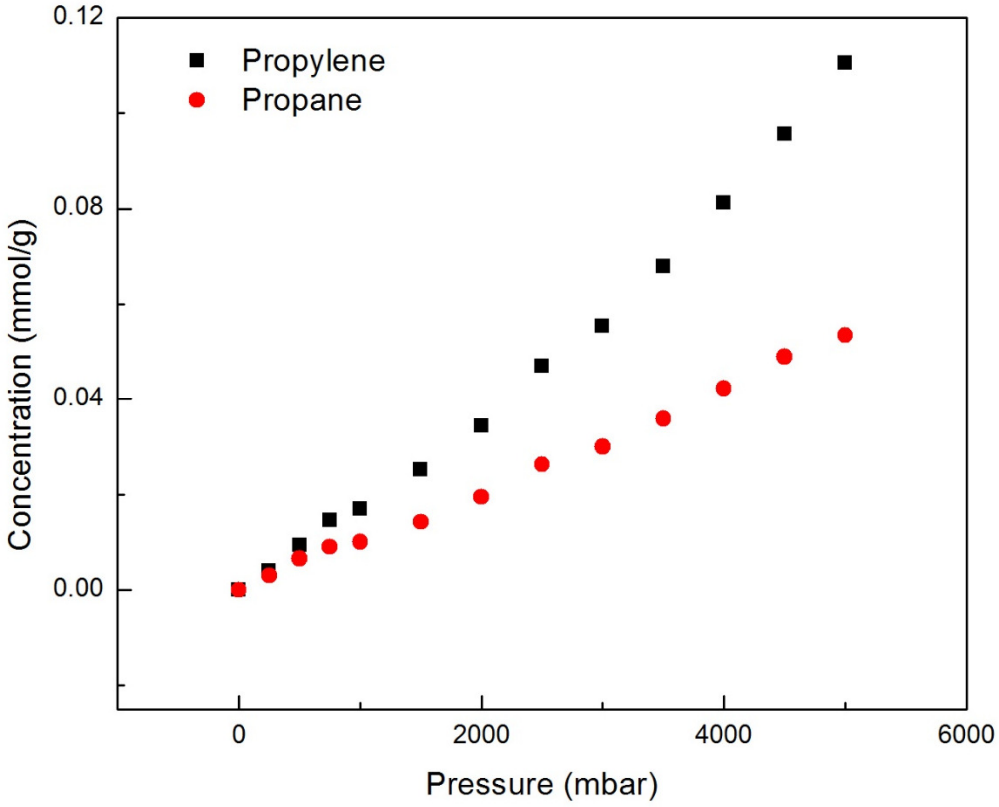

Figure 5.5: Propane and propylene sorption with BDLC in the smectic mesophase at 50 °C

5.5.3 Light Gas Permeability at Room Temperature

Permeability tests were performed at room temperature for He, O_2, N_2, and CH_4. Figure 5.6 depicts the size dependent transport of the glassy PLC membrane at 21 °C. Permeability was highest for helium gas, which has the smallest kinetic diameter of 2.6 Å. This resulted in a He/CH_4 selectivity of 30. Permeability decreased with increasing kinetic diameter. This indicates that for light gas transport in the PLC membrane glassy state, gas transport is dominated by diffusion.

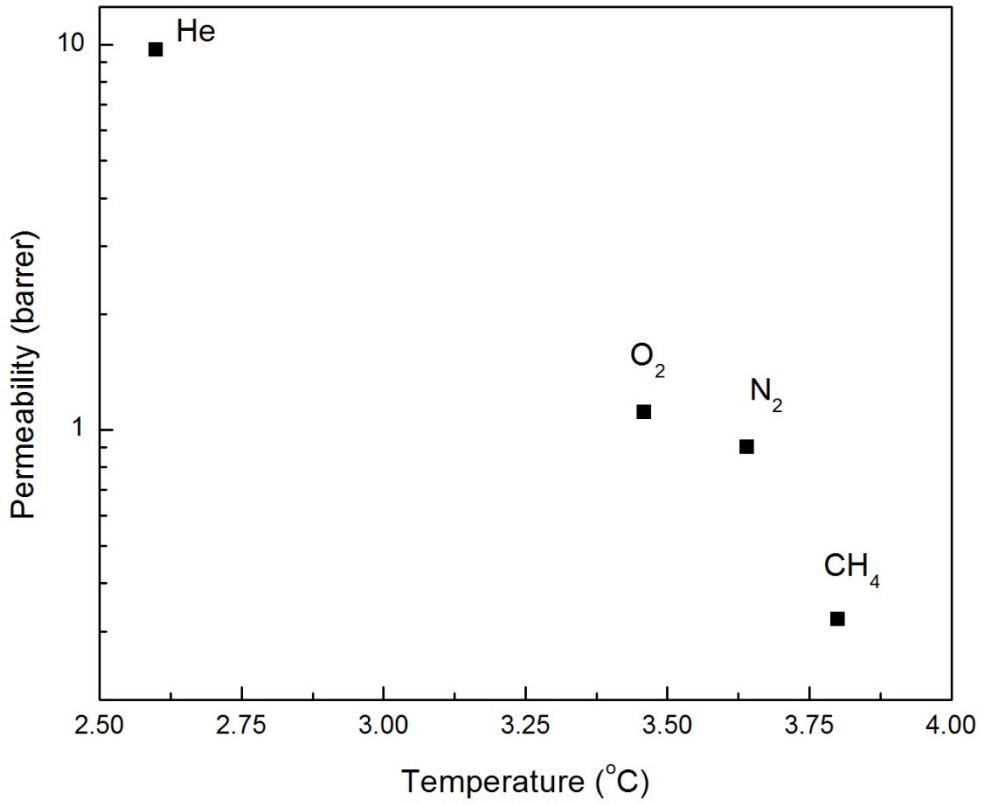

Figure 5.6: Permeability vs Kinetic Diameter of PBDLC at 21 °C

Table 5.1: Summary of permeability data obtained at 21 °C

Gas	Kinetic Diameter (Å)	Permeability (barrer)	He relative selectivity
He	2.60	9.7	1
O_2	3.46	1.1	8.7
N_2	3.64	0.9	10.8
CH_4	3.80	0.3	30.1

5.5.4 Effect of Pressure and Temperature on Permeability, Solubility and Diffusion

Single gas permeability experiments of propane and propylene were conducted in three the glassy, smectic, and isotropic phases. Figure 5.7 contains data for propylene permeability and propylene/propane permeability selectivity at a feed pressures of 1.5 atm. A selectivity of about 1.9 was observed at the glassy-smectic phase. Permeability was lowest at this temperature. At lower temperatures in the LC state, an initial decrease in selectivity, to 1.2, was observed. Permeability and selectivity increased with increasing temperature in the LC phase. This agrees with the sorption data asthe sorption of propylene increased with increasing temperatures while the sorption of propane remained relatively constant. In the isotropic state, selectivity decreased with increasing temperature. Figure 5.8 contains propylene permeability and selectivity data at a feed pressure of 6 atm. Similar trends were found at the higher feed pressure. An increase of propylene permeability and selectivity was observed with increasing temperatures in both the glassy smectic and smectic phases.. A selectivity of about 3.0 was observed in the glassy-smectic phase. The highest selectivity of 3.4 was found at temperatures close to the smectic/isotropic transition.

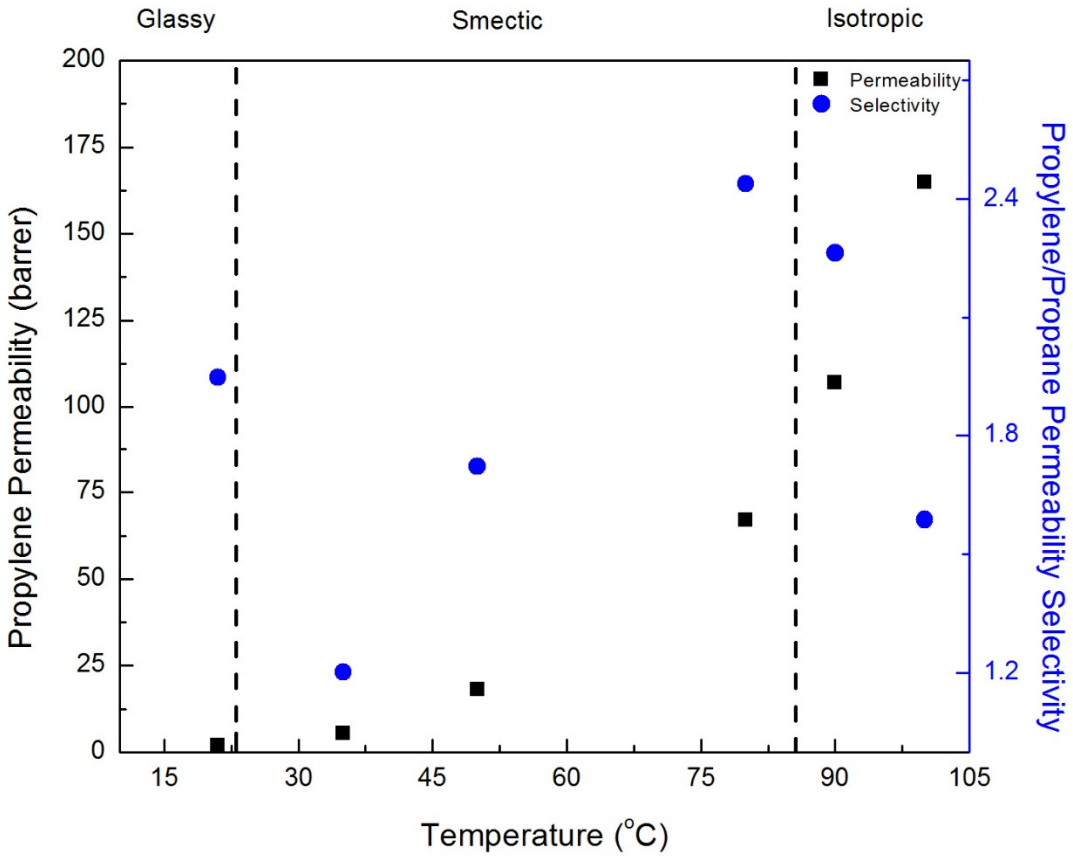

Figure 5.7: Permeability and permeability selectivity at 1.5 atm.

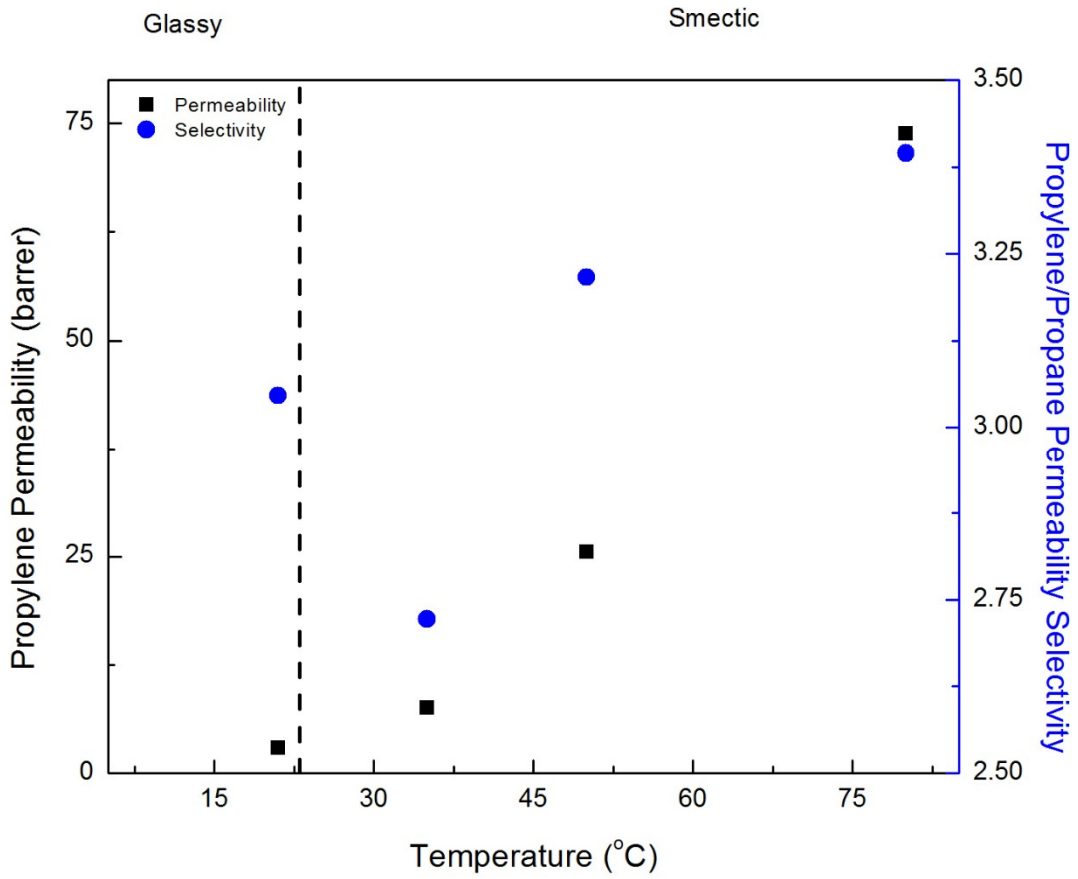

Figure 5.8: Permeability and permeability selectivity at 6.0 atm.

Figure 5.9 contains propylene diffusion and propylene/propane diffusion selectivity. For the smectic and isotropic phase, an increase in propylene diffusion was observed with increasing temperature. The lowest diffusion and the highest diffusion selectivity for propylene was found in the glassy state. The macroscopic mobility of the polymer backbone is lowest at temperatures in the glassy state. In addition, the LC mesogens are 'frozen' due to steric hindrance with the polymer backbone. This results in a stronger size discrimination between propane and propylene.[92] A large decrease in diffusion selectivity was present when crossing the glass transition temperature. This correlated well to permeability selectivity data. Furthermore, within all phases, diffusion selectivity decreased with increasing temperature. The isotropic state exhibited a selectivity of about 1. The temperature and phase change increased the molecular mobility of the polymer and diminished the ordering of the mesogen, which reduced gas diffusion selectivity.[93-94] Figure 5.10 contains diffusion and diffusion selectivity data obtained at a feed pressure of 6 atm. The magnitude of the diffusivities of propylene and propane showed no correlation with the feed pressure. Larger diffusion selectivities were also present at

temperatures below the T_g. In addition, gas diffusion increased and diffusion selectivity decreased with increasing temperature.

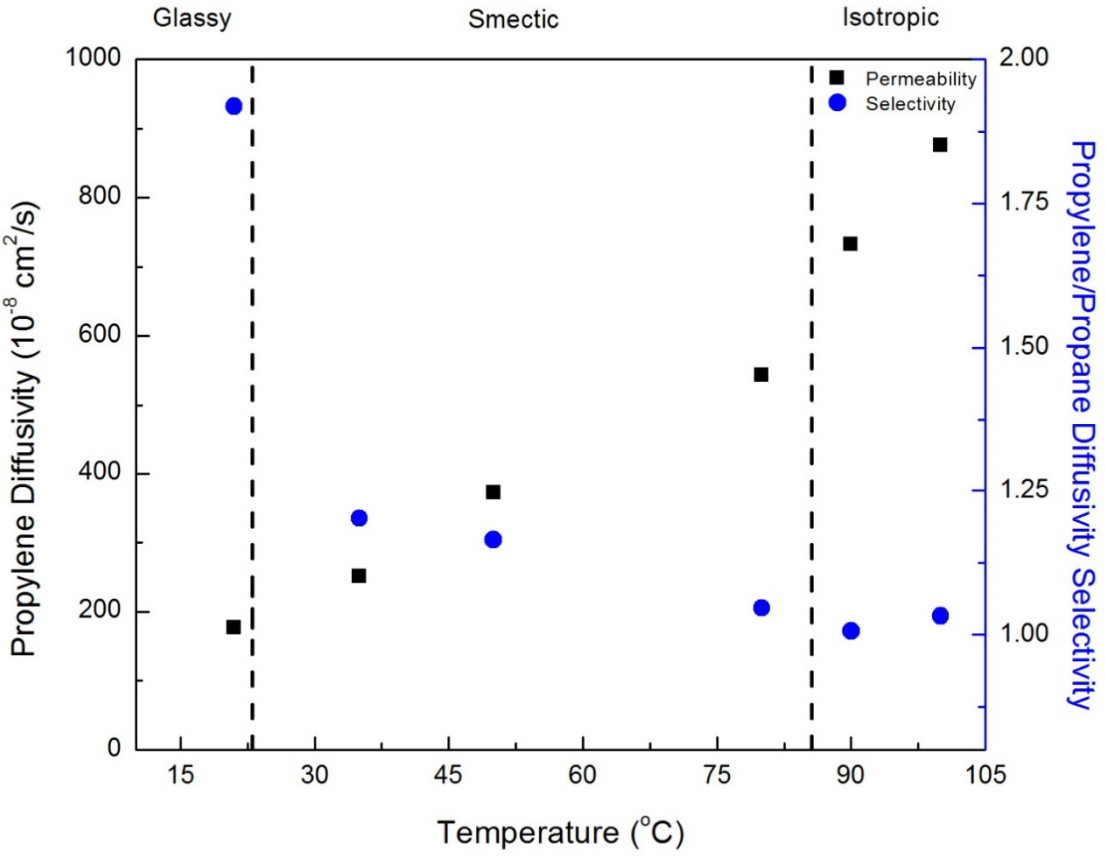

Figure 5.9: Diffusion and diffusion selectivity at 1.5 atm

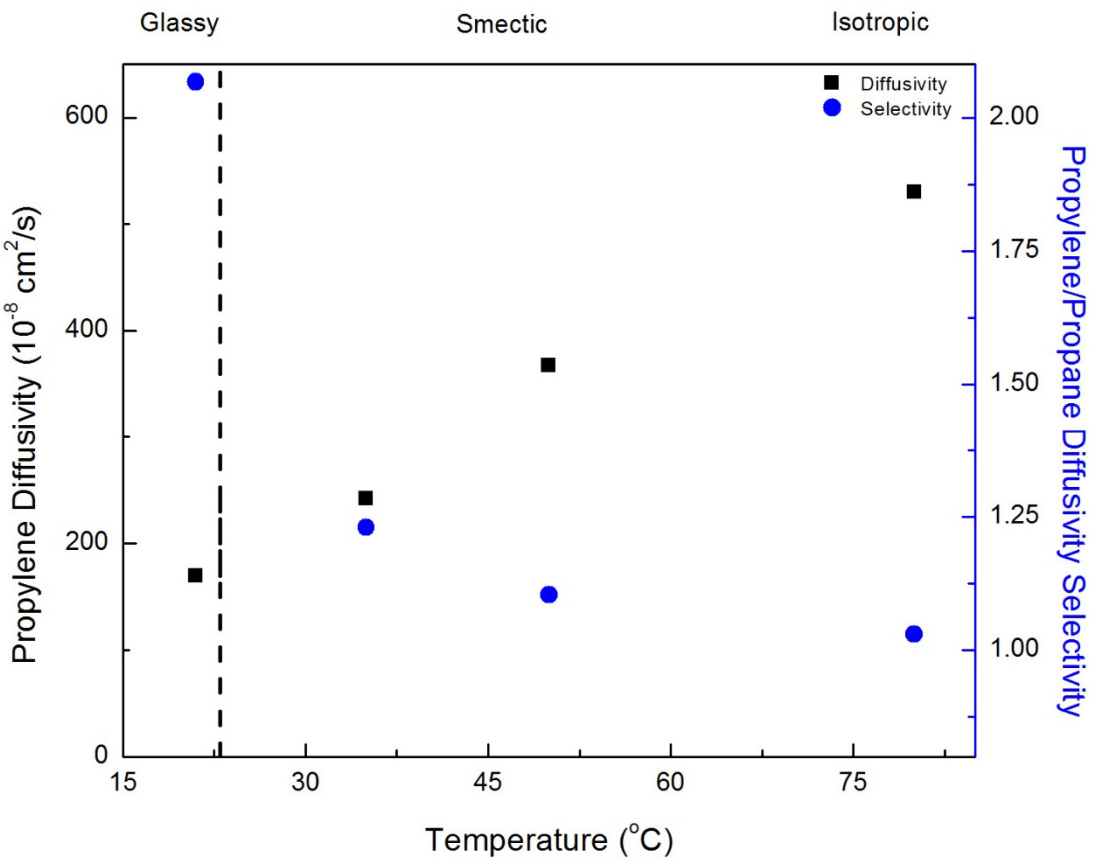

Figure 5.10: Diffusion and diffusion selectivity at 6.0 atm

Figure 5.11 contains solubility and solubility selectivity data for propane and propylene in the LCP membrane calculated from the permeability and diffusivity data. Data was collected for several temperatures at a feed pressure of 1.5 atm. The gas solubilities were lowest in the glassy state. Solubility approximately doubled to 0.017 mmol/g when crossing the glass transition temperature. Propylene solubility increased with increasing temperature across all phases. In addition, solubility selectivity increased with increasing temperature in the LC state. This trend correlates well with permeability selectivity results. The increase in permeability selectivity with temperature is due to an increase in solubility selectivity. Solubility of gases occurs between the polymer backbone and ordered mesogenic side-chains. The segmental motional of the mesogenic units are frozen at temperatures below the T_g and consequently are considered as barriers for the gases. For temperatures above the T_g, the polymer chains are free to move which also results in an increase in mesogen mobility. Thus, permeability increases with temperature, but the highest selectivity occurs at temperatures approaching the T_g.[69-70, 72] In this particular case, the glass transition was not detectable using DSC, suggesting that there is little

morphological change between the glassy and rubbery polymer and no significant increase in mesogenic mobility across the putative glass transition.

It is interesting to note that propylene solubility increases continuously across the isotropic transition temperature, while a slight decrease in selectivity is observed. This indicates that the solubility depression of gases by the liquid crystal order and mesogen immobility is more significant for propane than propylene. Therefore, propylene/propane solubility selectivity decreased above the isotropic transition and continued to decrease with increasing temperature. Propylene solubility increased at feed pressures of 6 atm, which can be seen in Figure 5.12. An increase in solubility selectivity was observed at higher pressures. These results agree with the sorption isotherms, which exhibited an increase in sorption selectivity with an increase in temperature and pressure.

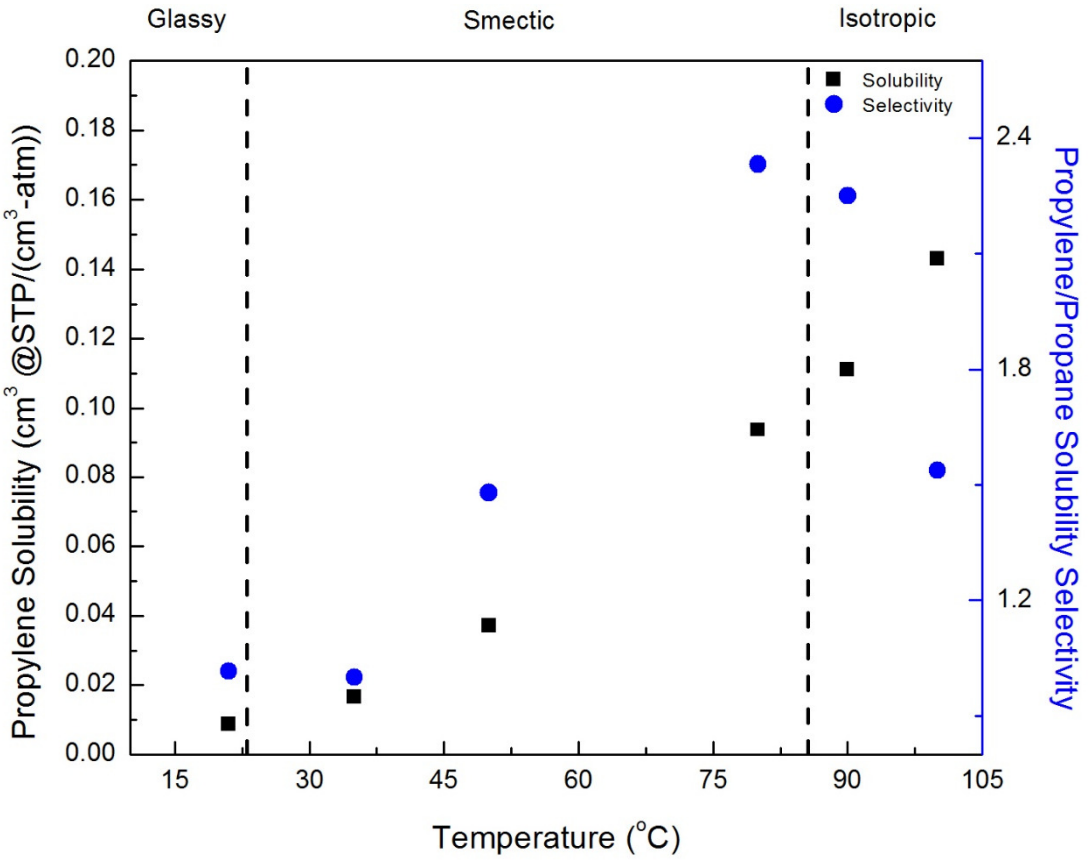

Figure 5.11: Solubilities and solubility selectivities at 1.5 atm

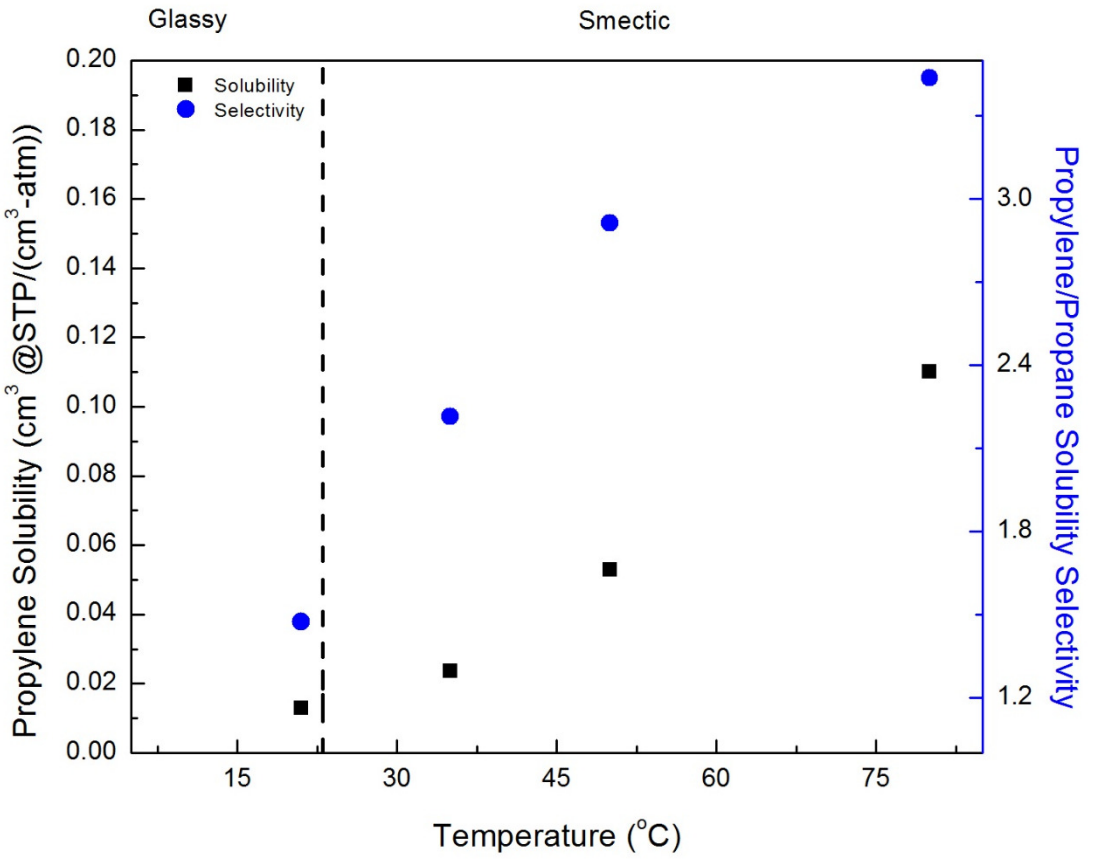

Figure 5.12: Solubilities and solubility selectivities at 6.0 atm

5.5.5 Propane and Propylene Mixed Gas Permeation

Mixed gas permeation measurements were performed with a 50/50 gas mixture of propane and propylene. The feed pressure was 3 atm and a steady-state flow rate of 20 sccm was used. Permeate pressure was held at 1.1 atm (helium). For gas transport in the glassy state, propylene and propane permeabilities decreased slightly, compared to single gas runs at a feed pressure of 1.5 atm. The solubility of both components were depressed by the presence of the second one. This behavior is commonly found in glassy polymers.[95] This resulted in the mixed gas selectivity increasing to 2.2. Mixed gas permeation of propylene at 40 °C in the smectic phase were higher than single gas permeation. In addition, propane permeabilities decreased. Selectivity of mixed gas transport increased to 2.6 (propylene/propane) at 40 °C. The LCP competitively permeated propylene over propane indicating preferential interactions with a more polar compound.

Table 5.2: Propylene and propane mixed gas permeabilities

Temperature (°C)	Propylene (barrer)	Propane (barrer)	Selectivity
21	1.9	0.9	2.2
40	12.3	4.8	2.6

5.6 Conclusions

The gas transport properties of a cyanobiphenyl liquid crystal attached to a polybutadiene backbone via a flexible alkane spacer were investigated. LCP gas diffusion selectivity is dominated by the mobility of the polymer backbone. The highest diffusion selectivities were observed below the glass transition temperature. The smectic mesophase exhibited an increase in diffusivity and a decrease in diffusion selectivity with increasing temperature. Permeability selectivity in the smectic phase was dominated by the solubility differences of propane and propylene in the LCP, which lead to an increase in permeability and permeability selectivity with increasing temperature. Gas solubilities were depressed due to the polymer main chain restricting side-chain LC mobility. As the temperature increase within the LC phase the segmental motion of the LC mesogenes increased resulting in larger solubility differences between propane and propylene. This agreed well with gas sorption isotherms. Mixed gas permeability measurements showed an increase in selectivity below and above the T_g, indicating competitive sorption between propylene and propane.

A large excess of LC monomer was needed to obtain an LCP with grafting densities higher than 0.60, making it difficult to control the final LC content. In addition, the LCP membrane stability was an issue at higher temperatures in the LC phase and in the isotropic phase, and attempts to crosslink the material were unsuccessful. There were incentives to derive a simple synthetic scheme for which the LCP crosslinker density, mesogen structure, mesogen content and phase behavior can be relatively easily altered without changing the fundamental chemistry of process. As a result, a new system consisting of cyanobiphenyl or nitroazobenzene meth(acrylate) mesogens were synthesized and polymerized with 2-ethylehexyl acrylate and ethylene glycol dimethacrylate to produce stable, cross-linked LCP membanes. Details of this work is presented in Chapters 7 and 8.

Chapter 6: Dynamic Mechanical and Thermal Behavior of Novel Liquid-Crystalline Polybutadiene-Diols with Azobenzene Groups in Side Chains

6.1 Abstract

Liquid-crystalline (LC) polymers containing methoxy- or butoxy-substituted azobenzene in side chains have been prepared via radical addition of the in advance synthesized nematic thiols onto double bonds of poly(butadiene)diol.[22] In the present work, thermal behavior of these comb-like polymers has been characterized by differential scanning calorimetry and polarizing optical microscopy. LC transitions have been also determined by rheological measurement. Time-temperature superposition of mechanical functions has been successfully applied to samples undergoing direct nematic/glassy state transition.

6.2 Introduction

In the last few decades, thermotropic liquid-crystalline polymer (LCP) materials are attracting great attention, especially due to their unique potential in the field of technical applications. From LCPs, processable films could be made for photonic, ferroelectric and antiferroelectric applications and second harmonic generation in non-linear optics.[96-98] LCPs usually consist of a polymer backbone and a mesogenic group. Mesogens can be bound on the polymer backbone (side chain LCPs) or can be incorporated directly in the polymer backbone (main chain LCPs). To synthesize a thermotropic side chain LCP, the designed molecule should obey special rules. The polymer backbone needs to be relatively flexible with a suitable glass transition temperature, T_g. Incorporation of the mesogenic units onto the polymer should not result in T_g greater than LC transition temperatures. To enable rigid mesogenic groups to form a mesophase, mesogens should be bound on the backbone through a flexible and sufficiently long spacer. Finkelmann *et al.* (1978) predicted that such spacer (usually consisted of more than 5 or 6 methylene units) contributes to effective decoupling of motions of mesogens involved in the ordered state from motions of the polymer segments. [99]

The polymer nature of the LCPs allows for application of rheological methods for characterization of these materials. Ilavsky *et al.* (1998), Hotta and Terentjev (2003), Colby and Gillmor (1993) and many others used rheological measurements for characterization of LCPs.[25, 100-101] It was found that both temperature and frequency dependences of mechanical functions are sensitive to a presence of ordered LC structure due to more or less aligned parts in the macromolecule. Upon certain circumstances, frequency dependences of mechanical functions can be superimposed to obtain information about the sample behavior at conditions that are not accessible by a simple measurement.

Structure of the thiols **MA** and **BA** are shown in Figure 6.1. Both possess a *para*-substituted azobenzene as a mesogenic core and a thiol-terminated pentamethylene spacer attached by an ether bond to the mesogen. The synthesized mesogenic thiols have been grafted onto double bonds of commercially available poly(butadiene)diol Krasol LBH 3 000 (PBD, Figure 6.1) with varying initial mole ratio of thiol/double bonds (from 0.2 to 1.0). After a purification process, the structure and composition of the resulted comb-like PBDs have been determined.

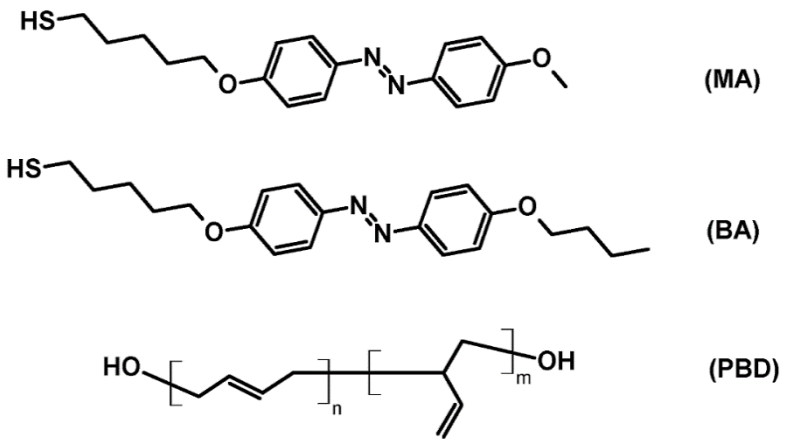

Figure 6.1: The structure of the synthesized liquid-crystalline thiols **MA** and **BA** and the poly(butadiene)diol (PBD) used for the grafting reactions of these thiols.

This present work is based on the detailed characterization of the thermal behavior of both the synthesized thiols and related comb-like PBDs with respect to a mesophase formation. For the thermal behavior investigation, differential scanning calorimetry and polarizing optical microscopy have been employed. Mechanical properties of the polymer samples (loss and storage moduli, loss tangent) have been determined using rheological measurements. Time-temperature superposition of the moduli and loss tangent has been successfully applied for some of these LC PBDs.

6.3 Methods of Measurements

6.3.1 Differential Scanning Calorimetry

Calorimetric measurements were performed using a Pyris 1 DSC (Perkin–Elmer). Purge gas (helium) was let through the DSC cell with a flow rate of 20 mL/min. The temperature of the equipment was calibrated with mercury, H_2O and indium. The melting heat of indium was used for calibrating the heat flow.

Samples of typical mass ca 10 mg were first heated from 30 °C to 130 °C at 40 °C/min, held at 130 °C for 5 min, then subjected to a cooling scan to -60 °C at 10 °C/min, held at -60 °C for 15 min, followed by a second heating scan to 130 °C at 10 °C/min. The reason, why the rate 10 °C/min was chosen, achieves in the nature of the poly(butadiene)-based polymers. As follows from our own experience, the higher heating/cooling rate, the better detectability of glass transition and mesophase transitions in these samples during DSC measurement.

6.3.2 Polarizing Optical Microscopy

The texture of crystalline and LC phases and phase transition temperatures were determined by a polarizing optical microscope (POM) Nikon Eclipse 80i equipped with a heating stage Linkam LTS350. The heating and cooling rate was 5 °C/min and 2 °C/min. These rates enabled us a better development of phase structures in grafted PBDs than the rate 10 °C/min used in DSC method.

6.3.3 Rheological Measurement

Dynamic mechanical measurements were performed on a Bohlin CVOR 200 instrument with the parallel-plate geometry. Diameter of the used plates was 6 mm (for modulus higher than 10^4 Pa), 15 mm (for modulus from 10^4 Pa to 10^7 Pa) and 25 mm (for modulus lower than 10^5 Pa). Both components of the complex shear modulus G^* ($G^* = G' + iG''$, where G' and G'' are the storage and loss modulus, respectively) and the loss tangent, tan $\delta = G''/G'$ were determined.

Preparation of all polymer samples (measured with various plate diameters) was carried out by the following procedure. The polymer powder was placed between plates of the rheometer and heated until the isotropic state of the sample was reached.

Two types of measurements were made: measurement of temperature dependence at constant frequency and isothermal frequency sweep. The temperature dependences of mechanical functions were

measured at a constant frequency *f* = 1 Hz during cooling at the rate 2 °C/min, the strain was kept within a linear region of viscoelastic behavior. Isothermal measurements (frequency dependencies) of mechanical functions were made during the cooling regime. Small-strain oscillatory shear measurements were performed in the frequency range from 0.05 to 50 Hz at several isotherms (between -15 °C and 100 °C, temperature range was dependent on the phase behavior of the sample, step of the temperature was 5 °C) and frequency dependences of the storage *G*′ and loss *G*″ moduli were measured at each temperature. The strain for those measurements was carried out within a linear viscoelastic regime; amplitude sweep (dependence of the modulus and strain on stress) was measured at several temperatures and frequencies to set the region of viscoelastic behavior. Using the frequency-temperature superposition data, the superimposed curves of reduced moduli $G'_p = G' \cdot b_T$, $G''_p = G'' \cdot b_T$ and loss tangent $\tan\delta_p = \tan\delta$ vs. reduced frequency $\omega \cdot a_T$ were obtained (where a_T is horizontal and b_T is vertical shift factor). The horizontal shift factor a_T was obtained from superposition of the loss tangent (for tan δ no vertical shift is necessary).

6.4 Results and Discusion

6.4.1 Thermal Behavior

DSC data for thiol **MA**, neat PBD and PBDs modified with thiol **MA** are summarized in Table 6.1. Two peaks in the DSC curves occurred in the neat thiol.

Table 6.1: DSC-data of the thiol **MA**, neat PBD and PBDs grafted by thiol **MA** (R_e – degree of modification, estimated from elemental analysis). Heating and cooling rate was 10 °C/min.

Sample	R_e	Run	T_g	Δc_p	T_{m1}	ΔH	T_{m2}	ΔH	T_{m3}	ΔH
			°C	J/g×°C	°C	J/g	°C	J/g	°C	J/g
PBD	0.00	H	-47.3	0.49	–	–	–	–	–	–
		C	-44.2	0.42	–	–	–	–	–	–
MA	–	H	–	–	88.0	90.7	110.0	2.9	–	–

		C	–	–	71.0	-83.1	108.0	-2.6	–	–
MA 0.2	0.21	H	-5.1	0.54	33.6	0.3	–	–	–	–
		C	-8.1	0.37	–	–	–	–	–	–
MA 0.4	0.30	H	7.2	0.56	39.1	1.1	–	–	–	–
		C	3.5	0.49	34.8	-0.7	–	–	–	–
MA 0.6	0.42	H	18.9	0.56	74.6	1.3	–	–	–	–
		C	19.0	0.77	73.1	-1.4	–	–	–	–
MA 0.8	0.57	H	[a]	[a]	35.7	5.2	63.1	-0.2	87.8	1.3
		C	[a]	[a]	27.5	[a]	34.8	[a]	86.9	-1.5
MA 1.0	0.55	H	[a]	[a]	62.5	-0.3	75.1	25.6	88.9	1.3
		C	[a]	[a]	47.0	-16.1	87.8	-1.7	–	–

[a] not determined

During heating, the first peak at ~ 88.0 °C is responsible for a transition from a crystalline phase to a mesophase, which resulted in a relatively high value of enthalpy (ΔH ~ 90.7 J/g). A POM image of this sample at 90 °C (heating regime 5 °C/min) is shown in Figure 6.2a. Inversion walls (grey field) with a Schlieren texture with disclinations of ± 0.5 (points with two arms) are typical for presence of a nematic phase. The homogenous black area corresponds to a place without sample. The nematic mesophase is stable up to 110.0 °C, which then begins to melt to an isotropic liquid (ΔH ~ 2.9 J/g). Position of this peak was confirmed by a cooling run (~ 108 °C, ΔH ~ -2.6 J/g), while the nematic-crystalline transition peak was slightly shifted (~ 71.0 °C, ΔH ~ 2.9 J/g), probably due to a supercooling process at the cooling rate (10 °C/min).

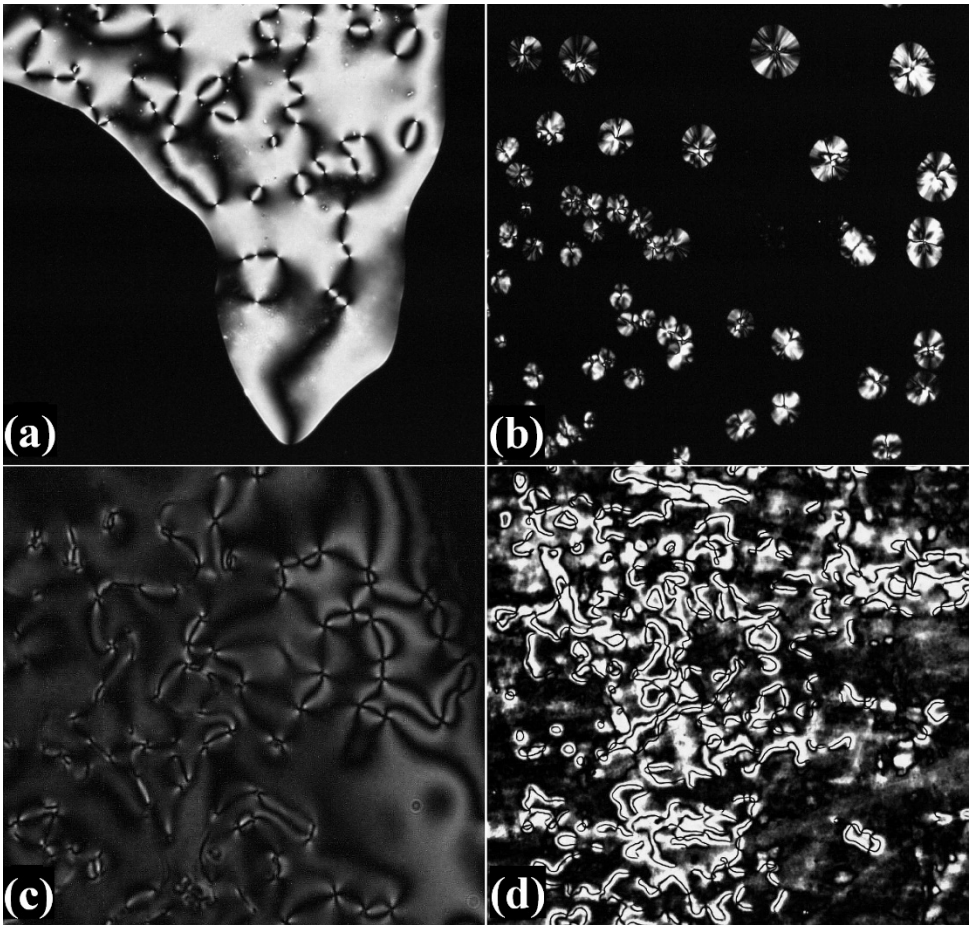

Figure 6.2: POM images of thiol **MA** (a, 90 °C, heating run) and related PBDs **MA 0.2** (b, 25 °C, cooling run), **MA 0.6** (c, 25 °C, cooling run) and **MA 0.8** (d, 72 °C, cooling run). Width of these pictures is 350 μm.

After grafting of thiol **MA** onto double bonds of PBDs, related comb-like polymers with varying amount of LC side chains (**MA 0.2** to **MA 1.0**) were obtained. DSC curves from cooling run for these polymers are shown in Figure 6.3a. Glass transition temperatures (T_g) of these structures and their Δc_p increase with increasing degree of modification, R_e (estimated from elemental analysis, see Tab. 1), namely from -47.3 °C and 0.49 J/g×°C (neat PBD) up to 18.9 °C and 0.56 J/g×°C (**MA 0.6**). In polymers with R_e > 0.42, glass transition was not detectable on DSC upon measurement conditions, probably due to overlapping with a crystallization process. During heating, a small peak connected with melting of a mesophase to an isotropic liquid occurred in each polymer sample (Tab. 1). Its temperature and enthalpy also increase with increasing amount of LC grafts, namely from 33.6 °C to 88.9 °C and from 0.3 J/g to 1.3 J/g, respectively. Position of this peak was confirmed during cooling runs, with the exception of sample **MA 0.2**. As follows from our observation under polarizing microscope (rate 2 °C/min), when cooling **MA 0.2** from an isotropic state, a mesophase can be not easily induced in the whole area of this sample,

probably due to lower content of mesogenic grafts (~ 21 mol%). Figure 6.2b shows a place with nematic droplets of **MA 0.2** (25 °C, cooling run) in the black field indicating the presence of an isotropic liquid. Presence of nematics was observed in each polymer sample in the related temperature range above T_g. Namely, **MA 0.6** exhibits a very well-developed Schlieren texture with disclinations of both ± 0.5 and ± 1.0 (Figure 6.2c, at 25 °C, cooling run, 5 °C/min). Disclination lines in **MA 0.8** can be seen as a typical thread-like texture (Figure 6.2d, 72 °C, cooling run, 5 °C/min). Comparing the temperatures and enthalpies of the Iso/N transition in both original low-molecular thiol **MA** (~ 108 °C, -2.6 J/g) and PBD with the highest degree of modification (~ 88 °C, -1.7 J/g) and of the N/Iso transition in the thiol **MA** (~ 110 °C, 2.9 J/g) and PBD **MA 1.0** (~ 89 °C, 1.3 J/g), we can conclude that LC properties of the *para*-methoxyazobenzene are still influenced by the presence of the poly(butadiene) backbone.

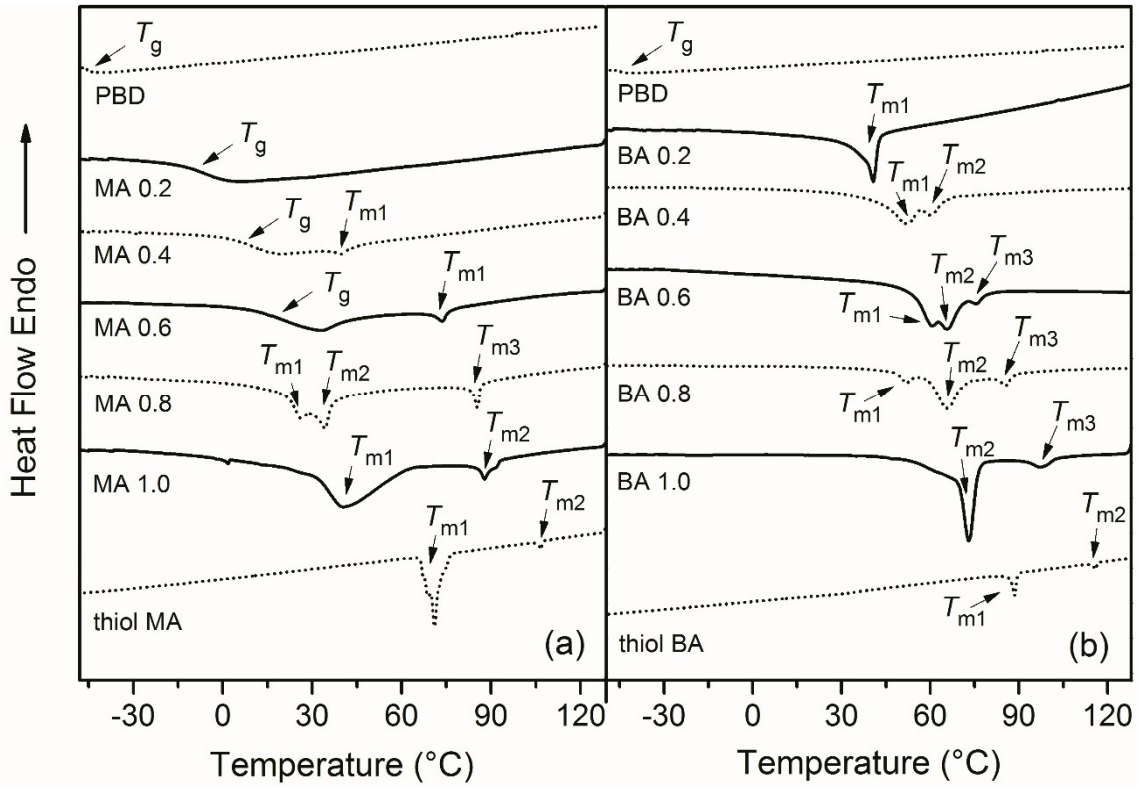

Figure 6.3 DSC curves for neat PBD and PBDs grafted with thiol **MA** (a) and with thiol **BA** (b). Data collected from cooling run, rate 10 °C/min.

Thermal behavior of the thiol **BA** (containing a butoxy group in the azobenzene *para*- position) differs significantly from the thiol **MA**. Tab. 2 summarizes results obtained by DSC for thiol **BA**. A sequence of several crystallization transitions, that was observed in a relatively broad temperature range (70–93 °C, heating run), resulted in a mesophase formation. An image of coexistence of this mesophase and a

crystalline structure at 97 °C (heating run, 5 °C/min) is shown in Figure 6.4a. A black background indicating homeotropic alignment of the rod-like molecules and a Schlieren texture with four arms can be observed in both the nematic and smectic mesophase. However, Figure 6.4b presents a different area of the sample where a rare marbled texture occurred, typical for the presence of nematics only. Hence, we concluded that thiol **BA** exhibits the presence of a nematic mesophase.

Table 6.2: DSC-data of the thiol BA, neat PBD and PBDs grafted by thiol BA (Re – degree of modification, calculated from elemental analysis). Heating and cooling rate was 10 °C/min.

Sample	R_e	Run	T_g	Δc_p	T_{m1}	ΔH	T_{m2}	ΔH	T_{m3}	ΔH	T_{m4}	ΔH
			°C	J/g×°C	°C	J/g	°C	J/g	°C	J/g	°C	J/g
PBD	0.00	H	-47.3	0.49	–	–	–	–	–	–	–	–
		C	-44.2	0.42	–	–	–	–	–	–	–	–
BA	–	H	–	–	72.0	14.5	82.0	17.0	93.0	36.3	116.0	3.4
		C	–	–	89.0	-36.5	115.0	-3.5	–	–	–	–
BA 0.2	0.22	H	[a]	[a]	55.6	16.2	–	–	–	–	–	–
		C	[a]	[a]	40.5	-15.5	–	–	–	–	–	–
BA 0.4	0.30	H	[a]	[a]	60.4	5.8	73.2	5.9	–	–	–	–
		C	[a]	[a]	53.7	[a]	62.8	[a]	–	–	–	–
BA 0.6	0.36	H	[a]	[a]	69.8	14.1	91.9	3.5	98.1	0.7	–	–
		C	[a]	[a]	60.8	[a]	66.1	[a]	75.8	[a]	–	–
BA 0.8	0.44	H	[a]	[a]	81.7	7.6	96.0	3.5	103.3	1.6	–	–
		C	[a]	[a]	53.0	-1.2	66.6	-9.1	87.2	-1.3	–	–
BA 1.0	0.52	H	[a]	[a]	91.2	21.1	106.2	0.6	–	–	–	–
		C	[a]	[a]	73.4	-22.1	98.2	-2.4	–	–	–	–

[a] not determined

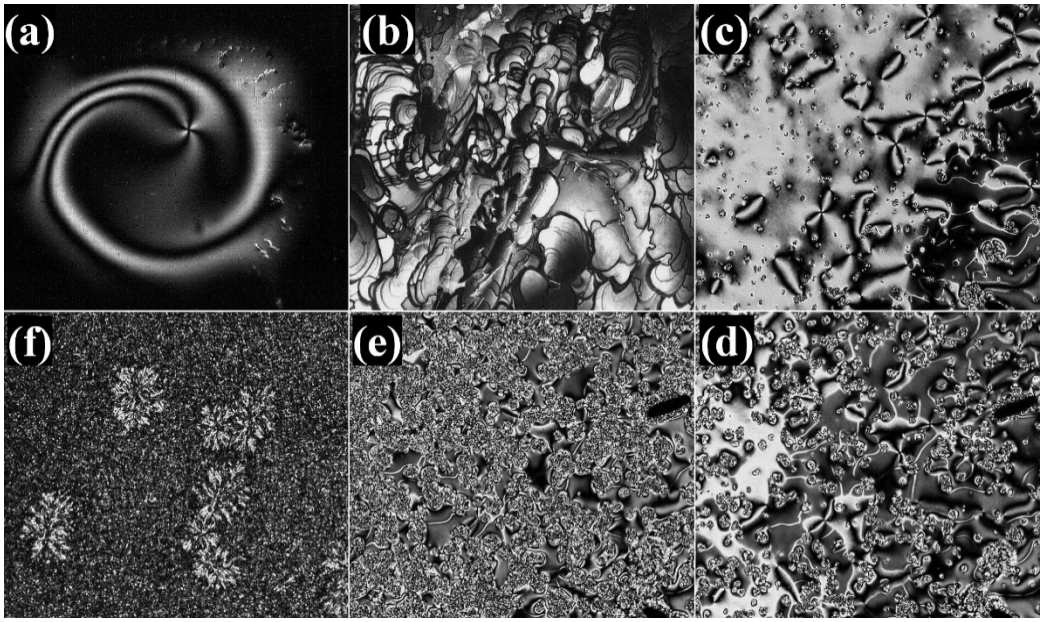

Figure 6.4: POM images of thiol **BA** at 97 °C (a – Schlieren texture, b – marbled nematic texture; heating run) and N → Cr transition of polymer **BA 1.0** (c – 78 °C, d – 76 °C, e – 74 °C, f – 60 °C, cooling run). Width of pictures is 350 µm.

Strong tendencies for the thiol **BA** to form crystalline structures has a significant impact on the phase and mesophase behavior of the related PBDs. Figure 6.3b presents DSC curves from cooling regimes for these polymers. Corresponding values of temperatures and enthalpies for all DSC transitions can be found in Tab. 2. As follows from these data, no glass transition was detected, even in the case of the sample with the lowest content of grafts (**BA 0.2**, ~ 22 mol%). In this sample, only a semi-crystalline structure was observed under POM. This corresponds to one broad peak on the cooling and heating curve. In all PBDs with higher amount of LC side-chains ($R_e \geq 0.30$), a small peak responsible for a mesophase formation occurred on cooling curves, moving to higher temperature values with increasing R_e. For **BA 0.4** and **BA 0.6**, this peak is still slightly overlapped by a crystallization peak, so it was not possible to determine enthalpy for each peak separately. Concluded from cooling curve DSC results, Figure 6.3b, temperature ranges, in which there is a mesophase, are broadened in accordance with increasing degree of modification of the sample. After grafting of the LC thiol on a polymer chain, the resulting comb-like polymer should exhibit a mesophase at a maximum of the same level of arrangement as in the case of the neat thiol. Hence we assumed the mesophase in polymers **BA 0.4 – BA 1.0** is a nematic one. This fact was confirmed by polarizing microscope. An interesting sequence of images of mesophase/semi-crystalline state transition were obtained for the polymer with the highest reached grafting density, sample **BA 1.0** (R_e ~ 0.52; Figure 6.4c-f). In the nematic Schlieren texture with homogenously aligned layers, in which the

molecules are arranged parallel to a substrate layer, small crystallization centres start to appear (Figure 6.4c, 78 °C). During continuous cooling, these centres with a spherullite structure became larger (Figure 6.4d,e) and finally fill the entire sample space (Figure 6.4f, 60 °C). The cooling rate of POM method was in this case of PBD with the highest degree of modification 5 °C/min and the temperature values of the N/Cr transition are relatively comparable with those obtained from DSC-cooling (10 °C/min). When comparing DSC results obtained for the neat thiol **BA** and for the LC PBDs **BA 0.4 – BA 1.0**, presence of the polymer chain has a significant influence on the thermal behavior of the *para*-butoxyazobenzene LC unit, i.e. temperature shift of the Iso/N transitions during cooling and heating run, narrower temperature intervals of the mesophase existence and shifting of these intervals to lower values of temperatures. As also follows from the cooling curves for PBDs grafted with thiol **MA** (Figure 6.3a) and with thiol **BA** (Figure 6.3b), mesophase in LC PBDs **MA 0.4 – MA 1.0** exists at lower temperatures and in broader temperature ranges than this in **BA 0.4 – BA 1.0**.

6.4.2 Rheological Testing

Temperature dependences of storage and loss moduli G' , G'' and loss tangent, tan δ, of the selected PBDs grafted by thiol **MA** are shown in Figure 6.5. During the cooling of PBDs **MA 0.2-0.6** from an isotropic state, a pronounced increase in G' is observed. The temperatures of Iso/N transition in **MA 0.4** and **MA 0.6** are slightly shifted to higher values in comparison with those found from DSC, due to higher cooling rate used in DSC measurement (10 °C/min). Continued cooling is accompanied with an increase in G', resulting finally in the glassy state with the highest values of the modulus corresponding to ~ 10^9 Pa. In PBD **MA 0.8** (and **MA 1.0**, not presented), transition from a semi-crystalline phase to a glassy state results in a much sharper increase of G' in comparison to samples with lower grafting degree undergoing a direct nematic/glassy state transition.

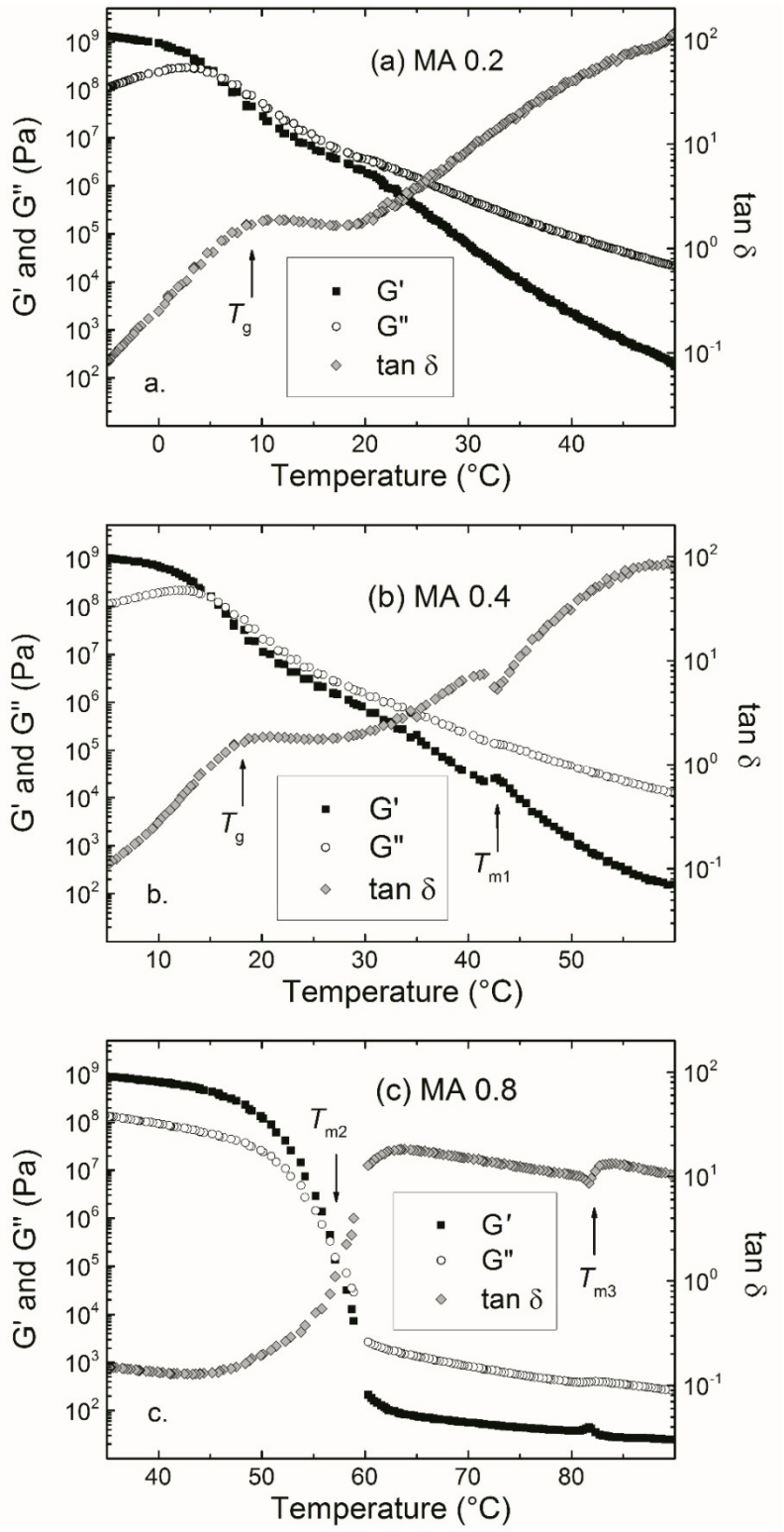

Figure 6.5: Temperature dependences of moduli *G'*, *G"* and loss tangent tan *δ* for LC PBDs **MA 0.2** (a), **MA 0.4** (b) and **MA 0.8** (c). Measured at *f* = 1 Hz, cooling rate 2 °C/min.

As presented by Yu *et al.* (2007), the temperature regions for transitions in the material can be also detected from the much sensitive tan δ vs. T plot.[102] When cooling samples **MA 0.2-0.6** from an isotropic state, a nematic mesophase is formed. This results in a small drop in the loss tangent (marked as T_{m1} in Figure 6.5). This drop was reprodubly obtained during measurement with all types of plates. For temperatures below this local maximum, the material is purely nematic. With continuing cooling, the system is preparing for the glass transition resulting in the lowest values of loss tangent. A different behavior is present in samples with the highest content of mesogenic side chains, **MA 0.8-MA 1.0**. These materials exhibit semi-crystalline phases, resulting in a loss of elastic properties. Crystallization of mesogens involved in the nematic liquid-crystalline arrangement is a very fast process in these PBDs. Due to the formation of growing crystals, the mobility of the polymer backbone segments is inhibited until a glassy state is reached.

Similar behavior was also expected in PBDs grafted by thiol **BA**. Figure 6.6 presents temperature dependencies of both moduli and loss tangent for PBDs **BA 0.4** (a) and **BA 0.8** (b). Common feature for these polymers is a Cr/glassy state transition exhibiting a very fast increase of both moduli and decrease of loss tangent as in cases of PBDs **MA 0.8-1.0**. During cooling of polymer **BA 0.4** from an isotropic state, moduli G' and G'' are slightly increasing. The Iso/Cr transition at ca 70 °C is accompanied by a sharp increase of both moduli. Transition from a crystalline phase to a glassy state can be also clearly seen at ca 54 °C (T_{m1}). After polymer reached the glassy state, value of G' corresponds to ~ 10^9 Pa. During cooling of the LC polymer **BA 0.8**, a formation of a semi-crystalline structure from a mesophase was followed by a very sharp increase in G' , G''. After the sample reached the glassy state, elastic and viscous moduli remained almost constant (~ 10^9 and 10^8 Pa, respectively).

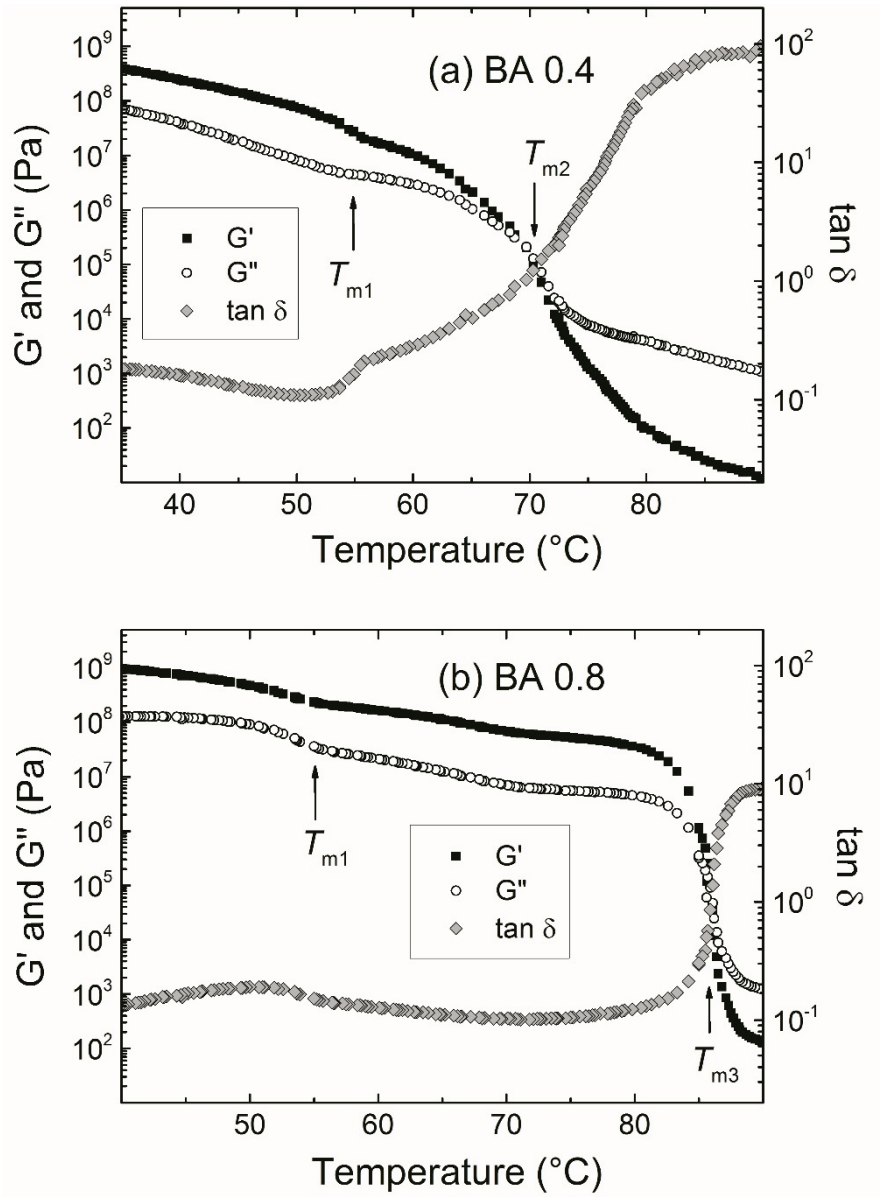

Figure 6.6 Temperature dependences of moduli *G*′, *G*″ and loss tangent tan *δ* for PBDs **BA 0.4** (a) and **BA 0.8** (b). Measured at *f* = 1 Hz, cooling rate 2 °C/min.

Thermal behavior of an LC compound is strongly influenced by structure of the molecule. In this study, azobenzene mesogens possess an alkoxy- substituent (methoxy-, butoxy-) in the *para*-position of the aromatic core. The length of the alkoxy- substituent plays an important role in thermal behavior of the compound. Galewski *et al.* (1999) determined a strong tendency to a formation of several polymorphic crystalline structures in some low-molecular azobenzenes possessing butoxy- substituents.[103] In a certain temperature interval, the crystalline/crystalline transition in polymorphic phases is thermodynamically

more favourable than direct crystalline/nematic phase transition for molecules containing the butoxy- substituent.

The tendency to a formation of semi-crystalline phases is preserved in the azobenzene with butoxy- substituent grafted on a flexible PBD backbone. We have observed that even small amount of BA units in side chains ($R_e \geq 0.22$) is sufficient for the formation of semi-crystalline structures in the related polymer sample.

Different behavior was observed for methoxy- substituent on the azobenzene core. The neat mesogenic unit exhibits only one crystalline phase and the presence of a semi-crystalline structure in PBDs grafted with MA is dependent on their degree of modification. Whereas a direct transition from a nematic phase to a glassy state was observed for PBDs with $R_e \leq 0.42$ during cooling, a semi-crystalline phase occurred in these PBDs at higher degree of modification ($R_e > 0.42$).

The presence of the semi-crystalline structure has a strong impact on the possibility to apply a temperature-frequency superposition for these LC polymer samples. For illustration, Figure 6.7 presents the raw data of elastic modulus in dependence on frequency during isothermal measurements for two representative samples **MA 1.0** (a) and **BA 0.4** (b). A mesophase formation during cooling of polymer **MA 1.0** is accompanied by an increase of storage modulus. This fluent increase is disrupted when a semi-crystalline oriented structure appeared in the sample (see Figure 6.3a). In the PBD **BA 0.4**, a mesophase exists in a relatively short temperature interval. As a consequence, an isotropic state/nematic transition is followed by a very fast nematic/semi-crystalline transition. This process is connected with a rapid, discontinuous increase in storage modulus resulting in the impossibility to superimpose these points with only simple horizontal shift. From this angle of view, a superposition of mechanical functions G', G'' and tan δ was applicable only for the samples undergoing direct nematic/glassy state transition.

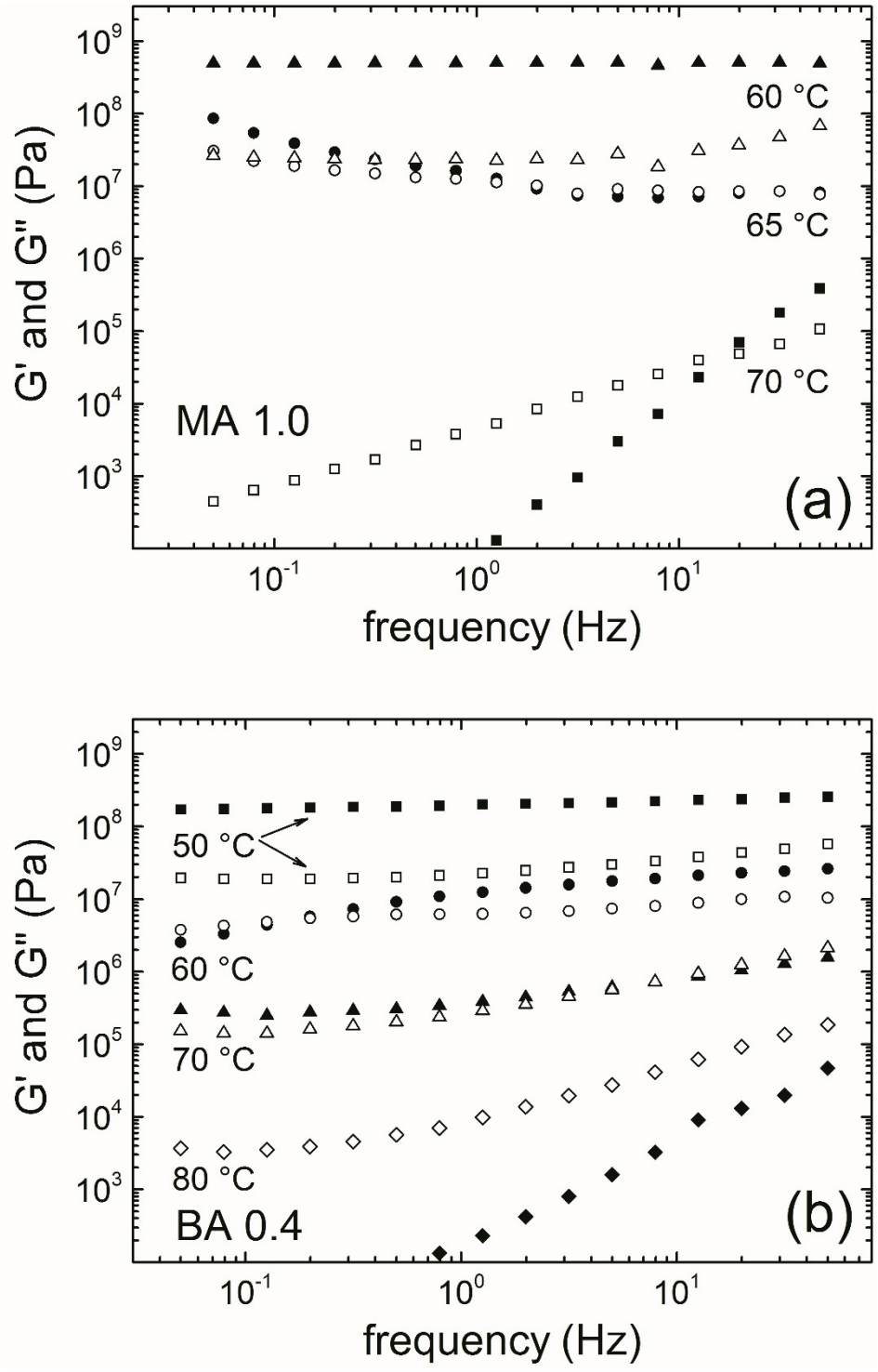

Figure 6.7: Raw data for *G'* and *G"* vs. frequency of the PBDs **MA 1.0** (a) and **BA 0.4** (b). Data collected during cooling regime, T_{ref} = 20 °C. Close symbols – *G'*, open symbols – *G"*.

During cooling from an isotropic state, a frequency-temperature superposition of dynamic mechanical functions has been successfully applied for the PDBs **MA 0.2**-**MA 0.6**. The horizontal shift

factor, a_T, was obtained from the superposition of the loss tangent, tan δ. Using these a_T values, also G' and G'' dependencies could be superimposed. The temperature dependencies of the log a_T of the neat PBD and of the measured LC samples are shown in Figure 6.8. They follow the Williams–Landel–Ferry (WLF) equation in the form:[104]

$$\log a_T = -c_1(T - T_{ref})/(c_2 + T - T_{ref})\,(1) \qquad (5.1)$$

where T_{ref} is a reference temperature and c_1, c_2 are constants (Tab. 3). Reference temperature was chosen as 20 °C. This value of T satisfies the condition of WLF equation, $T_g < T < T_g + 100$, for all superimposed samples. In addition, the selection of the same T_{ref} for all samples enabled us a comparison of superimposed curves. The values of the vertical shift factor, b_T, were found to be close unity. From c_1 and c_2, the fractional free volume at the reference temperature, f_0, and the coefficient of thermal expansion of the fractional free volume, α_f, were calculated ($f_0 = 1/2.3c_1$ and $\alpha_f = 1/2.3c_1c_2$, Tab. 3). As expected, the free volume value was the highest in the case of the neat PBD ($f_0 = 0.111$), where the difference $T_{ref} - T_g$ is approximately 60 °C. Values of f_0 calculated for other samples are getting closer to the universal value 0.025 as T_g is approaching T_{ref}. A thermal expansion coefficient, α_f, that is independent on the reference temperature, exhibited values very close to the universal one (= 4.8×10^{-4} K^{-1}) in the case of the grafted PBDs. Nevertheless, values of both f_0 and α_f are within the range found for amorphous polymers, as follows from Sperling (2006).

Table 6.3 Constants of WLF equation and free volume parameters for the neat PBD and selected LC PBDs. T_{ref} was 20 °C.

Sample	R_e	c_1	c_2 (K)	f_0	$\alpha_f \times10^4$ (K^{-1})
neat PBD	0	3.9	94.6	0.111	11.8
MA 0.2	0.21	17.4	52.0	0.025	4.8
MA 0.4	0.30	18.2	35.4	0.024	6.7
MA 0.6	0.42	26.1	23.7	0.017	7.0

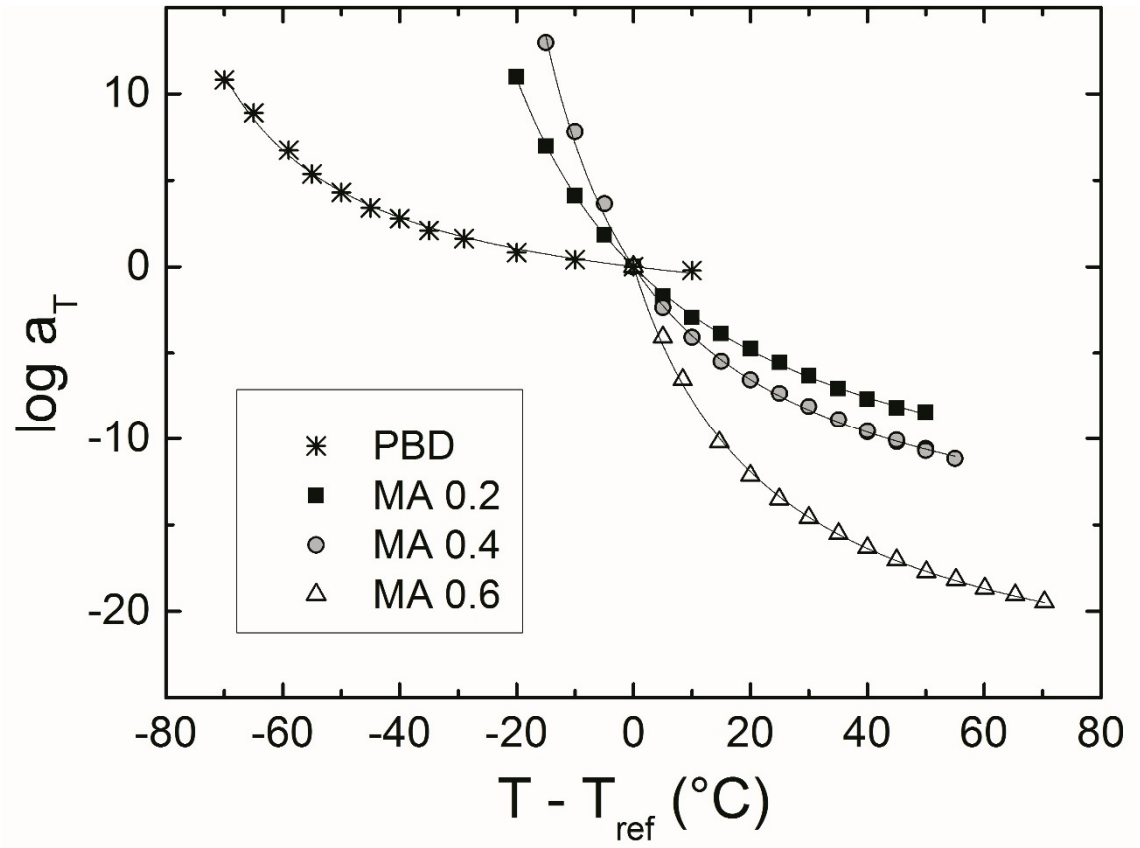

Figure 6.8 Log a_T vs. temperature for the neat PBD (✳) and PBDs **MA 0.2** (■), **MA 0.4** (●) and **MA 0.6** (△). Solid lines follow the WLF-dependencies.

The superimposed dependences of moduli G_p', G_p'' and tan δ on the reduced frequency $\omega \cdot a_T$ for the LC PBD samples modified with thiol **MA** are shown in Figure 6.9. As the amount of grafted mesogenic chains increases, the dependences of moduli of the polymer (with respect to frequency) also increase. This results in a lower frequency extrapolation or longer predicted times. In the region of highest frequency (lowest temperature), G_p' of all the samples exhibits values above 10^9 Pa. The primary softening region causes, in all samples, a decrease in the superimposed moduli with decreasing frequency. Then, the grafted polymers are going through a glassy state/nematic transition which is accompanied by a continuing decrease of both moduli. When the sample exhibits a presence of a nematic phase, the loss component, G_p'', is higher than the elastic component, G_p'. At lowest frequencies, when polymers enter the flow region, the same trend of the moduli is observed. In this terminal region of the lowest frequencies, the slopes of dependencies of all mechanical functions vs. $\omega \cdot a_T$ that are typical for viscoelastic liquids [$G_p' \sim (\omega \cdot a_T)^2$; $G_p'' \sim (\omega \cdot a_T)^1$; tan $\delta \sim (\omega \cdot a_T)^{-1}$] were found for the three grafted PBDs.[105]

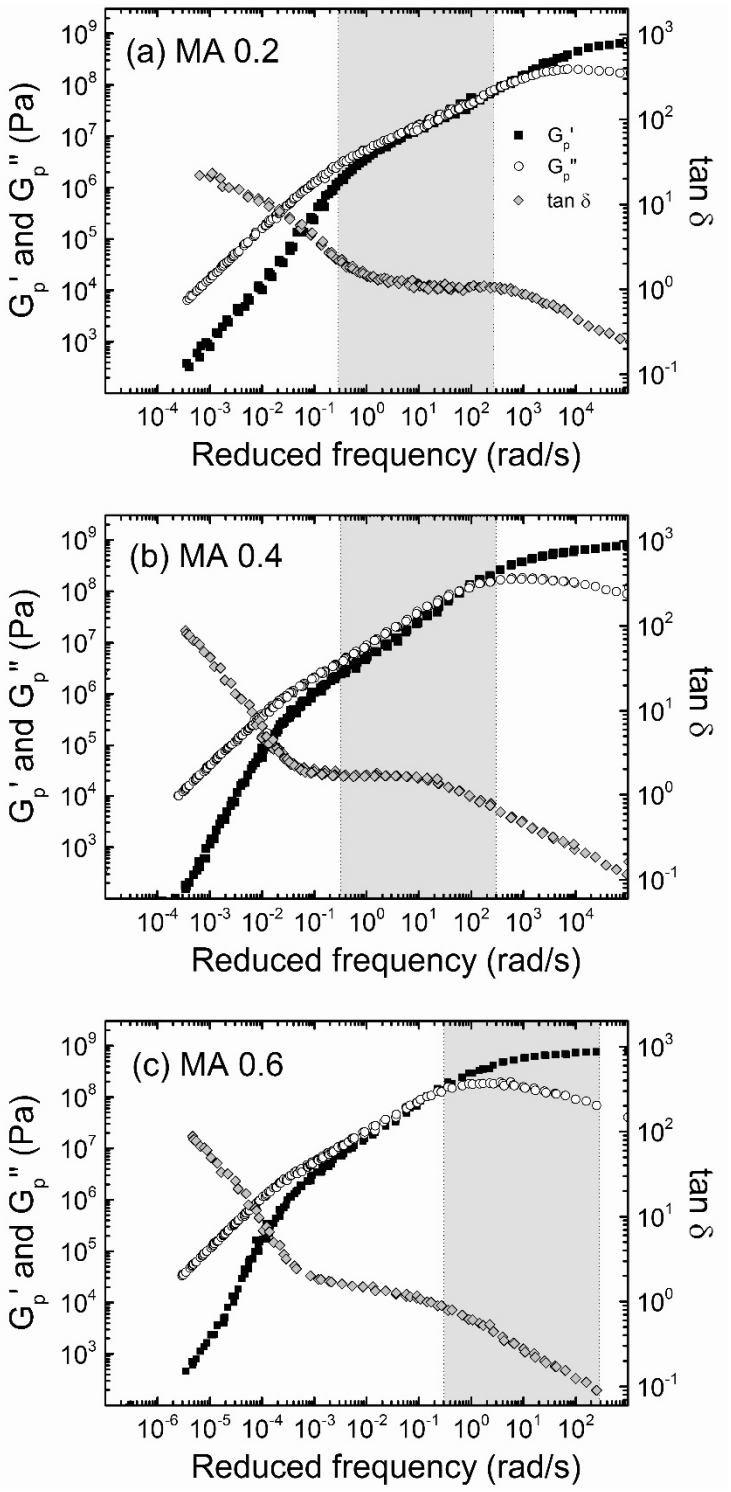

Figure 6.9 Dependencies of the superimposed moduli G_p', G_p'' and tan δ on reduced frequency for the samples **MA 0.2** (a), **MA 0.4** (b) and **MA 0.6** (c). Data collected during cooling regime. Grey field presents the real frequency window (corresponding to T_{ref} = 20 °C).

It is interesting to note that the master curves cover fluently transitions both from a glassy state to a nematic mesophase and from the mesophase to an isotropic state. The similar phenomenon was observed previously of a time-temperature superposition for cyanobiphenyl-containing mesogens grafted also on the poly(butadiene)-based polymer backbone.[91] The master curves for both moduli and loss tangent were constructed over a broad frequency region comprising direct transition from a glassy state to a smectic A mesophase and melting of the mesophase to an isotropic liquid. According to our knowledge, only a few published works have been focused on the applicability of the time-temperature superposition for the side-chains liquid crystalline polymers containing an azobenzene or a cyanobiphenyl mesogens. The polymer backbones were in these cases based on acrylates, methacrylates or siloxanes.[100-101, 106-108] However, the superposition worked mostly only during a mesophase/isotropic state transition. As a contrast, our unique synthetic route comprising grafting of the selected mesogens onto double bonds of poly(butadiene) enables to prepare LC polymers with very flexible polymer backbone. When the polymer sample exhibits a direct transition from a glassy state to a mesophase, a superposition during both the glass/mesophase and mesophase/isotropic transition is possible.

6.5 Conclusions

The synthesized comb-like LC poly(butadiene)diols have been characterized by differential scanning calorimetry and polarizing optical microscopy. T_g of these polymers increased with increasing degree of grafting. In samples with higher amount of grafts, glass transition was not detectable due to overlapping by a crystallization process. The polymers exhibit a presence of a nematic mesophase when containing at least 21 mol.% of thiol **MA** or 30 mol.% of thiol **BA** in side chains. Dynamic mechanical measurement was used to investigate mechanical properties of the samples. A superposition of mechanical functions (storage and loss moduli and loss tangent) was successfully construct for neat poly(butadiene)diol and for LC polymer samples with direct nematic/glassy state transitions.

Chapter 7: (Meth)acrylate Liquid Crystalline Polymers for Membrane Gas Separation Applications

7.1 Abstract

The synthesis and characterization of a series of linear copolymers with liquid crystalline side chains based on novel mesogenic monomers is reported. Methacrylate monomers containing nitroazobenzene or cyanobiphenyl as a mesogenic group were prepared. These monomers were then copolymerized with 2-ethylhexyl acrylate in varying molar ratios. The structure and composition of the monomers and corresponding polymers were determined by ^{1}H-NMR, elemental analysis and size-exclusion chromatography. Thermal properties of the polymers were studied using differential scanning calorimetry, polarized optical microscopy and X-ray scattering techniques. Increasing mesogen content resulted in a decrease of the glass transition temperature of the copolymers. In addition, above a threshold mesogen content, both nitroazobenzene and cyanobiphenyl containing copolymers exhibited Smectic-A mesophases.

7.2 Introduction

Polymer materials exhibiting liquid crystalline (LC) properties have been investigated for many applications [8-9, 24]. Polymers possessing azobenzene, azomethine, stilbene, cyanobiphenyl or other mesogens have been used in photonic, ferroelectric and antiferroelectric applications and in non-linear optics [99, 109-110]. Research on liquid crystal polymer (LCP) membranes for commercial and industrial applications has been limited due to the rheological properties and difficulty in processing of side-chain and main chain LCPs. Several studies have investigated light gas transport properties in linear LCPs aiding in the understanding of the fundamental mechanisms of gas transport [69-70, 72]. Unfortunately, heating a linear LCP membranes above the glass transition (T_g) and into the LC or isotropic states increases polymer mobility, which results in an undesirable decrease in the loss and storage moduli [91]. This results in decrease in membrane stability, resulting in an inability to withstand the pressure gradients used in gas separation applications. For this reason, a cross-linkable LCP material is desirable for the production of stable LCP membranes.

Cross-linked polysiloxane (PS) based LC elastomers have already been synthesized for membrane separation applications [68]. The preparation of these membranes requires the use of a precious metal catalyst, making it potentially too expensive for scale up. To our knowledge, there have been no reported cross-linkable LCP materials that could be used to produce membranes in a cost effective manner.

In-situ free radical polymerization of certain LC monomers with a crosslinking agent can result temperature independent 'form retaining' polymeric materials that also exhibit LC properties. The use of a single reaction scheme to produce multiple LCPs with various mesogen types allows for the facile optimization of LCP membranes for specific applications. Common synthetic routes, such as azocoupling, Williamson reaction and esterification, can be used for the preparation of a variety of mesogenic monomers. These routes can be applied to common precursors to allow control over both the mesogenic group and the spacer group. Free radical polymerization as a means of LCP membrane fabrication also allows for flexibility in the selection and ratios of the mesogenic monomer and the non-mesogenic comonomer, providing control over phase transition temperatures (e.g. glass transition, mesophase, and isotropic), specific volumes, and interactions with permeating gases.

Herein we present the preparation and characterization of a set of novel (meth)acrylate copolymers with nitroazobenzene or cyanobiphenyl based mesogenic side chains, as depicted in Figure 7.1. These materials were prepared in order to demonstrate the use of free radical polymerization as a means of producing a series of polymers with varying mesogen type and mesogen content, and to study

their effect on the phase behaviour. The preparation of cross-linked methacrylate LCPs for membrane applications will be addressed in a future paper.

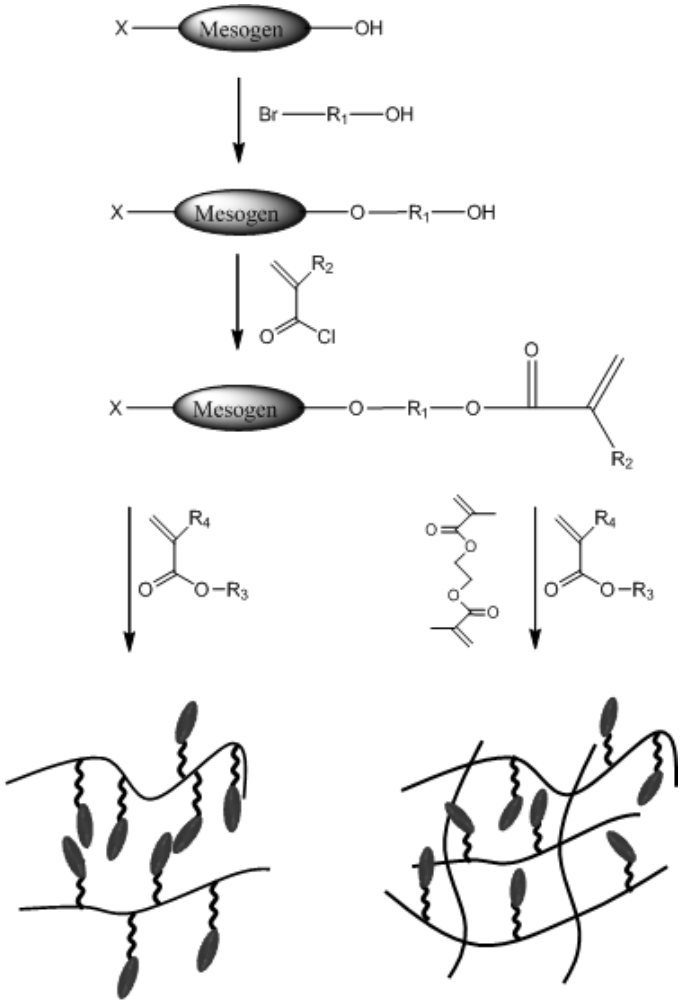

Figure 7.1: Scheme of the synthetic route for the preparation of linear (left) or crosslinked (right) liquid crystal polymers.

7.3 Materials

4-nitroaniline (m.p. 146 °C, Sigma Aldrich), 4'-hydroxy-4-biphenylcarbonitrile (m.p. 192 °C, Sigma Aldrich), 36% hydrochloric acid (b.p. > 100 °C), 98% 11-bromo-1-undecanol (m.p. 46 °C, Sigma Aldrich), sodium nitrite (Sigma Aldrich), sodium hydroxide (VWR), triethylamine (b.p. 89 °C, VWR), toluene (b.p. 110 °C), heptane (b.p. 98 °C), ethanol (b.p. 78 °C), chloroform (b.p. 61 °C) were used as received. Phenol (m.p. 40.5 °C, VWR) was distilled under vacuum. Methacryloyl chloride (b.p. 96 °C) and 2-ethylhexyl

acrylate (b.p. 91 °C/13 mbar) were distilled with DPPH as a stabilizer under vaccum prior to use. Acetone (b.p. 56°C, HPLC grade) was dried using as received calcium carbonate. Potassium carbonate (VWR) and anhydrous calcium chloride were annealed for several hours prior to use. 2,2´-azobisisobutyronitrile (m.p. 103 °C, Sigma Aldrich) was re-crystallized with methanol several times prior to use.

7.4 Methods of Measurements

^{1}H NMR and elemental analysis were used to determine the structure and composition of the low-molecular weight and polymeric compounds. ^{1}H NMR spectroscopy was performed at 300 MHz using deuterated chloroform ($CDCl_3$) as the solvent. Molecular weights of the synthesized polymers and their distributions were estimated using size-exclusion chromatography (SEC) with poly(methyl methacrylate) as a standard.

Thermal behavior of the copolymers was determined using differential scanning calorimetry (DSC). Measurements were performed using a Perkin Elmer DSC-2 instrument. The sample was first cooled to -50 °C or -70 °C and then heated to a temperature of 150 °C, at a rate of 10 °C/min. Liquid crystalline textures were observed using polarized optical microscopy (POM) using an Olympus BX51 equipped with a polarizer/analyser, a Linkam LTS 350 hot stage and a Linkam TMS 94 temperature programmer. SAXS and WAXD experiments were performed using a Rigaku S-Max 3000 system, equipped with a copper rotating anode emitting X-rays with a wavelength of 0.154nm (Cu Kα) and a Linkam Scientific Instruments hot stage and temperature controller. The calibration standard for both SAXS and WAXD was silver behenate. SAXS patterns were obtained using a 2D gas-filled multiwire, proportional counting detector. A Rigaku RAXIA-DI was used to read WAXD sample image plates. Temperature ramp rates of 10 °C/min, equilibrium times of 30 minutes, and exposure times of 2 hours were used for all SAXS and WAXD measurements.

7.5 Synthesis and Characterization

Methacrylate monomers containing azobenzene (A) and biphenyl (B), as depicted in Figure 7.2, were synthesized for use in the preparation of linear LCPs.

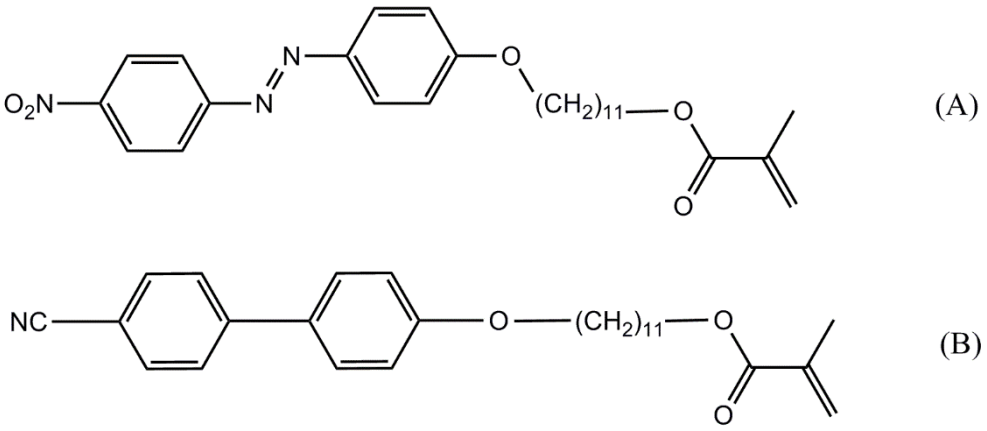

Figure 7.2: Monomers synthesized for use in the preparation of LCPs: 11-(4-nitroazobenzene-4´-yloxy)undecyl methacrylate (A); and 11-(4-cyanobiphenyl-4´-yloxy)undecyl methacrylate (B)

7.5.1 Synthesis of 11-(4-nitroazobenzene-4´-yloxy)undecyl methacrylate (A)

Monomer A was synthesized using a multi-step process consisting of an azocoupling followed by a Williamson reaction and an esterification (Figure 7.3).

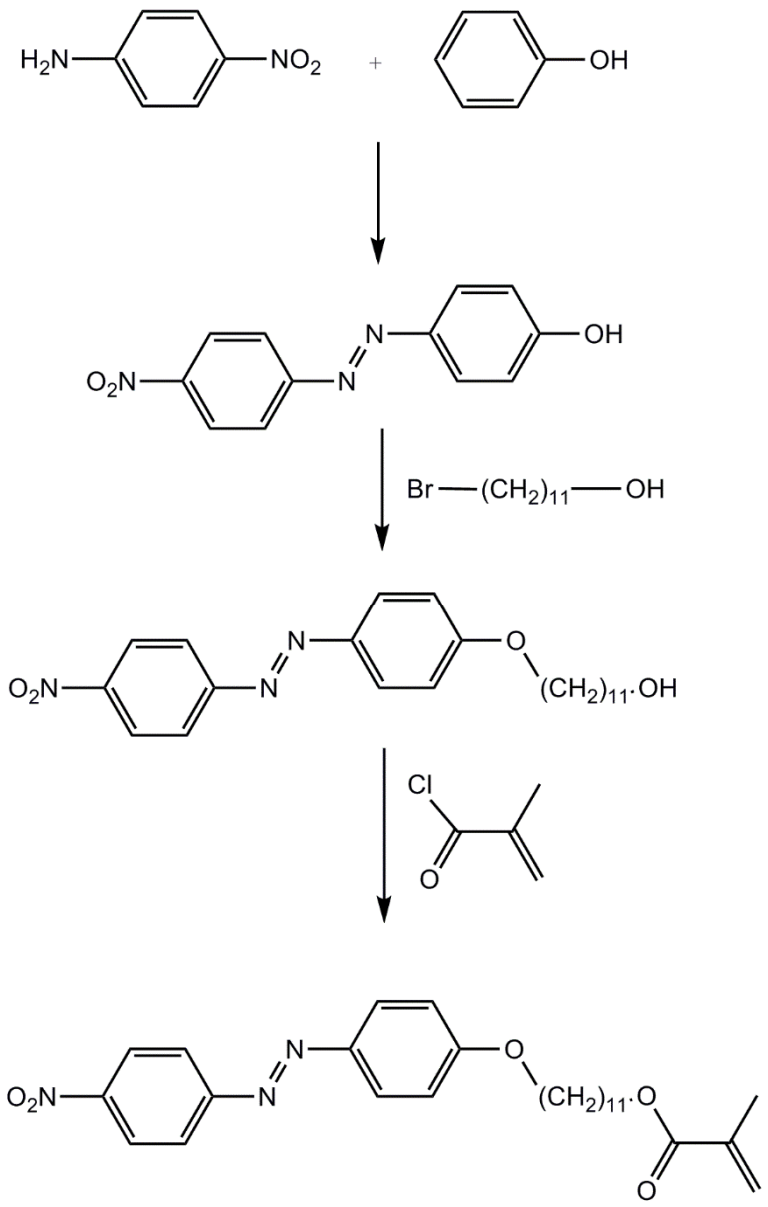

Figure 7.3: Reaction scheme for the preparation of 11-(4-nitroazobenzene-4´-yloxy)undecyl methacrylate (monomer A.)

7.5.1.1 Synthesis of 4´-hydroxy-4-nitroazobenzene (1)

21.5 g of 4-nitroaniline (0.16 mol) was dissolved in a hot mixture of 60 ml of 36% HCl (0.69 mol) and 50 ml of DI H_2O. The resulting solution (solution I) was poured onto 200 g of crushed ice and kept between 0 °C and 5 °C. At this temperature, 11.0 g of $NaNO_2$ (0.16 mol) in 110 ml of H_2O was added dropwise to solution I. The reaction mixture was then stirred at a temperature below 5 ^oC for 30 minutes. The resulting diazonium salt solution was then added dropwise to a solution of 15.0 g of phenol (0.16 mol) and 19.6 g of NaOH (0.48 mol) in 200 ml of iced water. The reaction temperature was maintained below

5 °C for the duration of the reaction. After the reaction was complete, the resulting orange precipitate was filtered off, washed with ice water and dried. The crude product was recrystallized twice from toluene and dried on ceramic plates overnight. M.p. 225-229 °C, yield – 19.7 g (54%). ^{1}H NMR data (300.1 MHz, $CDCl_3$): 8.36 (d, 2H, ortho to –NO_2), 7.94 (dd, 4H, ortho to –N=N–), 6.98 (d, 2H, ortho to –OH).

7.5.1.2 Synthesis of 4´-(11-hydroxy-undecyloxy)-4-nitroazobenzene (2)

12.0 g of *(1)* (49.3 mmol), 27.0 g of 11-bromo-1-undecanol (107.4 mmol) and 24 g of just annealed K_2CO_3 (173.6 mmol) were dissolved in 360 ml of dry acetone. The solution was bubbled with nitrogen for several minutes, sealed and heated under reflux for 48 hrs. The reaction mixture was then cooled down to room temperature and the solid was filtered off. The filtrate was concentrated in vacuum until crystallization occurred. The precipitated crystals were filtered off and recrystallized from a toluene/heptane mixture (1/4). M.p. 99-102 °C, yield – 17.0 g (85%). ^{1}H NMR data (300.1 MHz, $CDCl_3$): 8.34 (d, 2H, ortho to –NO_2), 7.96 (dd, 4H, ortho to –N=N–), 7.00 (d, 2H, ortho to –O–CH_2–), 4.05 (t, 2H, –O–CH_2–), 3.63 (q, 2H, –CH_2–OH), 1.79 (qui, 2H, –O–CH_2–CH_2–), 1.19 to 1.56 (m, 16H, aliphatic).

7.5.1.3 Synthesis of 11-(4-nitroazobenzene-4´-yloxy)undecyl methacrylate (A)

In a three-necked round bottom flask equipped with a thermometer and a drying tube filled with anhydrous calcium chloride, 8.0 g of *(2)* (19.4 mmol) was dissolved in 460 mL of dry chloroform and 10.5 ml of triethylamine (75.0 mmol). The resulting solution was cooled to 0 °C using an ethanol/dry ice bath under constant stirring. 6.9 mL of freshly distilled methacryloyl chloride (69.7 mmol) in 50 mL of dry methylene chloride was added dropwise. Formation of HCl vapor was observed as the methacryloyl chloride was added. The reaction temperature was maintained between 0 °C and 4 °C for 16 hours. Half of the solvent in the reaction mixture was then removed under reduced pressure, and the mixture was kept for 7 days to ensure that the reaction was complete. The mixture was then shaken with an aqueous solution of $NaHCO_3$ (8.0 g per 500 mL of water) and KOH (6.0 g per 500 mL of water) to remove dissolved triethylammonium chloride and methacrylic acid. The organic phase was dried with anhydrous magnesium sulphate and the solvent was removed under reduced pressure. The resulting crystals were dried on a ceramic plate. Yield – 7.3 g (79%). ^{1}H NMR data (300.1 MHz, $CDCl_3$): 8.34 (d, 2h, ortho to –NO_2), 7.96 (dd, 4H, ortho to –N=N–), 7.00 (d, 2H, ortho to –O–CH_2–), 5.53 and 6.08 (s+s, 2H, CH_2=C(CH_3)–), 4.12 (t, 2H, –CH_2–O–CO–), 4.05 (t, 2H, Ar–O–CH_2–), 1.93 (s, 3H, –CH_3), 1.24 to 1.84 (m, 18H, aliphatic).

7.5.2 Synthesis of 11-(4-cyanobiphenyl-4´-yloxy)undecyl methacrylate (B)

Monomer B was synthesized using the two-step synthesis depicted schematically in Figure 7.4.

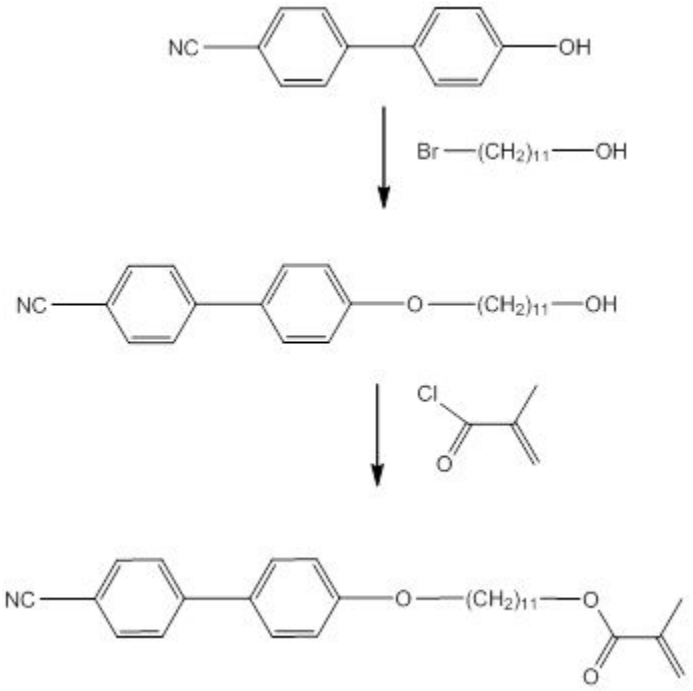

Fig. 7.4: Reaction scheme for the preparation of 11-(4-cyanobiphenyl-4´-yloxy)undecyl methacrylate (monomer B.)

7.5.2.1 Synthesis of 4′-(11-hydroxy-undecyloxy)-4-biphenylcarbonitrile (3)

5.8 grams of 4'-hydroxy-4-biphenylcarbonitrile (30 mmol), 11.3 grams of 11-bromo-1-undecanol (45 mmol), and 8.0 grams of annealed K_2CO_3 (60 mmol) were added to 150 mL of acetone. The solution was bubbled with nitrogen for several minutes, sealed, and heated to reflux for 72 hours. After cooling to room temperature, the solid present in the solution was filtered off. The solvent in the filtrate was removed under reduced pressure. The resulting solid was recrystallized several times in heptane. M.p. 98-100 °C, yield – 43%. ^{1}H NMR data (300 MHz, $CDCl_3$): 7.58 (dd,4H, ortho, meta to –CN), 7.46 (d, 2H, meta to alkoxy), 6.92 (d, 2H, ortho to alkoxy), 3.93 (t, 2H, Ph–O–CH_2–), 3.58 (q, 2H, –CH_2–OH), 1.79 (qui, 2H, –O–CH_2–CH_2–), 1.19 to 1.56 (m, 16H, aliphatic).

7.5.2.2 Synthesis of 11-(4-cyanobiphenyl-4´-yloxy)undecyl methacrylate (B)

2.0 grams of *(3)* (5.5 mmol) and 830 µL of triethylamine (6 mmol) were dissolved in 20 mL of dry THF. The solution was cooled to -5 °C using ethanol and dry ice. 0.8 mL of a freshly distilled methacryloyl chloride (8 mmol) in 5 mL of THF was added drop wise to the solution. The solution was stirred at a temperature between 0 °C and 5°C for several hours followed by several days at room temperature to ensure the reaction was complete. Solid triethylammonium chloride was filtered off and the solvent in the filtrate was removed under reduced pressure. The resulting solid was recrystallized several times in methanol. M.p. 75-77 °C, yield – 63%. ^{1}H NMR data (300 MHz, $CDCl_3$): 7.58 (dd, 4H, ortho, meta to –CN), 7.46 (d, 2H, meta to alkoxy), 6.92 (d, 2H, ortho to alkoxy), 5.48 and 6.04 (s+s, 2H, CH_2=C(CH_3)–), 3.93 (t, 2H, Ph–O–CH_2–), 3.58 (q, 2H, –CH_2–OH), 1.79 (qui, 2H, –O–CH_2–CH_2–), 1.19 to 1.56 (m, 16H, aliphatic).

7.5.3 Preparation of copolymers of 2-EHA with comonomer A or B

Monomer A or B, 2-EHA, and AIBN were dissolved in toluene and poured into an ampule. The concentration of monomer A or B varied from 0 to 0.9 grams per mL of toluene, but the total amount of acrylate and methacrylate stayed constant at 2.5 mmol/mL of toluene. The initial molar ratio of AIBN to the comonomers was 1.5×10^{-2}. The solution was bubbled and blanketed with nitrogen for several minutes and then the ampule was immediately sealed. The ampule was heated to 80 °C for 48 hours to induce polymerization. The resulting viscous solution was re-precipitated several times in a methanol/THF mixture (decreasing solvent ratio with increasing A or B ratio with respect to 2-EHA) and dried under vacuum overnight at a temperature of 80 °C.

The structure and composition of the resulting (co)polymers was determined using ^{1}H NMR and elemental analysis. Number-average molecular weights and polydispersity indices of these materials were estimated by size-exclusion chromatography.

7.6 Results and Discussion

7.6.1 Characterization of the Synthesized Polymers

A/2-EHA and B/2-EHA copolymers were synthesized by a free radical polymerization method. The initial ration of the mesogenic monomer (A or B) to the non-mesogenic comonomer (2-EHA) in the feed

varied from 0 to 1. The final mesogen fractions, molecular weights and polydispersity indices are reported in Table 7.1.

Table 7.1: Main characteristics of the synthesized polymers

Sample	F_{LC}[a]	f_{LC}[b]	M_n x 10^{-4} [c]	M_W/M_n[c]
poly(2-EHA)	0.00	0.00	1.2	3.5
A-15	0.15	0.16 (0.18 [d])	2.1	2.0
A-30	0.30	0.33 (0.36 [d])	2.1	1.9
A-50	0.50	0.44 (0.48 [d])	2.0	1.8
A-60	0.60	0.49 (0.56 [d])	2.1	1.8
A-75	0.75	0.60 (0.67 [d])	2.1	1.9
A-100	1.00	1.00	2.2	1.6
B-33	0.33	0.19 (0.24 [d])	2.5	3.3
B-50	0.50	0.36 (0.42 [d])	2.8	2.9
B-75	0.75	0.66 (0.68 [d])	2.7	2.6
B-100	1.00	1.00	2.8	2.3

[a] mole fraction of mesogenic monomer in the feed
[b] mole fraction of mesogenic monomer units in the (co)polymer, estimated from ^{1}H-NMR
[c] determined from SEC using PMMA as a standard
[d] mole fraction of LC comonomer content in the sample, estimated from elemental analysis

As expected, the fraction of mesogenic comonomer units (A or B) incorporated into the copolymer increased with the increasing mesogenic comonomer content in the feed. The values found using NMR are in relatively good agreement with those from elemental analysis. All the homopolymers and copolymers exhibited a unimodal distribution of molecular weights. The ratio M_w/M_n found for these polymers varied from 1.6 to 3.5. This is in accordance with the nature of the free radical polymerization

process [111]. The presence of the mesogenic comonomer in the feed contributed to a significantly narrower molecular weight distribution in the resulting polymer in comparison to the neat non-LC homopolymer poly(2-EHA) (M_w/M_n = 3.5). This is to be attributed to a decrease in the overall reaction rate caused by the addition of the bulky azobenzene or biphenyl containing monomers.

7.6.2 The Effects of Copolymer Composition on Phase Transitions

Thermal properties of the homopolymers and copolymers were determined using differential scanning calorimetry, polarized optical microscopy and X-ray scattering.

5.2.1 Differential Scanning Calorimetry (DSC)

DSC-curves for polymers containing mesogenic comonomer A and 2-EHA are depicted in Figure 7.5. The associated DSC-data are summarized in Table 7.2.

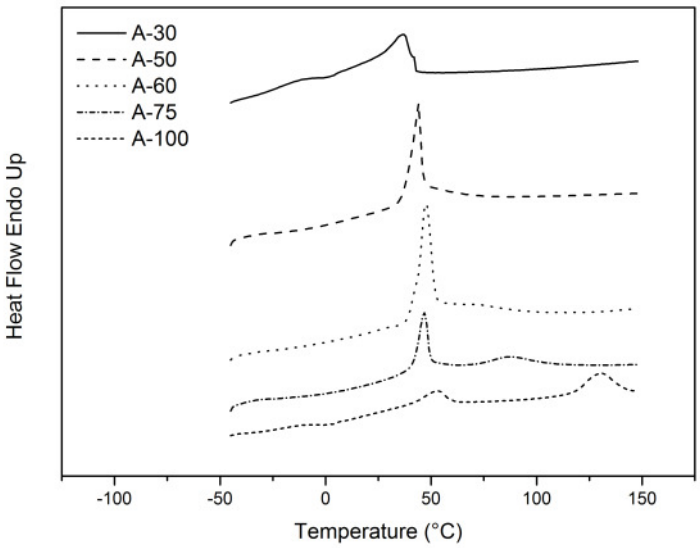

Figure 7.5: DSC heating curves for polymers containing mesogenic comonomer A, with a temperature ramp of 10 °C/min

As expected, only the homopolymer poly(2-EHA) exhibited a simple thermal behavior with one glass transition [112]. The values found for this transition (T_g ~ -50 °C and Δc_p ~ 0.05 J/g×°C) are typical for amorphous polymers [113]. Incorporation of A into the polymer chains dramatically influenced the thermal behavior of the resulted polymer. With increasing content of A in the polymer structure, the glass

transition is shifted to higher temperature values. A slight increase of its Δc_p is also observed. When the content of A exceeds 44%, the glass transition peak overlaps with a peak corresponding to a semi-crystalline/mesophase transition. An increase in the amount of comonomer A in the polymer samples A-50 through A-100 results in increasing mesophasic order in the polymer structure [114]. As a result, a decrease of the change in enthalpy of semi-crystalline/mesophase transition and an increase of the change of enthalpy of a mesophase/isotropic state transition with increasing LC is observed. The temperature interval over which the LC mesophase is stable also occurs with increasing monomer A content [115], from only a few °C in the case of A-50 to a range of 80 °C in the homopolymer A-100.

Table 7.2: DSC-data for copolymers containing 2-EHA and mesogenic comonomer A. The heating/cooling rate was 10 °C/min.

Sample	Run	T_g (°C)	Δc_p (J/g×°C)	T_{m1} (°C)	ΔH (J/g)	T_{m2} (°C)	ΔH (J/g)
poly(2-EHA)	H	-46.0	0.05				
	C	-51.9	0.06				
A-33	H	-23.3	0.32	36.9	8.2		
	C	-27.4	0.30	19.7	-7.2		
A-50	H	-10.5	0.34	44.2	15.4		
	C			25.3	-5.9		
A-60	H			45.4	12.2	73.7	0.5
	C			33.0	-6.4	49.7	-1.0
A-75	H			46.9	6.6	87.5	3.0
	C			28.9	-7.0	73.8	-3.3
A-100	H			52.9	3.7	130.6	6.4
	C			33.1	-3.4	124.9	-6.5

DSC-curves for polymers containing mesogenic comonomer B and 2-EHA are depicted in Figure 7.6. The associated DSC-data are summarized in Table 7.3.

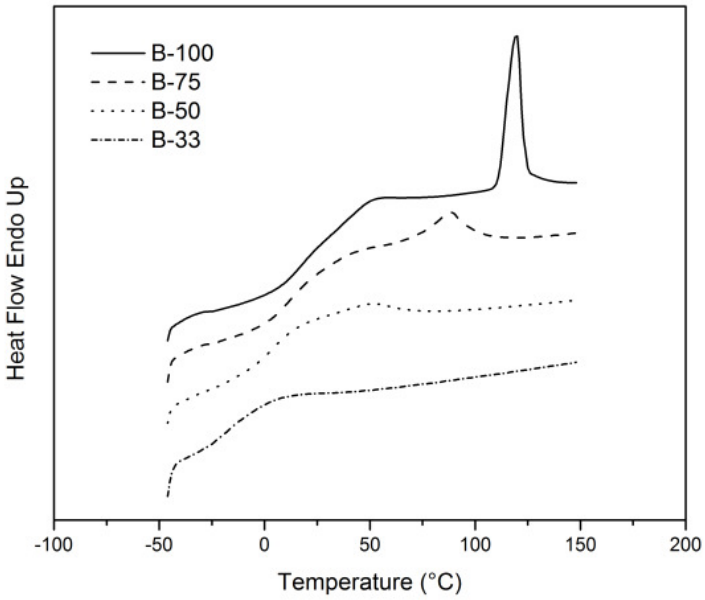

Figure 7.6: DSC-curves of polymers containing LC comonomer B. Heating run, 10 °C/min

As observed in the A/2-EHA polymers, the temperature and Δc_p of glass transition of the B/2-EHA polymers increased with increasing B content, from -46 °C and 0.05 J/g×°C for the homopolymer poly(2-EHA) up to 18 °C and 0.93 J/g×°C for the homopolymer B-100. Polymer samples containing more than 19 mol% B exhibited a peak that can be connected with a mesophase/isotropic state transition. As the content of B increases, the peak shifts to higher temperatures and the change in enthalpy increases. Thus the thermal stability of the mesophase increases with the mesogenic monomer content. For the copolymer B-50, the width of the temperature interval of the mesophase is ~45 °C, whereas in the homopolymer B-100, the mesophase is stable over an interval of ~100 °C. In addition, the difference in isotropic state/mesophase transition peak position between heating and cooling decreased as B content increased.

Table 7.3 DSC-data for polymers containing 2-EHA and LC comonomer B. Heating/cooling rate was 10 °C/min

Sample	Run	T_g (°C)	Δc_p (J/g×°C)	T_m (°C)	ΔH (J/g)
poly(2-EHA)	H	-46.0	0.05		
	C	-51.9	0.06		
B-33	H	-15.7	0.39		
	C	-23.9	0.27		
B-50	H	4.6	0.58	50.3	2.4
	C	-9.4	0.53	37.2	-0.92
B-75	H	11.9	0.61	88.8	5.9
	C	1.1	0.60	79.2	-6.3
B-100	H	17.8	0.93	111.3	12.4
	C	7.9	0.91	111.7	-13.1

7.6.3 The Effects of Copolymer Coposition of LC Textures

POM was employed to confirm results obtained from DSC and to determine the optical textures of the LC samples. Heating and cooling rates were 10 °C/min. Tthe heating/cooling was stopped at various temperatures to allow the material to equilibriate prior to images being taken. No LC texture was observed in the sample with the lowest content of A (A-33), either upon heating and cooling. A clearing point at 50 °C was observed upon heating the A-50 sample, which is in agreement with DSC. During cooling, a frozen Schlieren texture with 4 brushes was observed at temperatures below 45 °C. This kind of 4-brush Schlieren texture is typical for both nematic and smectic A mesophases [40]. X-ray diffraction (see *5.2.3*) confirms the presence of a smectic A mesophase. Thus a smectic glassy phase occurred in the A-50 copolymer sample below 45 °C (Fig. 7.7a). Similar Schlieren textures with 4 brushes were observed in

copolymer samples with higher A content (Fig. 7.7b-d). The most pronounced textures were present in the A-75 copolymer and the A-100 homopolymer. The temperature intervals over which the mesophase was stable broadened with increasing A content, in agreement with the DSC results.

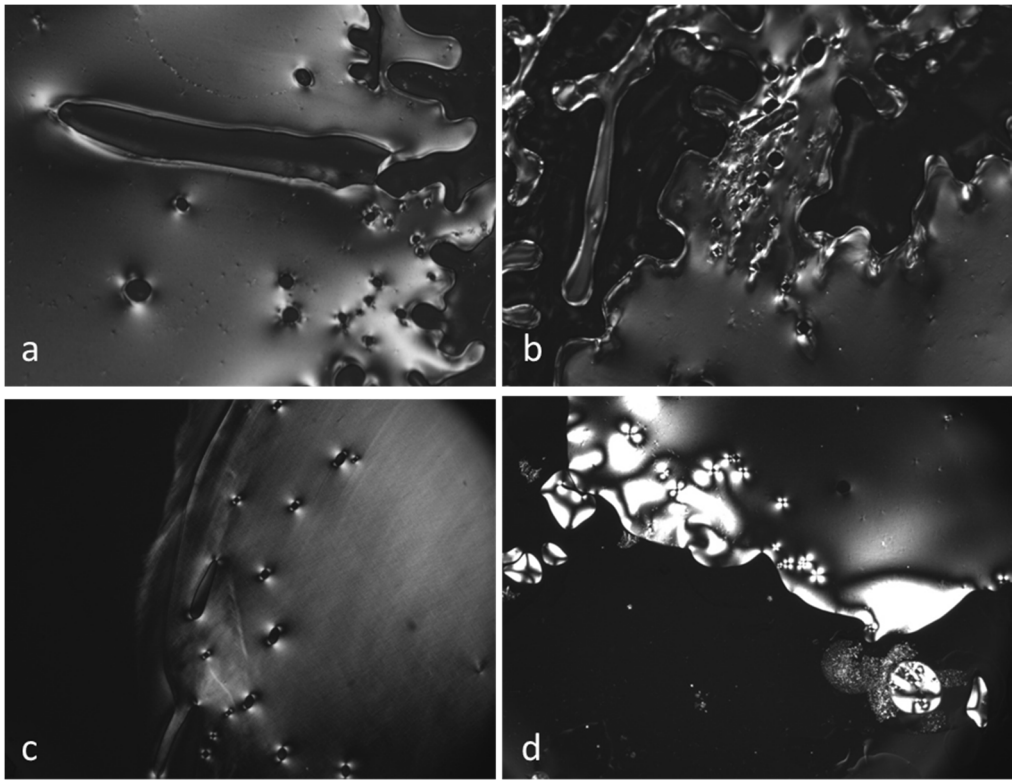

Figure 7.7: POM images of polymer samples: (a) A-50 at 40 °C, (b) A-60 at 50 °C, (c) A-75 at 60 °C, (d) A-100 at 120 °C. Cooling rate 10 °C/min. The width of the image is about 400 µm.

POM images for B/2-EHA copolymers are shown in Figure 7.8. The cyanogroup present in the B comonomers possesses a strong dipole moment, suggesting that the formation of a smectic mesophase with a layered structure is preferred [116]. Schlieren textures observed for polymers B-50, B-75 and B-100 exhibited singularities of ±1., in accordance with the assumption of a smectic mesophase. The smectic mesophase was also confirmed via X-ray diffraction (see *5.2.3*).

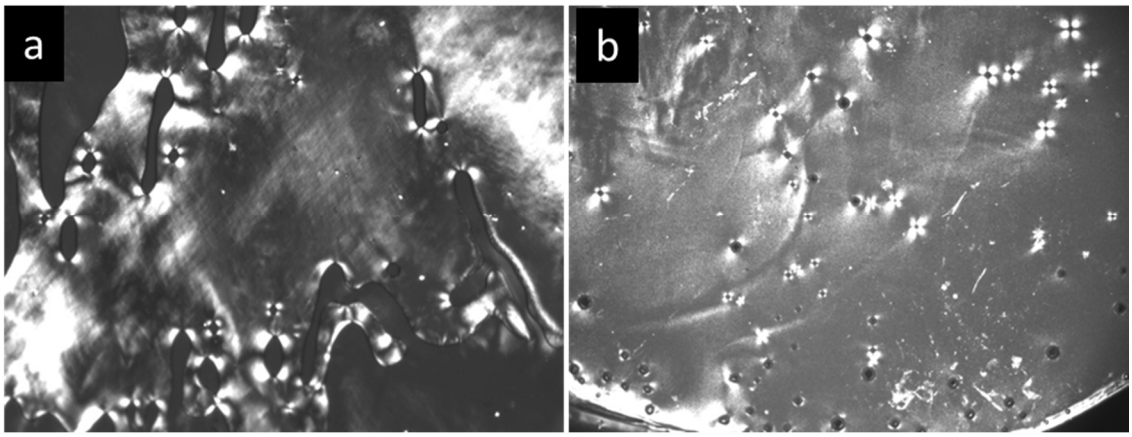

Figure 7.8: POM images of samples: (a) B-50 at 40 °C, (b) B-75 at 60 °C. Cooling rate 10 °C/min. The width of the image is about 400 µm .

7.6.4 LC Structural Property Characterization Using Small-Angle and Wide-Angle X-Ray Scattering

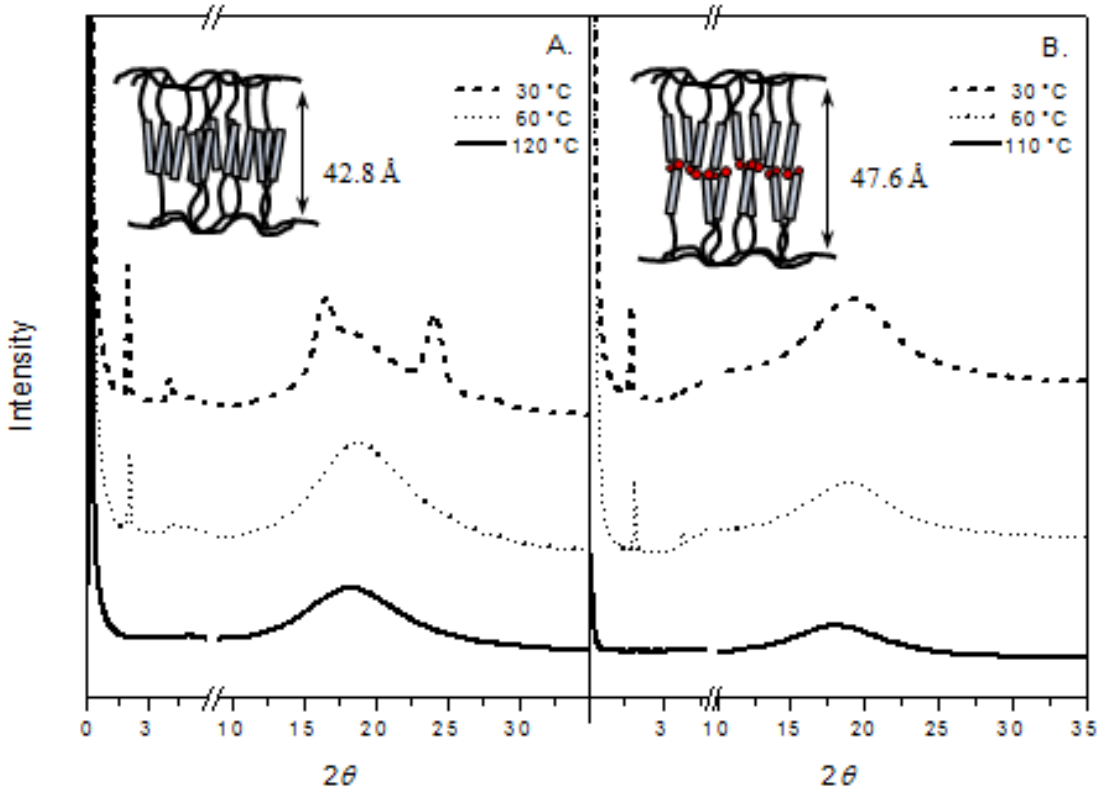

Figure 7.9: Temperature development of the X-ray diffractograms for samples A-75 (A) and B-75 (B). Cooling rate 10 °C/min

Figure 7.9a exhibits X-ray diffractograms for copolymer A-75 at several temperatures taken during cooling. The behaviour of A-75 is typical for the A/2-EHA polymers exhibiting an LC mesophase. In the isotropic state (120 °C), only a broad diffuse peak is observed in the wide-angle region. The maximum of this peak corresponds to a distance of 4.8 Å. When the material is cooled into the mesophase (60 °C), the wide-angle peak maximum shifts slightly and corresponds to an average between mesogens in the mesophase of 4.7 Å. In the small-angle region, two diffraction maxima are observed. These reflections are attributed to layered structure of a smectic mesophase. The first maximum at 42.8 Å corresponds to the thickness of the smectic A layer, and agrees well with the predicted value of 43.3 Å based on a model assuming the mesogens adopt an antiparallel arrangement (Figure 7.9a above). The second peak is a second order peak with a maximum at 21.1 Å. These periodicities are maintained in this material as it is cooled into the glassy state (43.2 Å and 21.7 Å respectively at 30 °C).

Diffractograms of the copolymer B-75 are shown in Figure 7.9b. In the isotropic state (110 °C), only a broad diffuse peak is observed corresponding to a distance of 4.9 Å. At 60 °C, when the polymer exhibits a LC mesophase, the position of the wide-angle maximum corresponds to an average distance between mesogens of 4.6 Å. In the small-angle region, two sharp reflections are observed at 47.6 Å (first order) and 23.8 Å (second order). The maximum at 47.6 Å is in a good agreement with the theoretical value calculated for the thickness of the smectic A bilayer (49.8 Å). Within this bilayer, mesogens are oriented antiparallel, strong interaction between polarized cyano groups takes place. The model of the mesophase is presented in Figure 7.9b above.

7.5 Conclusions

Methacrylates containing a nitroazobenzene (A) or a cyanobiphenyl (B) group as the rigid mesogen were synthesized and characterized. Thermally activated free-radical polymerization was used to produce copolymers of A or B with a non-mesogenic monomer 2-EHA. The fraction of A or B to 2-EHA in the feed of the copolymerization reaction was varied in the range from 0 to 1, and the content of A or B in the resulting polymer increased with increasing feed content. The resulting polymers had weight average molecular weights between 1.2×10^{-4} and 2.8×10^{-4}. The polydispersity indices of the copolymers decreased with increasing mesogen content, likely as a result of slower polymerization rates due to steric hindrance. The introduction of the mesogenic monomers into the polymer structure significantly influenced T_g values of the resulting copolymers; the T_g increased with increasing mesogen content. Liquid crystalline mesophases were observed in copolymers containing at least 44 mol% of A or 36 mol% of B.

Based on POM and X-ray scattering, the mesophases were identified as smectic A single layer (polymers containing A) or smectic A bilayer (polymers containing B.) The preference for these phases is due to the presence of the polarizable group in the comonomer structure. Increasing mesogenic comonomer content also lead to a broadening of the temperature intervals over which the LC mesophases were stable.

Chapter 8: Temperature-Dependent Gas Transport Properties of Cross-linked Liquid Crystalline Polyacrylate Membranes

8.1 Abstract

Stable cross-linked liquid crystal polymer films for membrane separation applications have been fabricated the mesogenic monomer 11-(4-cyanobiphenyl-4′-yloxy)undecyl methacrylate (CNBPh), non-mesogenic monomer 2-ethylhexyl acrylate (2-EHA), and cross-linker ethylene glycol dimethacrylate (EGDMA) using an *in situ* free radical polymerization technique with UV initiation. The phase behavior of the LCP membranes was characterized using DSC and X-ray scattering, and indicated the formation of a nematic liquid crystalline (LC) phase above the glass transition temperature. The single gas transport behavior of CO_2, H_2, CH_4, propane and propylene in the crosslinked LCP membranes were investigated for a range of temperatures in the LC mesophase and the isotropic phase. Solubility of the gases is dependent not only on condensability in the LC mesophase, but also on the polarity of the gases due to favorable interactions with the ordered polar mesogenic side chains of the LCP. Selectivities for various gas pairs generally decreased with increasing temperature and were discontinuous across the nematic/isotropic transition. Higher cross-link densities generally led to decreased selectivity at low temperatures when chain motion is limited by the lack of mesogen mobility in the ordered nematic phase, but increased selectivity at higher temperatures when the cross-links act to limit chain mobility. Mixed gas permeation measurements for propylene and propane showed close agreement with the results of the single gas permeation experiments.

8.2 Introduction

Membrane separation processes are of considerable scientific and economic interest due to their scalability and low energy requirements.[92] They also have the potential to perform separations that are difficult to achieve with other technologies such as desalination, natural gas purification, and paraffin/olefin separation.[44, 117-118] Liquid crystalline (LC) materials, which exhibit multiple temperature dependent mesophases with varying degrees of order, have not received significant scrutiny for membrane separations. The ordering of liquid crystalline materials presents a unique opportunity for gas

separation processes. These materials offer several options for tuning and controlling mass transport behavior, such as molecular orientation and temperature dependent phase behavior. The structure and molecular morphology of the membrane material have a direct effect on the transport mechanism.

Due to their intrinsic properties, liquid crystalline polymers (LCPs) are attractive in photonic, ferroelectric and antiferroelectric applications.[10, 24] LCPs are a distinct class of liquid crystals where the liquid crystal mesogens are attached to a polymer backbone, either by being incorporated in the main chain or attached with a flexible spacer to form a comb like structure. The flexible spacer decouples motion between the polymer backbone and the LC mesogens, giving the mesogens the ability to form independent phases.[25] In addition, the polymer backbone decreases the macroscopic mobility of the material, which enhances the mechanical stability. The introduction of a crosslinker results in the formation of a network structure that eliminates all macroscopic mobility in the material.

Investigations on the selective pervaporation of volatile organic compounds and the enantioselective properties of cholesteric liquid crystalline membranes have been reported. [66, 82, 89, 119] In addition, there have been several studies of side-chain LCPs focusing on the relationship between polymer microstructure and transport properties. [64, 68-70, 72, 120] For example Kawakami et. al.[72] have shown that the overall permeability of a LC polysiloxane with side chain mesogenic groups was governed by an activated diffusion mechanism as has been observed in other glassy polymers. In this particular case, the transport properties were dominated by the polysiloxane main chain, which has higher flexibility and free volume. On the other hand, the solubility increased with increasing temperature above the T_g apparently due to the increased sorption of the penetrant gas in the increasingly disordered liquid crystalline domains. In a series of similar studies, Chen and Hsiue have demonstrated that transport in liquid crystalline polymers does not necessarily follow a biphasic model[67]. In addition, Chen and Hsiue have examined the transport properties of a PDMS –side-chain LCP over a large temperature range spanning the glassy, nematic and isotropic states of the LCP.[69] Discontinuities in permeation were observed at the glass transition temperature and close to the nematic-isotropic transition. Permeation rates in the isotropic state were very fast and were attributed to the formation of micropores or cracks with convective flow. Sorption of the various penetrants also increased with temperature and the magnitude of this increase was related to the state of order of the mesogenic groups. Chen and Hsiue have also studied cross-linked LC polymers, showing that crosslinking significantly increased the permeability of the side-chain LCPs, most likely because it disrupts the packing order of the mesogenic units.[68]

The problem of LCP membrane stability has limited the study and potential industrial applications of these materials. LCPs often have relatively low viscosities in the liquid crystalline state, leading to failure

of the membranes. In addition, the mechanism of gas transport through LCP films has not been understood. Herein we report on the fabrication and gas transport behavior of cross-linked acrylate-based liquid crystal elastomer membranes. Gas permeation behavior has been studied for varying degrees of cross-linking and over a range of temperatures covering the nematic and isotropic phases, providing insight into the mechanism for transport in LCP materials.

8.3 Materials

2-Ethyl hexyl acrylate (2-EHA, b.p. 91 °C/13mbar, Sigma Aldrich) was distilled with DPPH as a stabilizer under vacuum prior to use. 2-Hydroxy-2-methylpropiophenone (b.p. 110 ˚C, Sigma Aldrich, 97%) , ethylene glycol dimethacrylate (EGDMA, b.p. 98 °C/5mmHg, Sigma Aldrich, 98%), tetrahydrofuran (THF, b.p. 66 ˚C, Sigma Aldrich, 99.9%) and ethanol (b.p. 78.4 ˚C, Decon Labs, 100%) were used as received.

8.4 Experimental Methods

Thermal characteristics of the cross-linked acrylate materials were determined using differential scanning calorimetry (DSC). Samples were tested using a Perkin Elmer Diamond DSC with an intercooler 2P unit. Samples were cycled from -50 ˚C to 175 ˚C at a rate of 10 ˚C/min. Phase transition temperatures were determined using the second heating-cooling cycle.

SAXS and WAXD experiments were performed using a Rigaku S-Max 3000 system, equipped with a copper rotating anode emitting X-rays with a wavelength of 0.154 nm (Cu Kα). The calibration standard for both SAXS and WAXD was silver behenate. SAXS patterns were obtained using a 2D gas-filled multiwire proportional counting detector, and a Rigaku RAXIA-DI was used to read WAXD sample image plates. Exposure times of 2 hours were used for all SAXS and WAXD measurements. A Linkam Scientific Instruments temperature controller was used to control sample temperature. Ramp rates 10 ˚C/min were used and the sample was allowed to equilibrate for 30 minutes prior to exposure.

Single gas permeation runs were performed using a constant volume-variable pressure permeation apparatus. Permeate volume was determined using a Swagelok 500 ml stainless steel cylinder. The permeate side was held at approximately 0.2 cmHg and the cylinder at approximately 1

cmHg. The two volumes were then equilibrated and the volume of the permeate side was determined using a mass balance. Membrane permeability was determined using the following relation:

$$\mathrm{P} = \frac{\mathrm{N_A l}}{\mathrm{p_2 - p_1}} \qquad (8.1)$$

P is the permeability, N_A is the gas flux across the membrane, l is the membrane thickness, and p_2 and p_1 are the feed and permeation pressures, respectively. The permeability can be related to the diffusivity and the solubility:

$$\mathrm{P} = \mathrm{DS} \qquad (8.2)$$

Where D and S are the diffusivity and solubility of a gas in the membrane. Membrane selectivities are defined based on permeability, diffusivity, and solubility as follows: $\alpha_{PAB} = \frac{P_A}{P_B}$, $\alpha_{DAB} = \frac{D_A}{D_B}$, and $\alpha_{SAB} = \frac{S_A}{S_B}$ where the subscripts refer to gas A and gas B.

Mixed gas permeation runs were performed using a constant pressure-variable volume apparatus. A Shimadzu GC-2014 with a Restek Rt-Alumina PLOT column and an automated 6-port valve were used to separate and measure the concentration of membrane permeate stream. The permeabilities of propane and propylene under mixed gas conditions was calculated using the following equation:

$$P_{C_3H_i} = \frac{x_{1,C3Hi} S_F l}{x_s^p A(P_2 x_{2,C3Hi} - P_1 x_{1,C3Hi})} \qquad (8.3)$$

where P_{C3Hi} is the permeability of propane or propylene. A subscript of 1 denotes the permeate side of the membrane and a subscript of 2 denotes the feed side of the membrane. P is the partial pressure of propane and propylene, *x* is the mole fraction of the feed or permeate stream, S_F is the sweep flow rate in the permeate gas (N_2 or He), A is the active separation area, and l is the thickness of the membrane. Permeation is an activated process and can be fitted using an Arrhenius equation.[121]

$$\mathrm{P} = \mathrm{P_o} \exp(-\frac{\mathrm{E_A}}{\mathrm{RT}}) \qquad (8.4)$$

E_A is the apparent activation energy of permeation, T is the system temperature and R is the ideal gas constant.

8.5 Synthesis and Membrane Fabrication

8.5.1 Synthesis of LC monomer, 11-(4-cyanobiphenyl-4´-yloxy)undecyl methacrylate

The synthesis of 11-(4-cyanobiphenyl-4´-yloxy)undecyl methacrylate was performed using a two-step synthesis via a Williamson and esterification reaction. A general scheme is shown in Figure 8.1.

8.5.1.1 Synthesis of 4′-(11-hydroxy-undecyloxy)-4-biphenylcarbonitrile

5.8 grams of 4'-hydroxy-4-biphenylcarbonitrile (30 mmol), 11.3 grams of 11-bromo-1-undecanol (45 mmol), and 8.0 grams of annealed K_2CO_3 (60 mmol) were added to 150 mL of acetone. The solution was bubbled with nitrogen for several minutes, sealed, and heated to reflux for 72 hours. After cooling to a room temperature, solid present in the solution was filtered off. The solvent in the filtrate was removed under reduced pressure. The resulting solid was recrystallized several times in heptane. M.p. 98-100 °C, yield – 43%. ^{1}H NMR data (300 MHz, $CDCl_3$): 7.58 (dd,4H, ortho, meta to –CN), 7.46 (d, 2H, meta to alkoxy), 6.92 (d, 2H, ortho to alkoxy), 3.93 (t, 2H, Ph–O–CH_2–), 3.58 (q, 2H, –CH_2–OH), 1.79 (qui, 2H, –O–CH_2–CH_2–), 1.19 to 1.56 (m, 16H, aliphatic).

8.5.1.2 Synthesis of 11-(4-cyanobiphenyl-4´-yloxy)undecyl methacrylate

2.0 grams of *(3)* (5.5 mmol) and 830 µL of triethylamine (6 mmol) was dissolved in 20 mL of dry THF. The solution was cooled to -5 °C using ethanol and dry ice. 0.8 mL of a freshly distilled methacryloyl chloride (8 mmol) in 5 mL of THF was added drop wise to the solution. The solution was stirred at a temperature of 0-5^{o}C for several hours followed by several days at room temperature to ensure the reaction went to completion. Triethylammonium chloride was filtered off and the solvent in the filtrate was removed under reduced pressure. The resulting solid was recrystallized several times in methanol. M.p. 75-77 °C, yield – 63%. ^{1}H NMR data (300 MHz, $CDCl_3$): 7.58 (dd, 4H, ortho, meta to –CN), 7.46 (d, 2H, meta to alkoxy), 6.92 (d, 2H, ortho to alkoxy), 5.48 and 6.04 (s+s, 2H, CH_2=C(CH_3)–), 3.93 (t, 2H, Ph–O–CH_2–), 3.58 (q, 2H, –CH_2–OH), 1.79 (qui, 2H, –O–CH_2–CH_2–), 1.19 to 1.56 (m, 16H, aliphatic).

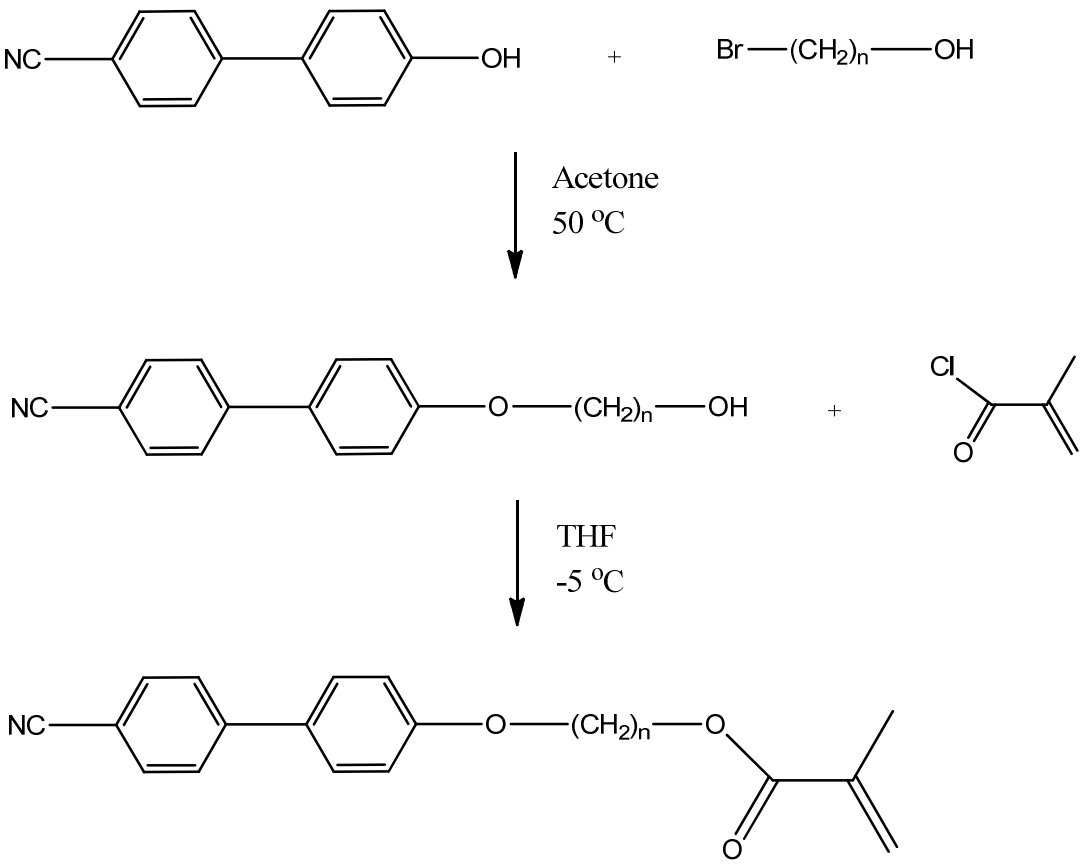

Figure 8.1: Synthesis of liquid crystalline monomer, 11-(4-cyanobiphenyl-4´-yloxy)undecyl methacrylate

8.5.2 Membrane Fabrication Procedure

The membrane fabrication apparatus is shown in Figures 8.2 and 8.3. A PTFE dense film with a rectangular orifice is sandwiched between two glass plates and is securely clamped together. A groove in the inner side of one glass plate allows for the injection of the reaction mixture. The apparatus is designed to minimize solvent loss due to evaporation and inhibition of the reaction caused by the presence of oxygen. The glass plates allow a UV light source to be used to initiate the polymerization.

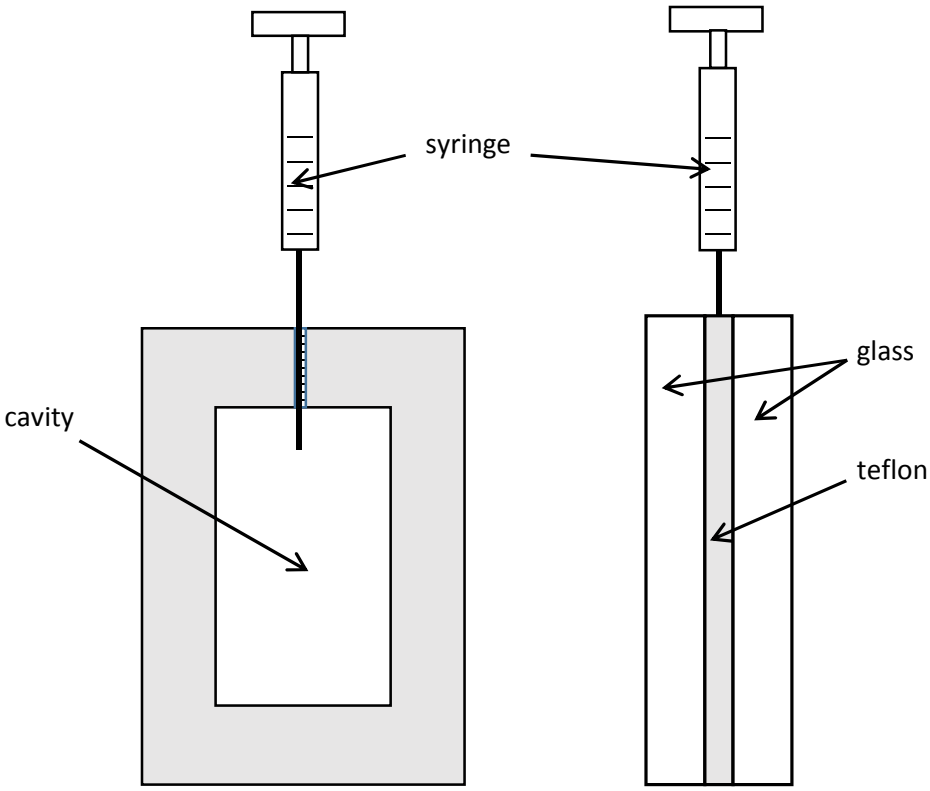

Figure 8.2: Schematic of the sandwich cell used for membrane fabrication via in situ free radical polymerization.

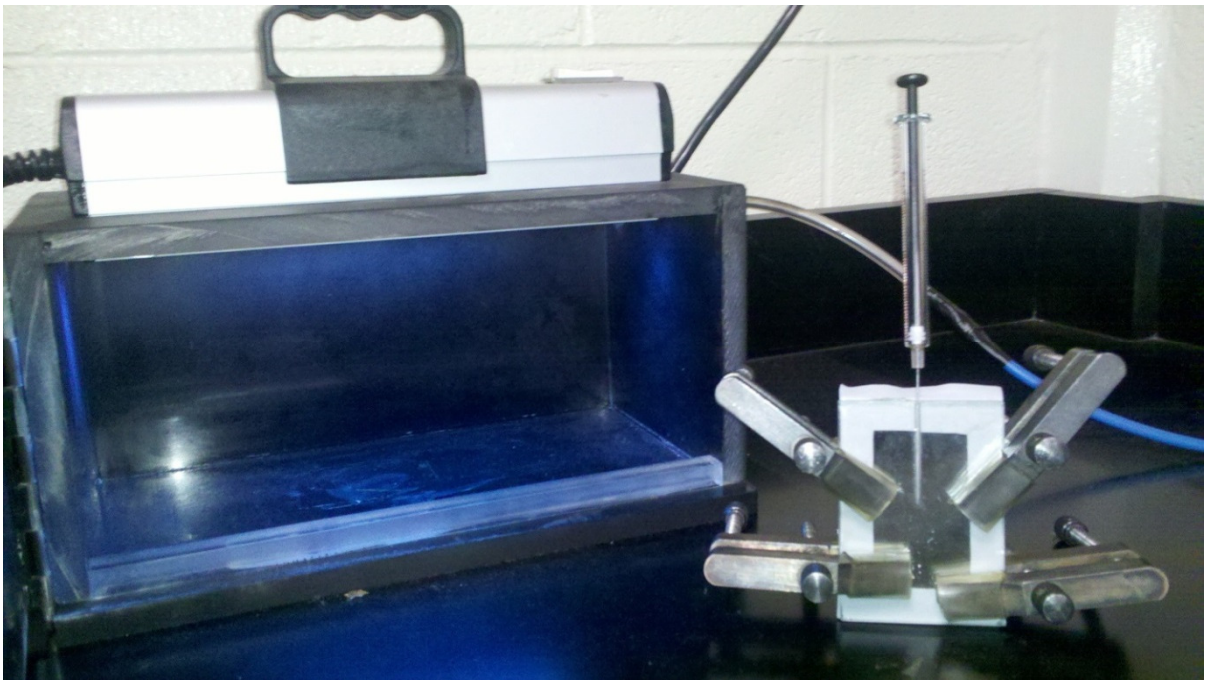

Figure 8.3: Photograph of the reaction cell and UV chamber.

Cross-linked LCP membranes were fabricated using 2.5 or 5.0 mol% crosslinker and 75 mol.% LC comonomer (denoted **CNBPh75_2.5** and **CNBPh75_5.0** respectively) according to the following procedure. 150 mg (0.33 mmol) of 11-(4-cyanobiphenyl-4´-yloxy)undecyl methacrylate, 2.1 µl of EGDMA (0.11 mmol, CNBPh75_2.5) or 4.2 µl of EGDMA (0.22 mmol, CNBPh75_5.0), 22.5 µl (0.11 mmol) 2-EHA, and 1.8 µl (0.12 mmol) Daracure were dissolved in 337.5 ml of THF to achieve a concentration of 1.3 mmol of comonomer per 1 mL of THF. The solution was bubbled with nitrogen for one minute and injected into the membrane reaction chamber. The chamber was blanketed with nitrogen and the injection port was sealed using silicone caulk. The sealed chamber was then exposed to a short wave UV source (254 nm) for 72 hours. Extraction of the membrane and removal of residual unpolymerized components was accomplished with several cycles of solvent swelling and exchange. THF was added dropwise to the membrane followed by immersing the membrane in ethanol for several minutes. The membrane was then placed under vacuum for 48 hours to remove residual solvent. The chemical structure of the cross-linked acrylate membrane is depicted in Figure 8.3. Figure 8.4 is an image of the resulting membrane. The film thickness was approximately 120 µm. This is the first example of a LC acrylate based cross-linked film to be produced as a membrane. The membrane was masked using aluminum tape and placed in a permeation cell. To avoid hysteresis and to further minimize any residual solvent affects the membrane chamber was degassed at 90 ˚C for 48 hours and cooled back to room temperature using a ramp rate of 5 ˚C/min. All permeation runs were performed from low to high temperature. The membrane and permeation cell were degassed for 5 hours between each permeation experiment.

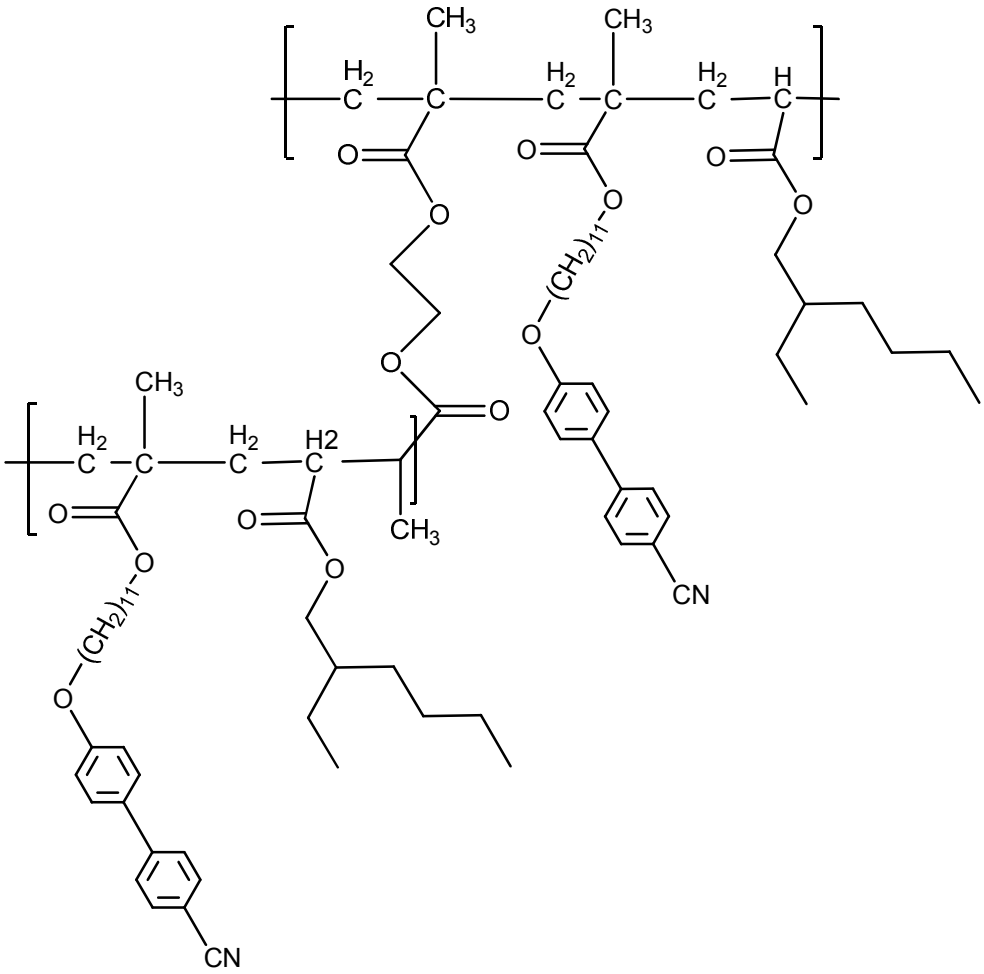

Figure 8.4: Chemical structure of the cross-linked liquid crystal polymer membrane.

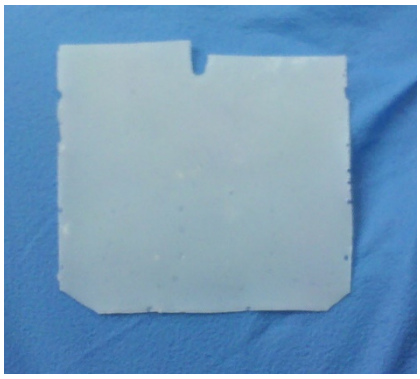

Figure 8.5: Image of the final CNBPh75_2.5 membrane following the swelling, solvent exchange and solvent evaporation steps.

8.6 Results and Discussion

8.6.1 The Dependence of LC Ordering on Crosslinker and Temperature

The phase behavior of the cross-linked CNBPh75_2.5 and CNBPh75_5.0 membranes were characterized using DSC. Figure 8.5 shows DSC isobars at temperatures between -50 °C and 150 °C. The glass transition temperature of CNBPh_5.0 (T_g = 12.2 °C) is slightly higher than that of CNBPh75_2.5 (T_g = 17.0 °C) due to the higher degree of cross-linking in the polymer structure. In addition the temperature of the LC/isotropic phase transition decreased from 73.5 °C for CNBPh75_2.5 to 63.4 °C for CNBPh75_5.0 as the degree of cross-linking increased. Chemical crosslinking imposes constraints on the motion of the chain segments that disrupts the formation of the ordered mesophase,[32] resulting in a decrease in the mesophase temperature range with increasing crosslinker content. The change in enthalpy of the LC/isotropic transition also decreases with increasing crosslinker content, indicating that the CNBPh75_2.5 samples (ΔH = 4.1 J/g) are more ordered than the CNBPh75_5.0 samples (ΔH= 2.3 J/g). Results are summarized in Table 8.1.

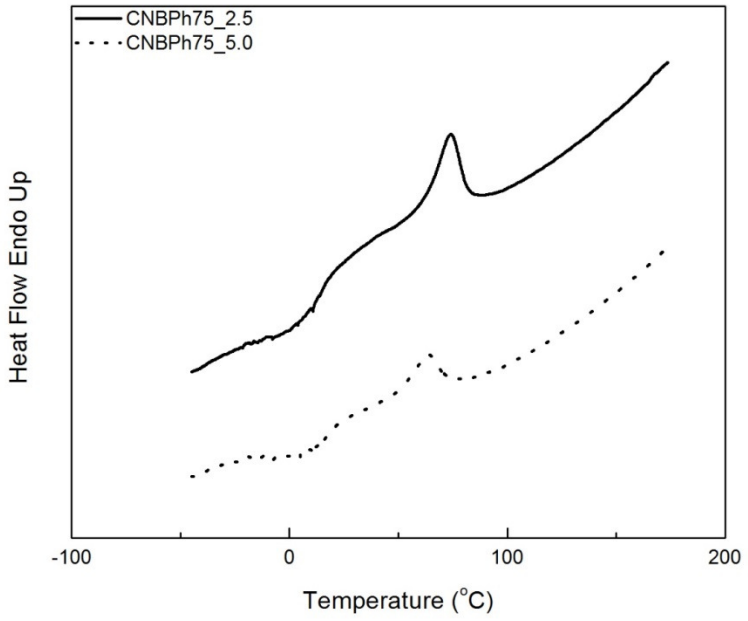

Figure 8.6: DSC heating curve for the CNBPh75_2.5 and CNBPh75_5.0 membranes.

Table 8.1: Summary of DSC data for CNBPh75_2.5 and CNBPh75_5.0 films.

Sample	Run	T_g (°C)	T_m (°C)	ΔH (J/g)
CNBPh75_2.5	Heating	12.2	73.5	4.1
CNBPh75_5.0	Heating	17.0	63.4	2.3

WAXD and SAXS experiments were conducted to characterize the type of LC mesophase present in the films and to determine the effect of temperature on the ordering of crosslinked LC material. Based on the DSC results, an LC mesophase is expected for CNBPh75_2.5 between 12.2 ˚C and 73.5 ˚C and an isotropic phase at higher temperatures. Figure 8.6 contains SAXS and WAXD data for CNBPh75_2.5 at 30 ˚C (LC), 50 ˚C (LC) and 100 ˚C (isotropic). The absence of a peak in the small angle region and the presence of a broad peak in the wide angle region (2ϑ = 19.1°) is characteristic of a nematic phase.[35] The corresponding average distance between mesogenic units is 4.6 Å. This peak is observed at temperatures of 30 ˚C and 50 ˚C. The WAXD data taken at 100 °C displays only a broad diffuse peak and is characteristic of an amorphous polymer.[122] The decrease in peak intensities from 30 ˚C to 50 ˚C indicates that the mesogens become less ordered as temperature increases within the mesophase.

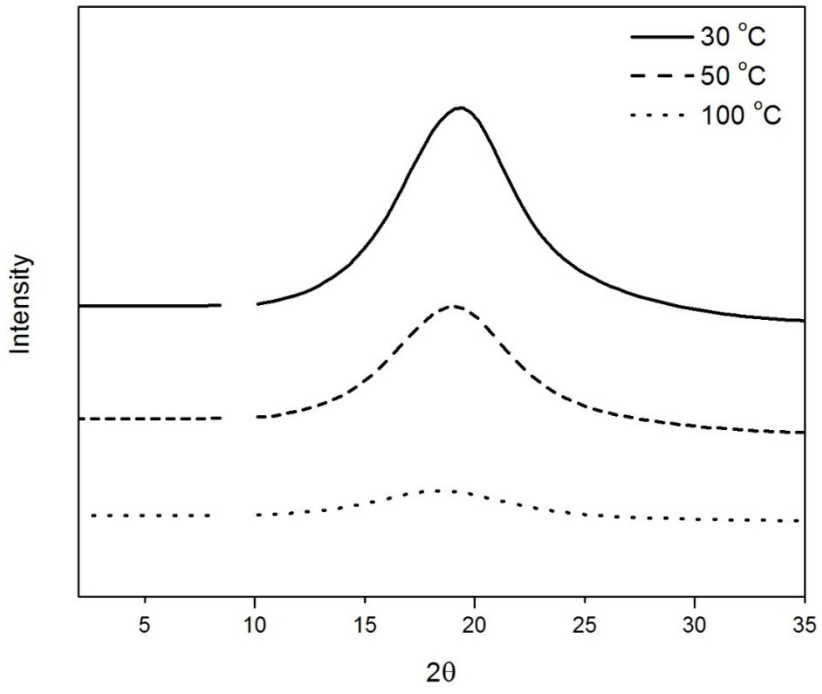

Figure 8.7**:** X-ray diffractograms of CNBPh75_2.5 at temperatures in the LC mesophase (30 °C and 50 °C) and isotropic phase (100 °C).

8.6.2 Permeability and Diffusivity Through LC Crosslinked Membranes

The results of single gas permeability measurements for CO_2, CH_4, H_2, propane, and propylene in CNBPh75_2.5 and CNBPh75_5.0 membranes are shown in Figure 8.7 and Figure 8.8 respectively. The measurements were performed over a range of temperatures both above and below the nematic/isotropic phase transition. As expected, an increase in permeability with incrasing temperature is observed for all gases and both membranes. Gas permeability is in increasing order of CH_4 > propane > propylene > H_2 > CO_2. In addition, increasing the crosslinker content from 2.5 mol% to 5.0 mol% results in a decrease in permeability for all gases studied. This indicates that the higher crosslinker content reduces the segmental motion of the polymer backbone, leading to a reduction in the diffusivity of the penetrant molecule and a lower permeability.[123]

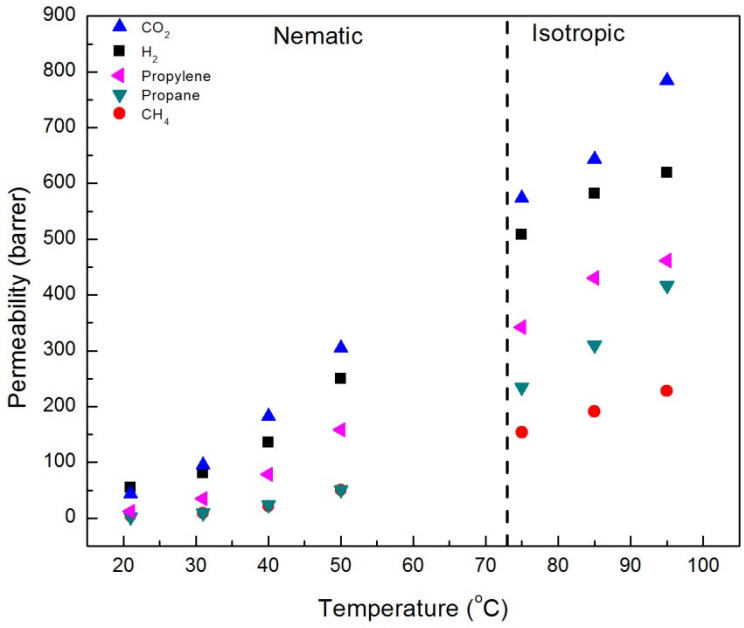

Figure 8.8: Single gas permeability for membrane CNBPh75_2.5 plotted as a function of temperature in the nematic and isotropic phases.

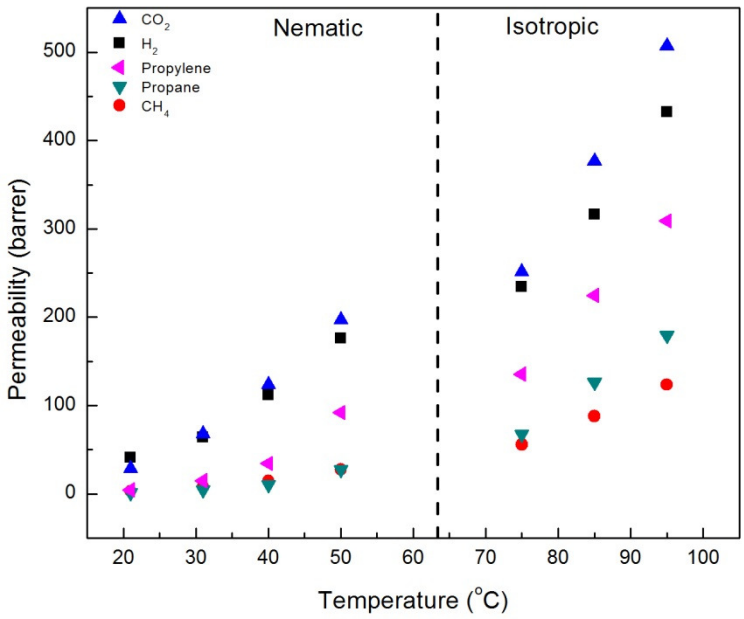

Figure 8.9: Single gas permeability for membrane CNBPh75_5.0 plotted as a function of temperature in the nematic and isotropic phases.

Figure 8.9 and Figure 8.10 contain plots of the diffusivities of gases in the CNBPh75_2.5 and CNBPh75_5.0 membranes respectively determined using the time-lag method. Diffusivity increases with temperature and the diffusivity decreases with increasing crosslinker content for all gases studied. This confirms that the increased cross-link density in the CNBPh75_5.0 membrane leads to decreased polymer backbone mobility. Diffusivities for the different gases studied were clearly dependent on the size of the penetrant molecule and decreased with increasing Lennard-Jones gas diameter: H_2 (2.83 Å) > CH_4 (3.76 Å) > CO_2 (3.94 Å) > propylene (4.68 Å) > propane (5.12 Å). This is consistent with the kinetic model proposed in the literature, which assumes that the diffusion of molecules occurs as a series of consecutive jumps facilitated by the temporal opening of the polymer matrix as a result of molecular fluctuations.[93]

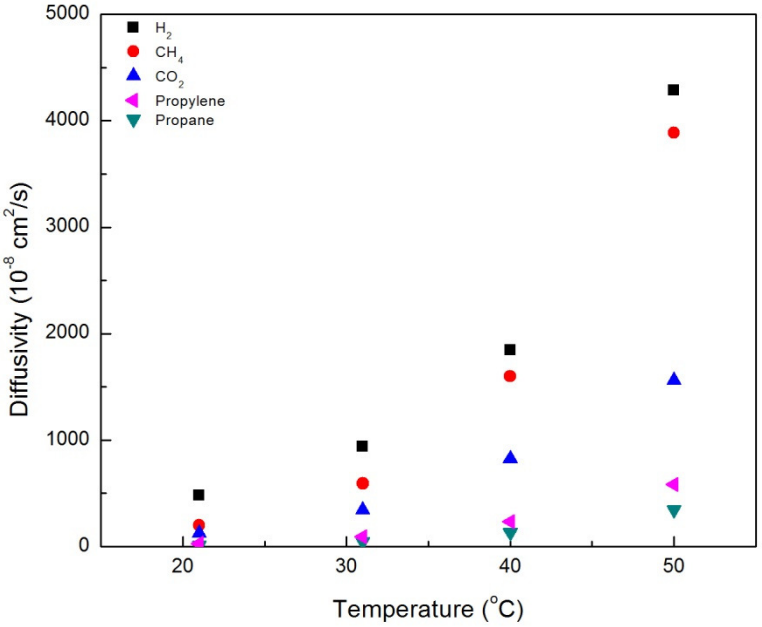

Figure 8.10: Diffusivity of various gases in the membrane CNBPh75_2.5 in the nematic phase.

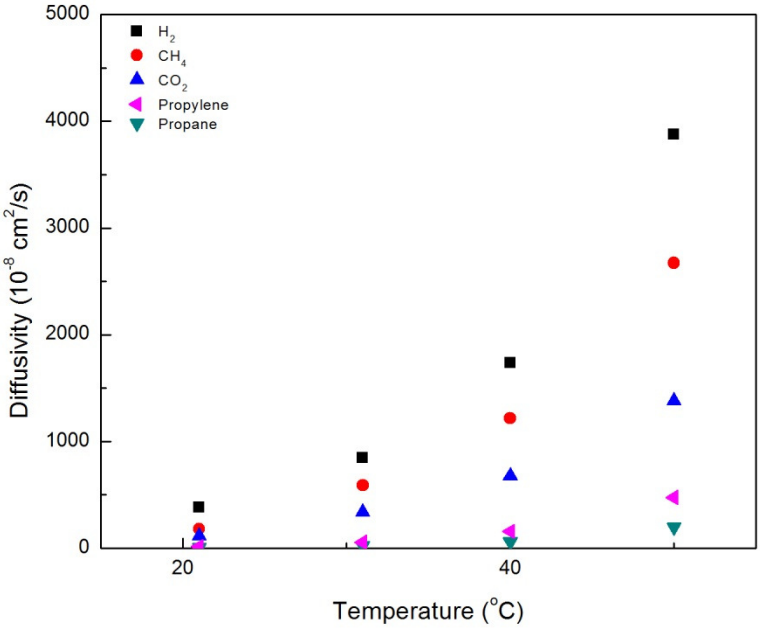

Figure 8.11: Diffusivity of various gases in the membrane CNBPh75_5.0 in the nematic phase.

8.6.3 Permeability Selectivity Dependence on Temperature and Crosslinker Density

Permeability selectivity values for the CNBPh75_2.5 and CNBPh75_5.0 membranes were calculated for the gas pairs propylene/propane, H_2/CH_4 and CO_2/CH_4 and are plotted over a range of temperatures in the nematic and isotropic phases in Figures 8.11, 8.12, and 8.13 respectively. The value of permeability selectivity decreased with increasing temperature for all gas pairs and for both membranes. The highest observed selectivities were $\alpha_{propane/propylene}$ = 6.4, α_{H2CH4} = 15, and $\alpha_{CO2/CH4}$ = 12 which were obtained at a temperature of 21 °C in the CNBPh75_2.5 membrane. In the nematic state CNBPh75_2.5 had a higher permeability selectivity than CNBPh75_5.0 at lower temperatures for all gas pairs; however, the permeability selectivity decreased more rapidly with increasing temperature in the CNBPh75_2.5 membrane so that at a temperature of 35-40 °C the CNBPh75_5.0 membrane exhibited higher selectivities. The CNBPh75_5.0 membrane also exhibited higher permeability selectivities for all temperatures and gas pairs in the isotropic state.

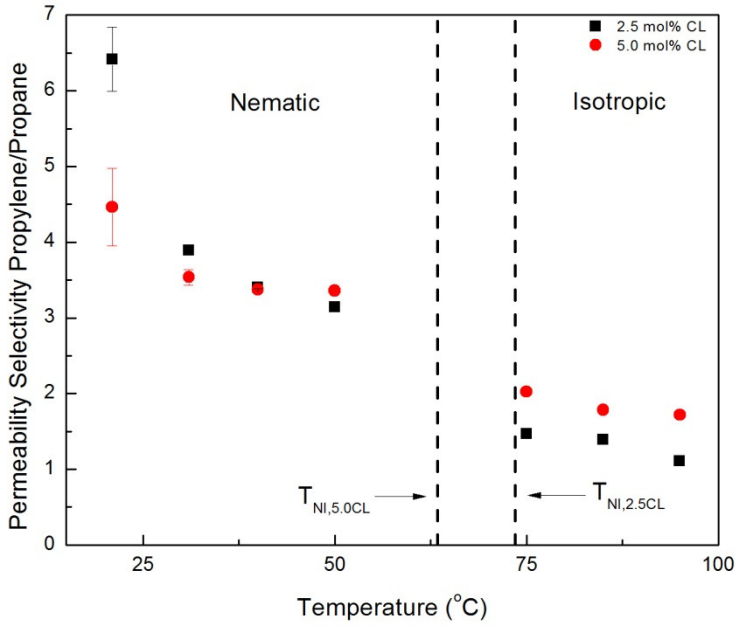

Figure 8.12: Propylene/propane permeability selectivity in the nematic and isotropic phases.

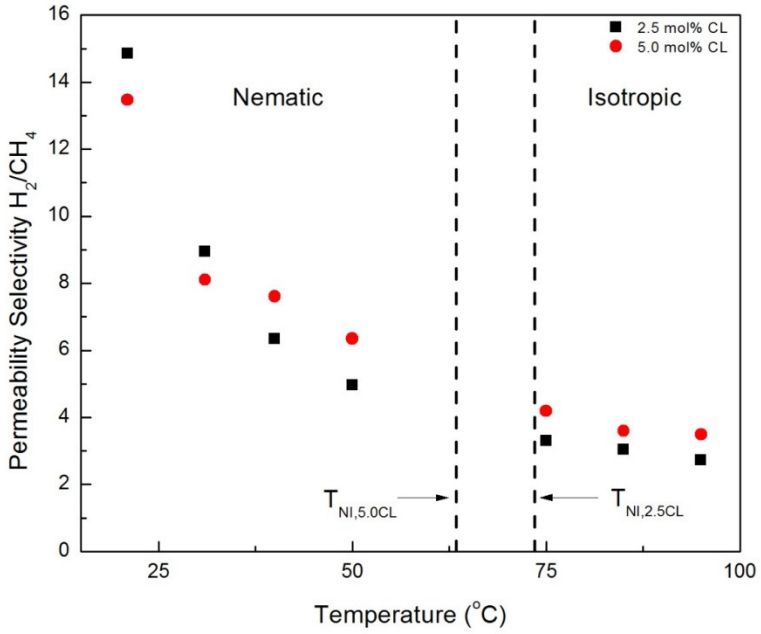

Figure 8.13: H_2/CH_4 permeability selectivity in the nematic and isotropic phases.

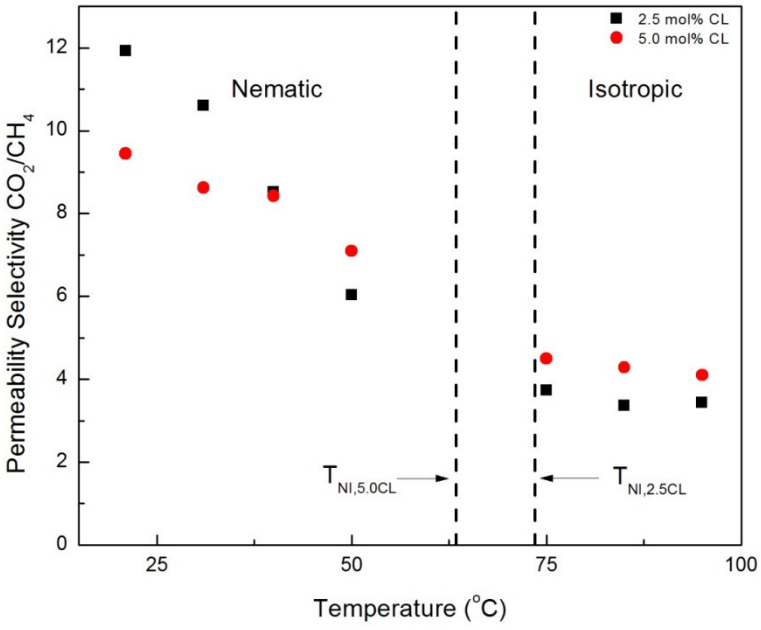

Figure 8.14: CO_2/CH_4 permeability selectivity in the nematic and isotropic.

8.6.4 Diffusion Selectivity Dependence on Temperature and Crosslinker Density

The crossover of permeability selectivity between the CNBPh75_2.5 and CNBPh75_5.0 membranes with increasing temperature in the nematic phase is attributed to differences in the temperature dependent diffusion selectivity in each membrane. Figures 8.14-8.16 compare diffusion selectivity in the CNBPh75_2.5 and CNBPh75_5.0 membranes for the gas pairs propylene/propane, H_2/CH_4 and CO_2/CH_4 over a range of temperatures in the nematic and isotropic phases. Diffusion selectivities for propylene/propane and H_2/CH_4 exhibited a similar dependence on temperature and crosslinker content as permeability selectivities. In the nematic phase, the CNBPh75_2.5 membranes exhibited higher diffusion selectivities at lower temperatures compared to the CNBPh75_5.0 membranes. At higher temperatures, the CNBPh75_5.0 membranes exhibited higher diffusion selectivities. CO_2/CH_4 diffusion selectivity in the CNBPh75_2.5 membrane is lower than that in the CNBPh75_5.0 membranes for all temperatures studied. In the nematic state, CO_2/CH_4 diffusion selectivity in the CNBPh75_2.5 membrane decreased with increasing temperature at a higher rate than CNBPh75_5.0. The fact that the CO_2/CH_4 diffusion selectivities for both membranes were less than one over the whole temperature range suggests that interactions between the quadrupole of CO_2 and the polar mesogens inhibit diffusion. The permeability selectivity remains greater than one because of the higher CO_2 solubility in the membrane, again due to favorable interactions between the CO_2 molecules and the polar mesogens. Increasing the temperature passed the isotropic transition resulted in an increase in CO_2/CH_4 selectivities, which further indicates these interactions can inhibit diffusion.

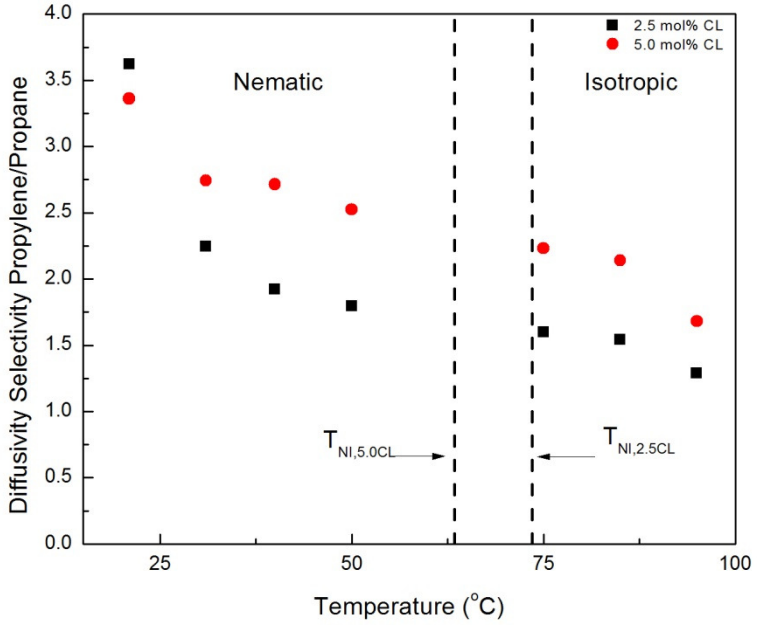

Figure 8.15: Propylene/propane diffusivity selectivity in the nematic and isotropic phases.

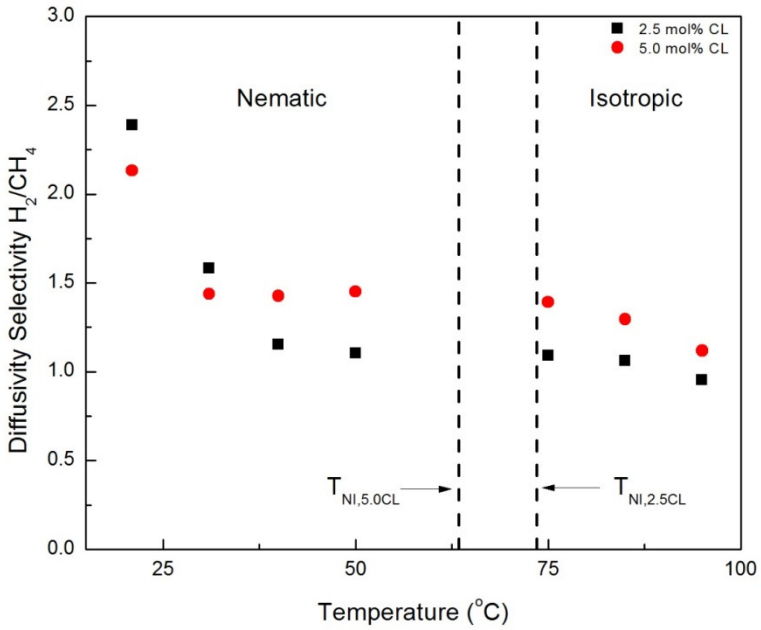

Figure 8.16: H_2/CH_4 diffusivity selectivity in the nematic and isotropic phases.

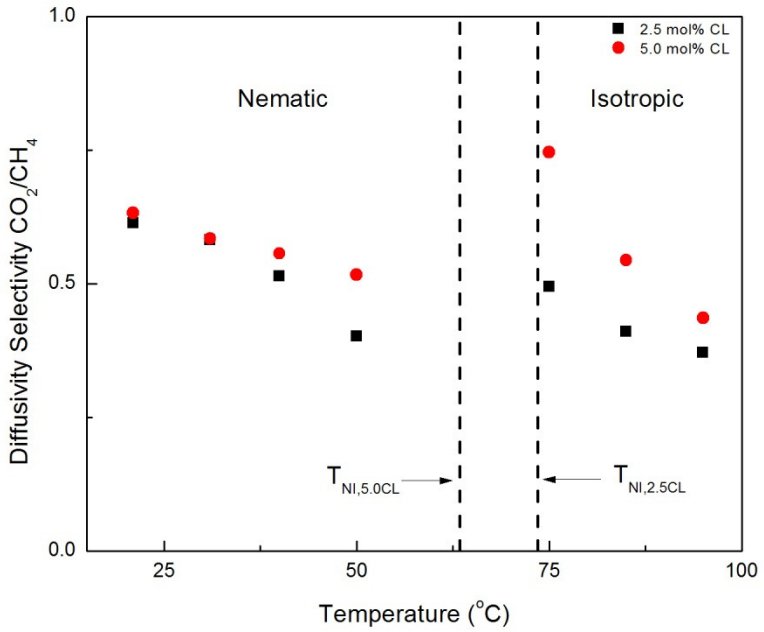

Figure 8.17: CO_2/CH_4 diffusivity selectivity in the nematic and isotropic.

WAXD experiments confirmed that the mesogens have higher ordering at lower temperatures in the LC phase compared to higher temperatures in the LC phase. In addition, DSC experiments determined CNBPh75_2.5 has a higher degree of ordering compared to CNBPh75_5.0. This resulted in higher diffusion selectivities at lower temperatures for membrane CNBPh75_2.5. This leads to the conclusions that ordering at lower LC temperatures has a greater effect on diffusion selectivity than polymer mobility. At higher LC temperatures, ordering for both membranes was reduced and resulted in a higher diffusion selectivity for membrane CNBPh75_5.0. A performance tradeoff between mesogen ordering and polymer mobility is present. This indicates penetrant gases are selectively diffusing between both LC mesogens and polymer backbones respectively.

8.6.5 The Effect of LC Phase and Crosslinker Density on Solubility of Gases

Calculated solubility values are shown in Figure 8.17 and Figure 8.18, for CNBPh75_2.5 and CNBPh75_5.0 membranes respectively. The permeability increase with temperature is result of the behavior of solubility and diffusion. The solubility of all penetrants decreases with temperature. This decrease is overcome by the large increase in diffusion. Solubilities for all gases were higher in the CNBPh75_2.5 membranes than the CNBPh75_5.0 membranes in the nematic and isotropic phase,

indicating that gas sorption decreases with an increasing crosslink density. The increase in crosslinker density decreased the free volume and segmental mobility of the material (diffusion results) which can This decrease in sorption is due to a decrease in the material free volume as crosslinker content increases.[124]

In general, the solubility decreases with increasing temperature in both the nematic and isotropic phases, however, there are distinct changes in behavior across the nematic/isotropic transition. In the isotropic phase, the relative solubilities of the gases studied are ordered (from highest to lowest solubility) propane > propylene > CO_2 > H_2 > CH_4. In contrast, the ordering of solubilities in the nematic state is propylene > CO_2 > propane > H_2 > CH_4. Thus propylene and CO_2, the more polar gases, exhibit higher solubilities than the non-polar gases in the nematic phase. Both membranes exhibited this behavior. This suggests that increased sorption of the polar penetrants is due tothe ordering of the LC mesogens. The increased interactions between the polar gas molecules and the mesogenic groups are attributed to ordering of the mesogens in the nematic mesophase.

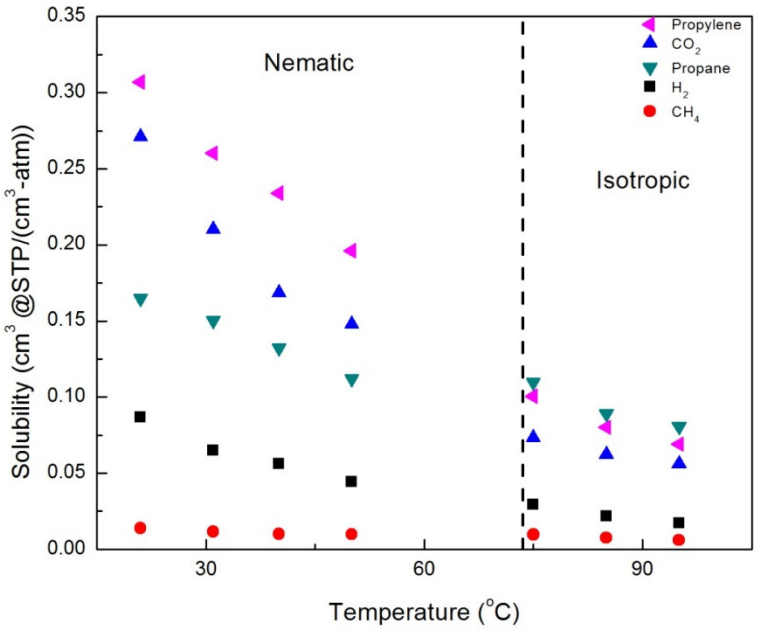

Figure 8.18: Solubilities for gases in the membrane CNBPh75_2.5 in the nematic and isotropic phases.

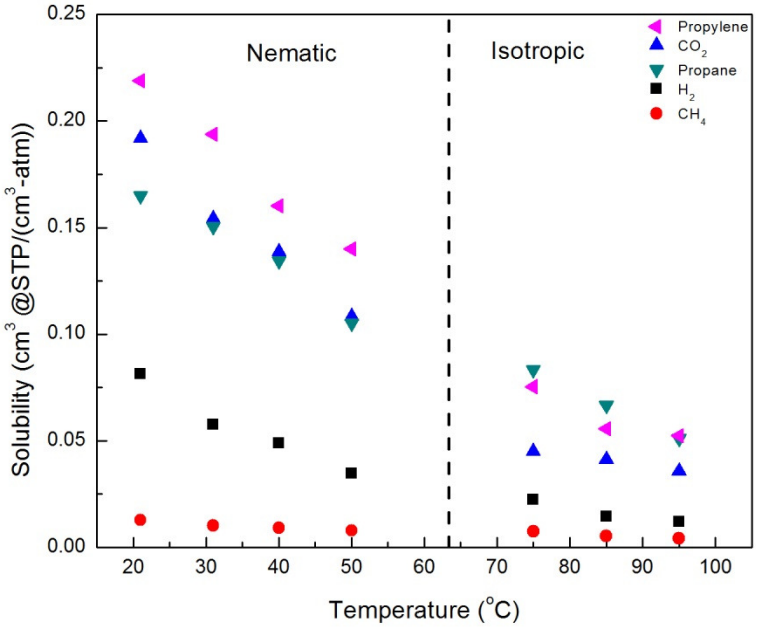

Figure 8.19: Solubilities for gases in the membrane CNBPh75_5.0 in the nematic and isotropic phases.

8.6.6 Activation Energies of Gas Transport in the Nematic and Isotropic LC Phase

Permeability is an activated process and follows Arrhenius behavior. [121] Figure 8.19 is an Arrhenius plot of ln(permeability) vs 1/T for transport in the CNBPh75_2.5 membrane. Activation energies were obtained from the slopes of the linear fits in both the nematic and isotropic phases and are reported in Table 8.2 and Table 8.3. The activation energy for permeation is higher in the nematic phase than the isotropic phase for all gases studied. This is expected, as the ordering in the nematic phase acts as a barrier to transport, and is in agreement with activation energies for transport in small molecule LC materials.[119] The relative activation energies for different gases do not correlate directly with the size of the gas molecules, indicating that interactions between the gases and polymer are important. In addition, the amount of crosslinker had little effect on the activation energies in the nematic state. The activation energies in the isotropic state were higher for membrane CNBPh75_5.0.

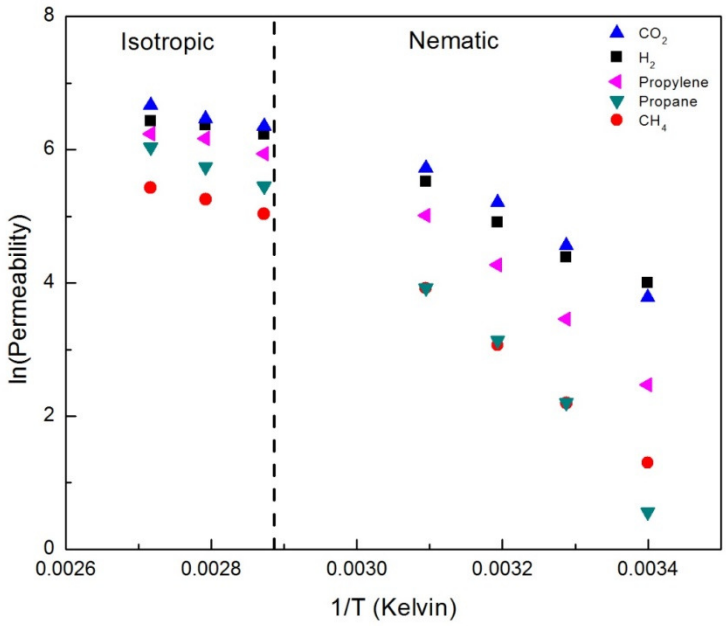

Figure 8.20: Arrhenius plot of permeability for gases in the CNBPh75_2.5 membrane.

Table8.2: Summary of mesophase and isotropic activation energies for CNBPh75_2.5

KJ/mol-K	**H_2**	**CO_2**	**Propylene**	**CH_4**	**Propane**
Isotropic E_A	10.5	16.5	16.0	20.9	30.8
Nematic E_A	41.8	53.3	72.3	71.8	91.2

Table 8.3: Summary of mesophase and isotropic activation energies for CNBPh75_5.0

KJ/mol-K	**H_2**	**CO_2**	**Propylene**	**CH_4**	**Propane**
Isotropic E_A	32.6	37.4	43.2	42.4	52.6
Nematic E_A	40.5	52.6	76.4	61.0	88.1

8.6.7 Mixed Gas Permeation of Propylene and Propane

Mixed gas permeation measurements were performed with a 50/50 propane/propylene gas mixture for CNBPh75_2.5. Figure 8.20 shows permeability and selectivity measurements at several

temperature in the nematic and isotropic state. A propylene/propane permeability selectivity of approximately 6 and a propylene permeability of 17 barrers were obtained at 25 °C. Permeability increased and selectivity decreased with increasing temperature. For all temperatures in the nematic state, mixed gas propylene permeabilities are in good agreement with single gas runs. The permeability of propane was depressed by the presence of propylene which can be seen by higher mixed gas propylene/propane selectivities. This behavior is commonly found in glassy polymers.[95] Table 8.4 summarizes activation energies of propane and propylene mixed gas permeation.

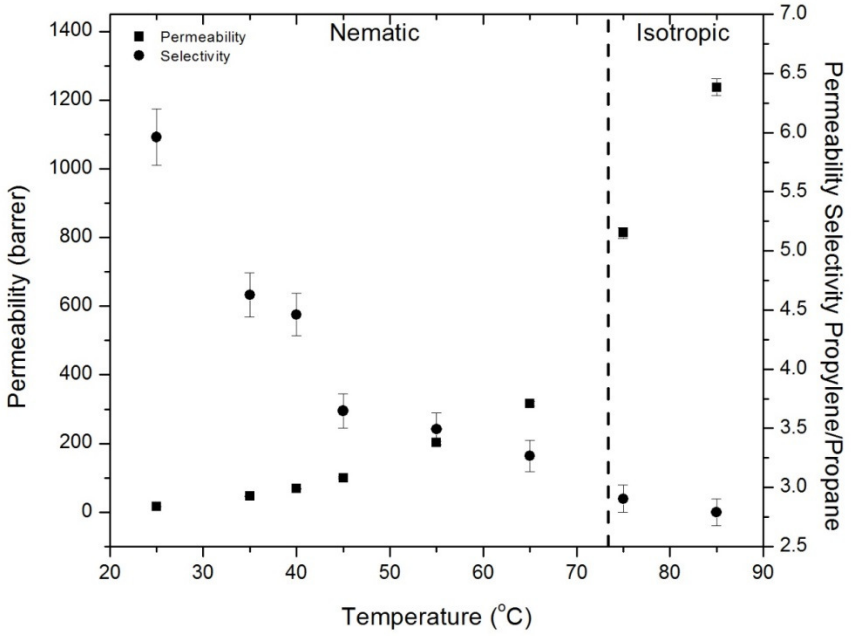

Figure 8.21: Mixed gas permeability and permeability selectivity for polypropylene and propane in the CNBPh75_2.5 membrane in the nematic and isotropic phases.

Table 8.4: Summary of mixed gas mesophase and isotropic activation energies for CNBPh75_2.5

KJ/mol-K	**Propane**	**Propylene**
Isotropic E_A	47.6	43.4
Nematic E_A	71.9	65.8

8.7 Conclusions

The development of a membrane fabrication scheme using a free radical polymerization technique, with a methacrylate cyanobiphenyl monomer, 2-EHA and ethylene glycol dimethacrylate (EGDMA) lead to the first reported acrylate-based cross-linked LCP film. Two membranes with 2.5 mol% (CNBPh75_2.5) and 5.0 mol% (CNBPh75_5.0) crosslinker were investigated. The ordering of LCP networks were dependent on temperature under the nematic/isotropic transition. X-ray scattering showed a decrease in molecular ordering with an increase in temperature. In addition, a decrease in the enthalpy of of the nematic-isotropic transition was observed with a higher crosslinker content. This indicates that the mesogens order more efficiently for membranes containing a lower crosslinker content because the cross-links limit the mobility of the mesogenic side chains. An increase in crosslinker content decreased the permeability for all gases tested (CO_2, CH_4, H_2, propane and propylene) due to a decrease in the diffusiivity. Within the LC phase of both membranes, the diffusivity increased with increasing temperature. In addition, the diffusivity of CNBPh75_2.5 increased at a higher rate resulting in a lower diffusion selectivity than that observed for the CNBPh75_5.0 membrane. This behavior is attributed to an interplay between the effect of LC morphology and polymer mobility. Trends in the gas solubility indicate that the ordering of the mesogens in the nematic phase enhanced interactions between the LCP and polar penetrant molecules. The solubilities of CO_2 and propylene were significantly higher in the nematic state than in the isotropic state. Mixed gas permeation experiments using propylene and propane resulted in an increase in propylene/propane permeability selectivity compared to that observed for single gas experiments. This is expected and is attributed to the effect of competitive transport between the propane and propylene molecules.

Chapter 9: Concluding Remarks and Recommendations

We have reported on the preparation and characterization of three different types of liquid crystal based membrane materials (polymer dispersed liquid crystals – PDLCs; linear side-chain liquid crystal polymers – LCPs; and cross-linked side-chain LCPs) and we have examined the gas permeation behavior in each of these materials. The separation of propylene and propane has received particular attention due to the important industrial applications of the separation and to the difficulty of achieving the separation with conventional membrane materials. The important conclusions and contributions from the work are summarized below.

An examination of the transport properties of the low molecular weight liquid crystal (LC) 4-octyl-4'-cyanobiphenyl (8CB) blended with the thermoplastic polymer polysulfone (PSf) revealed a strong dependence of the gas transport properties on the morphology of the membrane. Sorption of propane and propylene in pure 8CB decreased when crossing the nematic to isotropic transition. In addition, diffusion selectivity of propylene/propane increased upon crossing the isotropic/nematic transition. Polymer dispersed liquid crystals (PDLCs,) where isolated LC domains a surrounded by a polymer matrix, formed above a threshold LC concentration due to solubility differences between 8CB and PSf. The phase separation between the two constituents resulted in phase behavior that was governed by temperature and 8CB concentration. The blending of 8CB in PSf decreased the glass transition temperature of the polymer matrix. Interestingly, this plasticization effect enhanced the gas transport properties of PSf and resulted in an increase in both permeability and selectivity at temperatures below the T_g. An increase in LC concentration corresonded with a decrease in propane permeability resulting in an increase in selectivity for propylene over propane. Overall selectivities were low and membrane stability remained an issue at higher LC compositions. As a result, it was decided to examine LCP materials as an alternative to PDLCs.

The gas transport behavior of a cyanobiphenyl based side-chain LCPwith a polybutadiene di ol backbone was investigated. The linear polymer, possessing comb-like attached mesogens, exhibited a stable smectic LC mesophase. The linear LCP was impregnated in a porous PTFE support for gas transport studies. Diffusion dominated transport was observed in the glassy state. A selectivity of approximately 30 was found for He/CH_4. Gas transport in the smectic phase was solubility dominated. The mesogen mobility increased with increasing temperature in the mesophases, and the segmental motion of the mesogenic units facilitated the sorption of propylene resulting in an increase in solubility selectivity for

propylene with temperature. As a result, the permeability selectivity had a local maxima in the smectic phase near the isotropic transition. Permeability increased with temperature over the whole range studied. Selectivity decreased above the smectic/isotropic transition temperature. Increasing the feed pressure enhanced propylene selectivity by increasing propylene solubility and decreasing propane solubility. Mixed gas permeability measurements resulted in slightly higher selectivities than single gas experiments due to preferential interactions between the LCP and the polar propylene molecules. LCP single gas sorption experiments agreed well with the results of the membrane permeability experiments.

LCP membrane stability was an issue and we found it important to investigate the phase dependent viscoelastic behavior of the LCP material. To achieve this a scheme to synthesize LCP materials with improved long term stability was developed. LCPs based on Methoxy- or butoxy-substituted azobenzene mesogens grafted onto the double bonds of poly(butadiene)diol exhibited LC mesophases. The phase behavior was strongly dependent on the grafting densities of the LCs due to the cohesive forces between the mesogens. The transition from a glassy state to a semi-crystalline phase results in a large loss in the elastic properties in comparison to samples with a lower degree of grafting undergoing a direct glassy state/nematic transition. Therfore, viscoelastic properties for membrane applications can be enhanced by using higher degrees of grafting. The long term membrane stability for the LCP material was predicted using a time-temperature superposition. G' and G" decreased with a decrease in the superimposed frequency. This suggested that crosslinked LCPs are necessary to eliminate macroscopic mobility and produce membranes with long term stability.

Nitroazobenzene (A) or cyanobiphenyl (B) based mesogenic side chains were synthesized and characterized in the scope of demonstrating the use of free radical polymerization as means of producing networked LCPs. The introduction of the mesogenic monomers into the polymer structure significantly influenced the T_g values of the resulting copolymers, with the T_g increasing with mesogen content. Liquid crystalline mesophases were observed in copolymers containing at least 44 mol% of A or 36 mol% of B. The mesophases were identified as smectic A single layer (polymers containing A) or smectic A bilayer (polymers containing B.) The preference for these phases is due to the presence of the polarizable group in the comonomer structure. Increasing mesogenic comonomer content also lead to a broadening of the temperature intervals over which the LC mesophases were stable.

The development of a membrane fabrication scheme using a free radical polymerization technique, with a methacrylate cyanobiphenyl monomer, 2-EHA and ethylene glycol dimethacrylate (EGDMA) lead to the first recorded acrylate LCP networked film. The ordering of LCP networks were dependent on temperatures under the nematic/isotropic transition. X-ray scattering showed a decrease

in molecular ordering with an increase in temperature. In addition, a decrease in the enthalpy of transition was observed for increasing crosslinker content. This indicated that mesogens order more efficiently for membranes containing a lower crosslinker content. Two membranes with 2.5 mol% EGDMA (CNBPh75_2.5) and 5.0 mol% EGDMA (CNBPh75_5.0) crosslinker were investigated. An increase in crosslinker depressed permeability for all gases tested (CO_2, CH_4, H_2, propane and propylene) due to a decrease in the diffusions. Within the LC phase of both membranes, diffusion decreased with increasing temperature. In addition, diffusion of CNBPh75_2.5 decreased at a higher rate resulting in a higher diffusion selectivity for membrane CNBPh75_5.0. This behavior is attributed to an interplay between the effect of LC morphology and polymer mobility. In addition, LC mesogens in the ordered state enhanced interactions with polar constituents. Solubilities of CO_2 and propylene significantly increased in the nematic state compared to solubilities in the isotropic state. An increase in propylene/propane permeability selectivity was observed for mixed gas permeability measurements due to a lower propane permeability compared to single gas runs.

The work reported here has resulted in an increased understanding of the gas transport in liquid crystalline membranes. In particular, the use of side-chain LCPs as membrane materials shows promise for separations wherein a polarity difference can be exploited between gas species. In addition, the transport can be tuned by altering both the polymer structure (mesogen ratio, cross-link density, mesogen type, etc…) and by varying the temperature across multiple phases (e.g. glassy, smectic, nematic, isotropic.) Some recommendations for future work in this area are included in the next chapter.

We have studied the gas transport properties of propane, propylene and several light gases through three liquid crystal (LC) membrane systems. Preferential permeation of polar gases was observed at conditions with higher LC ordering. PDLC and L-BDLCP membranes showed highest selectivities in the smectic state. The crosslinked cyanobiphenyl membranes increase solubility and diffusion selectivities at conditions of highest mesogenic ordering. However, permeability and permeability selectivity was dependent on the segmental motion of the material. The plasticization of a polymer using LC material resulted in an increase in permeability and selectivity. In addition, L-BDLCP exhibited an increase in permeability and permeability selectivity with increasing temperature in the smectic mesophase. This was attributed to a “freeze” effect on LC mesogens caused by the rigidity of the polymer backbone and LC mesogens. Furthermore, a higher crosslinker density increased permeability selectivities at higher temperatures within the nematic phase, which was attributed to a loss in polymer backbone mobility. There is an interplay between molecular ordering and mobility which are effected by temperature, mesomorphic phase, crosslinker density and glass transition temperature and behavior.

Due to membrane stability concerns, the study of liquid crystal material for gas separation applications has been limited to only a few research groups. At high liquid crystal temperatures and in the isotropic phase, liquid crystal viscoelastic properties are negatively affected. To address this concern we developed a synthetic process that enables us to polymerize stabile crosslinked LCP membranes. This gives us the opportunity to further investigate the gas transport capability of LC materials. LC and alkyl comonomer ratios affect the mesophase and glass transition temperature and ordering, In addition, alkyl length can be varied without changing the fundamental chemistry. Chain length alters the phase behavior, mesophase structure, layer arrangements and free volume of LCP material.[26-27, 36-37] In addition, it would be interesting to investigate the effects of several polarizable group on propylene/LC intermolecular interactions.

References

1. Tschierske, C., Liquid crystalline materials with complex mesophase morphologies. *Current Opinion in Colloid & Interface Science* **2002,** *7* (1-2), 69-80.
2. Geary, J. M.; Goodby, J. W.; Kmetz, A. R.; Patel, J. S., The mechanism of polymer alignment of liquid-crystal materials. *Journal of Applied Physics* **1987,** *62* (10), 4100-4108.
3. Satyendra, K., Liquid Crystals. *Cambridge University Press* **1994**.
4. Demchenko, Y. A.; Studenovský, M.; Sedláková, Z.; Sikora, A.; Baldrian, J.; Ilavský, M., Formation, structure, thermal and dynamic mechanical behavior of polyurethane networks based on a diethanolamine derivative with mesogenic group. *European Polymer Journal* **2003,** *39* (8), 1521-1531.
5. Mysliwiec, J.; Czajkowski, M.; Miniewicz, A.; Kochalska, A.; Sedlakova, Z.; Nespurek, S., Grafted polybutadiene for fast retrieval of optical information. *Journal of Applied Physics* **2009,** *106* (5), 053108-4.
6. Grell, M.; Bradley, D. D. C.; Inbasekaran, M.; Woo, E. P., A glass-forming conjugated main-chain liquid crystal polymer for polarized electroluminescence applications. *Advanced Materials* **1997,** *9* (10), 798-802.
7. Goodyby, J., Liquid Crystal and Life. *Liquid Crystals* **1996,** *24* (1), 25-38.
8. Hsu, C.-S., The application of side-chain liquid-crystalline polymers. *Progress in Polymer Science* **1997,** *22* (4), 829-871.
9. Bunjes, H.; Rades, T., Thermotropic liquid crystalline drugs. *Journal of Pharmacy and Pharmacology* **2005,** *57* (7), 807-816.
10. Simonov, A. N.; et al., Holographic recording in films of azo-containing LC polymers in the presence of orienting electric field. *Quantum Electronics* **2000,** *30* (7), 635.
11. Park, Y.; Skelland, A. H. P.; Forney, L. J.; Kim, J.-H., Removal of phenol and substituted phenols by newly developed emulsion liquid membrane process. *Water Research* **2006,** *40* (9), 1763-1772.
12. Burducea, G., Lyotropic Liquid Crystals II. Structural Polymorphism. *Romanian Reports in Physics* **2004,** *56* (1), 87-100.
13. Panizza, P.; Archambault, P.; Roux, D., Effects of Shear on the Smectic A Phase of Thermotropic Liquid Crystals. HAL - CCSD: 1995.
14. Deuling, H. J., Deformation of Nematic Liquid Crystals in an Electric Field. *Mol. Cryst. Liquid Cryst.* **1972,** *19*, 123 - 131.
15. Jerome, B., Surface effects and anchoring in liquid crystals. *Reports on Progress in Physics* **1991,** *54* (3), 391.
16. Kumar, S., *Liquid Crystals: Experimental Study of Physical Properties and Phase Transitions*. Combridge University Press: 2001; p 483.
17. Chandrasekhar, S., *Frontmatter*
Liquid Crystals. Cambridge University Press: 1992.
18. Madhusudana, N. V., Statistical theories of nematic liquid crystals. *Bull. Mater Sci.* **1981,** *3*, 119-131.
19. Eelkema, R.; Feringa, B. L., Amplification of chirality in liquid crystals. *Organic & Biomolecular Chemistry* **2006,** *4* (20), 3729-3745.
20. Goodby, J. W., Chirality in liquid crystals. *Journal of Materials Chemistry* **1991,** *1* (3), 307-318.
21. Rodríguez, F. J.; Sánchez, C.; Villacampa, B.; Alcalá, R.; Cases, R.; Millaruelo, M.; Oriol, L., Optical anisotropy and non-linear optical properties of azobenzene methacrylic polymers. *Polymer* **2004,** *45* (7), 2341-2348.

22. Poláková, L.; Sedláková, Z.; Látalová, P., Synthesis and thermal behavior of telechelic poly(butadiene)diols with azobenzene-based liquid-crystalline units in side chains. *Polymer Bulletin* **2010,** *64* (4), 315-326.
23. Bladon, P.; Warner, M., Elasticity of nematic networks and nematic effects in conventional rubbers. *Macromolecules* **1993,** *26* (5), 1078-1085.
24. Brehmer, M.; Zentel, R., Ferroelectric liquid-crystalline elastomers with short switching times. *Macromolecular Rapid Communications* **1995,** *16* (9), 659-662.
25. Ilavsky, M.; Nedbal, J.; Polakova, L.; Sedlakova, Z., Thermal and Dielectric Behavior of Liquid-Crystalline Polybutadiene-Diols with Mesogenic Groups in Side Chains. *AIP Conference Proceedings* **2008,** *982* (1), 440-445.
26. Seiji, U.; Wataru, M.; Kazuyoshi, I., Influence of spacer length on liquid crystal microstructures of branched polyethyleneimines with mesogenic pendent groups. *Polym. J.* **2012,** *44* (6), 561-566.
27. Hu, T. H.; Yi, J.; Xiao, J. B.; Zhang, H. L., Effect of flexible spacer length on the mesophase structures of main-chain/side-chain liquid crystalline polymers based on ethyl cellulose. *Polym. J.* **2010,** *42* (9), 752-758.
28. Ilavsky, H. V. Z. S. J. N. M., Formation, structure, thermal and dynamic mechanical behavior of ordered polyurethane networks based on mesogenic diol. *European Polymer Journal* **2001,** *37*, 1511-1517.
29. Bubnov, A.; Kaspar, M.; Sedlakova, Z.; Ilavsky, M., Chiral liquid crystalline thiols for preparation of polybutadiene diols. *Liquid Crystals* **2008,** *35* (5), 653-660.
30. Jigounov, A.; Sedláková, Z.; Kripotou, R.; Pissis, P.; Nedbal, J.; Baldrian, J.; Ilavský, M., Dielectric and thermal behavior of liquid crystalline comb-like polybutadiene-diols with mesogenic groups in side chains. *Polymer* **2007,** *48* (19), 5721-5733.
31. Kourilová, H.; Stastná, J.; Hanyková, L.; Sedláková, Z.; Spevácek, J., 1H NMR study of temperature-induced phase separation in solutions of poly(N-isopropylmethacrylamide-co-acrylamide) copolymers. *European Polymer Journal* **2010,** *46* (6), 1299-1306.
32. Zhou, X.-h. W. H.-l. T. Y.-x. L. D. Z. X.-f. C. H.-l. Z. Q.-f., A New Strategy for the Design of Liquid Crystalline Polymers With Flexible and Apolar Building Blocks. *Chinese Journal of Polymer Science* **2003,** *21* (1), 21-27.
33. Xu, G.; Hou, J.; Zhu, S.; Yang, X.; Xu, M.; Zhou, Q., The peculiarity of side-chain liquid crystalline polymers with mesogenic units attached directly in a side-on mode. *Polymer* **1994,** *35* (25), 5441-5446.
34. Davidson, P., Selected Topics in X-Ray Scattering by Liquid-Crystalline Polymers. In *Liquid Crystals II*, Mingos, D., Ed. Springer Berlin / Heidelberg: 1999; Vol. 95, pp 1-39.
35. Pragliola, S.; Ober, C. K.; Mather, P. T.; Jeon, H. G., Mesogen-jacketed liquid crystalline polymers via stable free radical polymerization. *Macromolecular Chemistry and Physics* **1999,** *200* (10), 2338-2344.
36. Pereira, F. V.; Borsali, R.; Ritter, O. M. S.; Gonçalves, P. F.; Merlo, A. A.; Silveira, N. P. d., Structure-property relationships of smectic liquid crystalline polyacrylates as revealed by SAXS. *Journal of the Brazilian Chemical Society* **2006,** *17*, 333-341.
37. Pardey, R.; Zhang, A.; Gabori, P. A.; Harris, F. W.; Cheng, S. Z. D.; Adduci, J.; Facinelli, J. V.; Lenz, R. W., Monotropic liquid crystal behavior in two poly(ester imides) with even and odd flexible spacers. *Macromolecules* **1992,** *25* (19), 5060-5068.
38. Wu, S.-T.; Efron, U.; Hess, L. D., Birefringence measurements of liquid crystals. *Appl. Opt.* **1984,** *23* (21), 3911-3915.
39. Dierking, I., *Textures of Liquid Crystals*. Wiley-VCH 2003.
40. Nehring, J.; Saupe, A., On the schlieren texture in nematic and smectic liquid crystals. *Journal of the Chemical Society, Faraday Transactions 2: Molecular and Chemical Physics* **1972,** *68*, 1-15.
41. Kawanishi, Y.; Tamaki, T.; Seki, T.; Sakuragi, M.; Suzuki, Y.; Ichimura, K.; Aoki, K., Multifarious liquid crystalline textures formed on a photochromic azobenzene polymer film. *Langmuir* **1991,** *7* (7), 1314-1315.

42. Belfield, M. A. Q. K. D., Synthesis, Characterization and Texture Observations of Calamitic Liquid Crystalline Compounds. *International Journal of Molecular Science* **2009,** *10*, 4772-4788.
43. Wang, X.; Zhou, Q. F.; Zhou, Q., *Liquid crystalline polymers*. World Scientific Pub. Co.: 2004.
44. Bernardo, P.; Drioli, E.; Golemme, G., Membrane Gas Separation: A Review/State of the Art. *Industrial & Engineering Chemistry Research* **2009,** *48* (10), 4638-4663.
45. Graham, T., LV. On the absorption and dialytic separation of gases by colloid septa. *Philosophical Magazine Series 4 32* (218), 401 - 420.
46. Merkel, T. C.; Bondar, V. I.; Nagai, K.; Freeman, B. D.; Pinnau, I., Gas sorption, diffusion, and permeation in poly(dimethylsiloxane). *Journal of Polymer Science Part B: Polymer Physics* **2000,** *38* (3), 415-434.
47. Kamiya, Y.; Terada, K.; Mizoguchi, K.; Naito, Y., Sorption and partial molar volumes of organic gases in rubbery polymers. *Macromolecules* **1992,** *25* (17), 4321-4324.
48. Koros, W. J.; Paul, D. R., CO2 sorption in poly(ethylene terephthalate) above and below the glass transition. *Journal of Polymer Science: Polymer Physics Edition* **1978,** *16* (11), 1947-1963.
49. Costello, L. M.; Koros, W. J., Effect of structure on the temperature dependence of gas transport and sorption in a series of polycarbonates. *Journal of Polymer Science Part B: Polymer Physics* **1994,** *32* (4), 701-713.
50. Toi, K.; Morel, G.; Paul, D. R., Gas sorption and transport in poly(phenylene oxide) and comparisons with other glassy polymers. *Journal of Applied Polymer Science* **1982,** *27* (8), 2997-3005.
51. Paul, D. R., *Polymeric gas separation membranes*. CRC Press: 1994.
52. Staudt-Bickel, C.; J. Koros, W., Improvement of CO2/CH4 separation characteristics of polyimides by chemical crosslinking. *Journal of Membrane Science* **1999,** *155* (1), 145-154.
53. Bos, A.; Pünt, I. G. M.; Wessling, M.; Strathmann, H., Plasticization-resistant glassy polyimide membranes for CO2/CO4 separations. *Separation and Purification Technology* **1998,** *14* (1–3), 27-39.
54. Bos, A.; Pünt, I. G. M.; Wessling, M.; Strathmann, H., Suppression of CO2-plasticization by semiinterpenetrating polymer network formation. *Journal of Polymer Science Part B: Polymer Physics* **1998,** *36* (9), 1547-1556.
55. Chern R, T.; Koros W, J.; Hopfenberg H, B.; Stannett V, T., Material Selection for Membrane-Based Gas Separations. In *Materials Science of Synthetic Membranes*, American Chemical Society: 1985; Vol. 269, pp 25-46.
56. Amerongen, G. J. V., The Permeability of Different Rubbers to Gases and Its Relation to Diffusivity and Solubility. *Journal of Applied Physics* **1946,** *17* (11), 972-985.
57. Masuda, T.; Iguchi, Y.; Tang, B.-Z.; Higashimura, T., Diffusion and solution of gases in substituted polyacetylene membranes. *Polymer* **1988,** *29* (11), 2041-2049.
58. Chen, G.-H. S., Jurgen, Sorption and Diffusion of Gases in Liquid Crystalline Substances. *Mol. Cryst. Liq. Cryst.* **1999,** *339*, 31-44.
59. Kajiyama, T.; Washizu, S.; Takayanagi, M., Membrane structure and permeation properties of poly(vinyl chloride)/liquid crystal composite membrane. *Journal of Applied Polymer Science* **1984,** *29* (12), 3955-3964.
60. Kawakami, H.; Tsucla, K.; Yamane, K.; Nishide, H.; Tsuchida, E., Oxygen-binding and transport in the liquid crystal membrane containing cobaltporphyrin as an oxygen carrier. *Polymers for Advanced Technologies* **1990,** *1* (5-6), 319-323.
61. Li, X.-G.; Huang, M.-R.; Gang, L., Temperature dependence and stability of oxygen enrichment through liquid crystalline triheptyl cellulose-containing membranes cast from three solvents. *Journal of Membrane Science* **1996,** *116* (2), 143-148.
62. Li, X.-G.; Huang, M.-R.; Hu, L.; Lin, G.; Yang, P.-C., Cellulose derivative and liquid crystal blend membranes for oxygen enrichment. *European Polymer Journal* **1999,** *35* (1), 157-166.

63. Kajiyama, T.; Nagata, Y.; Washizu, S.; Takayanagi, M., Characterization and gas permeation of polycarbonateliquid crystal composite membrane. *Journal of Membrane Science* **1982,** *11* (1), 39-52.
64. Głowacki, E.; Horovitz, K.; Tang, C. W.; Marshall, K. L., Photoswitchable Gas Permeation Membranes Based on Liquid Crystals. *Advanced Functional Materials* **2010,** *20* (17), 2778-2785.
65. Inui, K.; Okazaki, K.; Miyata, T.; Uragami, T., Effect of mesogenic groups on characteristics of permeation and separation for benzene/cyclohexane mixtures of side-chain liquid-crystalline polymer membranes. *Journal of Membrane Science* **1998,** *143* (1-2), 93-104.
66. Inui, K.; Miyata, T.; Uragami, T., Effect of permeation temperature on permeation and separation of a benzene/cyclohexane mixture through liquid-crystalline polymer membranes. *Journal of Polymer Science Part B: Polymer Physics* **1998,** *36* (2), 281-288.
67. Chen, D.-S., Gas sorption in side-chain liquid crystalline polymers. *Polymer* **1993,** *35* (13).
68. Chen, D.-S.; Hsiue, G.-H., Gas transport properties of linear and crosslinked side-chain liquid crystalline polymers with variable spacer lengths. *Die Makromolekulare Chemie* **1993,** *194* (7), 2025-2033.
69. Chen, D.-S.; Hsiue, G.-H.; Hsu, C.-S., Gas permeation through a side-chain liquid-crystalline polysiloxane-based membrane. *Die Makromolekulare Chemie* **1991,** *192* (9), 2021-2029.
70. Chen, D.-S.; Hsiue, G.-H.; Hsu, C.-S., Gas permeation through two side-chain liquid-crystalline polyacrylate-based membranes containing 4-methoxyphenyl 4-hexyloxybenzoate or 4-cyanophenyl 4-hexyloxybenzoate mesogenic side groups. *Die Makromolekulare Chemie* **1992,** *193* (6), 1469-1479.
71. Kanehashi, S., Analysis of permeability; solubility and diffusivity of carbon dioxide; oxygen; and nitrogen in crystalline and liquid crystalline polymers. *Journal of Membrane Science* **2010**.
72. Kawakami, H., Gas transport properties of liquid crystalline polysiloxane with laterally attached side chain. *Journal of Membrane Science* **1997,** *133*, 245-253.
73. Yoshimizu, H. T., Mitsuhiro; Suzuki, Tomoyuki; Toida, Jiro; Ando, Aisuke; Watanabe, Junji; Tsujita, Yoshiharu, Layered structure and Xe sorption and diffusion properties of low-density liquid-crystalline polyesters with n-alkyl side chains. *Journal of Molecular Structure* **2004**, 19-26.
74. Dobb, M.; McIntyre, J., Properties and applications of liquid-crystalline main-chain polymers Liquid Crystal Polymers II/III. Platé, N., Ed. Springer Berlin / Heidelberg: 1984; Vol. 60, pp 61-98.
75. Chiou, J. S.; Paul, D. R., Gas transport in a thermotropic liquid-crystalline polyester. *Journal of Polymer Science Part B: Polymer Physics* **1987,** *25* (8), 1699-1707.
76. Weinkauf, D. H.; Paul, D. R., Gas transport properties of liquid crystalline poly (ethylene terephthalate-co-p-oxybenzoate). *Journal of Polymer Science Part B: Polymer Physics* **1991,** *29* (3), 329-340.
77. Hu, Y. S.; Wang, H. P.; Schiraldi, D. A.; Hiltner, A.; Baer, E., Oxygen-transport properties of liquid-crystalline polyesters based on 4,4′-bibenzoic acid. *Journal of Applied Polymer Science* **2007,** *105* (1), 30-37.
78. Hu, Y. S.; Hiltner, A.; Baer, E., Oxygen transport properties of liquid crystalline poly(pentamethylene 4,4'-bibenzoate). *Polymer* **2006,** *47* (11), 4058-4067.
79. Hu, Y. S.; Hiltner, A.; Baer, E., Solid state structure and oxygen transport properties of copolyesters based on smectic poly(hexamethylene 4,4'-bibenzoate). *Polymer* **2006,** *47* (7), 2423-2433.
80. Eldridge, R. B., Olefin/paraffin separation technology: a review. *Industrial & Engineering Chemistry Research* **1993,** *32* (10), 2208-2212.
81. Wentink, A. E.; Kuipers, N. J. M.; de Haan, A. B.; Scholtz, J.; Mulder, H., Olefin isomer separation by reactive extractive distillation: Modelling of vapour–liquid equilibria and conceptual design for 1-hexene purification. *Chemical Engineering and Processing: Process Intensification* **2007,** *46* (9), 800-809.
82. Han, S.; Martin, S. M., Diffusivity and Solubility of Organic Solutes in Supported Liquid Crystal Membranes. *The Journal of Physical Chemistry B* **2009,** *113* (38), 12696-12703.

83. Chen, L. G.; Shanks, R., Thermoplastic polymer-dispersed liquid crystals prepared from solvent-induced phase separation with predictions using solubility parameters. *Liquid Crystals* **2007,** *34* (12), 1349-1356.
84. Czichos, H.; Saito, T.; Smith, L. R.; Smith, L., *Springer handbook of materials measurement methods*. Springer: 2006.
85. Smith, G. W., Mixing and phase separation in liquid crystal/matrix systems: Determination of the excess specific heat of mixing. *Physical Review Letters* **1993,** *70* (2), 198-201.
86. Belfiore, L. A.; Cooper, S. L., Bisphenol-A polycarbonate–diluent interactions. *Journal of Polymer Science: Polymer Physics Edition* **1983,** *21* (10), 2135-2157.
87. Huh, W.; Weiss, R. A.; Nicolais, L., Thermal and rheological properties of blends of polystyrene and thermotropic liquid crystals. *Polymer Engineering & Science* **1983,** *23* (14), 779-783.
88. Chen, D.-S.; Hsiue, G.-H.; Schultze, J. D.; Song, B.; Springer, J., Gas Sorption Properties and Molecular States of a Liquid Crystal. *Molecular Crystals and Liquid Crystals Science and Technology. Section A. Molecular Crystals and Liquid Crystals* **1993,** *237* (1), 85-95.
89. Han, S.; Martin, S. M., Enantioselective cholesteric liquid crystalline membranes characterized using nonchiral HPLC with circular dichroism detection. *Journal of Membrane Science* **2011,** *367* (1–2), 1-6.
90. Fujii, N.; Kawase, Y.; Michinobu, T.; Shigehara, K., Phase transition behavior in side-chain liquid crystal polymers of different chain-backbones. *J. Photopolym Sci. Technol.* **2007,** *20* (1), 17-18.
91. Jigounov, A.; Sedláková, Z.; Spěváček, J.; Ilavský, M., Dynamic mechanical and thermal behavior of liquid-crystalline polybutadiene-diols with mesogenic groups in side chains. *European Polymer Journal* **2006,** *42* (10), 2450-2457.
92. Alexander Stern, S., Polymers for gas separations: the next decade. *Journal of Membrane Science* **1994,** *94* (1), 1-65.
93. Ghosal, K.; Freeman, B. D., Gas separation using polymer membranes: an overview. *Polymers for Advanced Technologies* **1994,** *5* (11), 673-697.
94. Weinkauf, D. H.; Paul, D. R., Gas transport properties of thermotropic liquid-crystalline copolyesters. I. The effects of orientation and annealing. *Journal of Polymer Science Part B: Polymer Physics* **1992,** *30* (8), 817-835.
95. Minelli, M.; Campagnoli, S.; De Angelis, M. G.; Doghieri, F.; Sarti, G. C., Predictive Model for the Solubility of Fluid Mixtures in Glassy Polymers. *Macromolecules* **2011,** *44* (12), 4852-4862.
96. Küpfer, J.; Finkelmann, H., Nematic liquid single crystal elastomers. *Die Makromolekulare Chemie, Rapid Communications* **1991,** *12* (12), 717-726.
97. Okano, K.; Shishido, A.; Tsutsumi, O.; Shiono, T.; Ikeda, T., Highly birefringent liquid-crystalline polymers for photonic applications: synthesis of liquid-crystalline polymers with side-chain azo-tolane mesogens and their holographic properties. *Journal of Materials Chemistry* **2005,** *15* (33), 3395-3401.
98. Mysliwiec, J.; Czajkowski, M.; Miniewicz, A.; Bartkiewicz, S.; Kochalska, A.; Polakova, L.; Sedlakova, Z.; Nespurek, S., Dynamics of photoinduced motions in azobenzene grafted polybutadienes. *Optical Materials* **2011,** *33* (9), 1398-1404.
99. Finkelmann, H.; Happ, M.; Portugal, M.; Ringsdorf, H., Liquid crystalline polymers with biphenyl-moieties as mesogenic group. *Die Makromolekulare Chemie* **1978,** *179* (10), 2541-2544.
100. Hotta, A.; Terentjev, E. M., Dynamic soft elasticity in monodomain nematic elastomers. *Eur Phys J E* **2003,** *10* (4), 291-301.
101. Colby, R. H.; Gillmor, J. R.; Galli, G.; Laus, M.; Ober, C. K.; Hall, E., Linear viscoelasticity of side chain liquid crystal polymer. *Liquid Crystals* **1993,** *13* (2), 233-245.
102. Yu, R.; Yu, W.; Zhou, C.; Feng, J. J., Rheology and relaxation processes in a melting thermotropic liquid–crystalline polymer. *Journal of Applied Polymer Science* **2007,** *104* (6), 3780-3787.

103. Galewski, Z. A. H. K. Z., Liquid crystalline properties of azobenzenes: I. 4-methoxy-, 4-ethoxy-, 4-propoxy- and 4-butoxy-4′-alkyloxyazobenzenes. *Polish Journal of Chemistry* **1999,** *73* (8), 1357-1371.
104. Sperling, L. H., *Introduction to Physical Polymer Science*. Wiley: 2005.
105. Ferry, J. D., *Viscoelastic Properties of Polymers*. Wiley: 1980.
106. Stein, P.; Aßfalg, N.; Finkelmann, H.; Martinoty, P., Shear modulus of polydomain, mono-domain and non-mesomorphic side-chain elastomers: Influence of the nematic order. *Eur Phys J E* **2001,** *4* (3), 255-262.
107. Fourmaux-Demange, V.; Brûlet, A.; Cotton, J. P.; Hilliou, L.; Martinoty, P.; Keller, P.; Boué, F., Rheology of a Comblike Liquid Crystalline Polymer as a Function of Its Molecular Weight. *Macromolecules* **1998,** *31* (21), 7445-7452.
108. Yang, I. K.; Chang, S., The Smectic Rheology of a Polysiloxane Side Chain Liquid Crystalline Polymer. *Journal of Polymer Research* **2002,** *9* (3), 163-168.
109. de Gennes, P. G.; Prost, J., *The Physics of Liquid Crystals*. Clarendon Press: 1995.
110. Finkelmann, H.; Ringsdorf, H.; Wendorff, J. H., Model considerations and examples of enantiotropic liquid crystalline polymers. Polyreactions in ordered systems, 14. *Die Makromolekulare Chemie* **1978,** *179* (1), 273-276.
111. Liu, X.; Jing, Y.; Bai, Y., Controlled/living photopolymerization of methyl methacrylate in miniemulsion mediated by HTEMPO. *Front. Chem. China* **2008,** *3* (1), 41-46.
112. Shojaei, A. H.; Paulson, J.; Honary, S., Evaluation of poly(acrylic acid-co-ethylhexyl acrylate) films for mucoadhesive transbuccal drug delivery: factors affecting the force of mucoadhesion. *Journal of Controlled Release* **2000,** *67* (2–3), 223-232.
113. Gaur, U.; Wunderlich, B., Heat capacity and other thermodynamic properties of linear macromolecules. IV. Polypropylene. *Journal of Physical and Chemical Reference Data* **1981,** *10* (4), 1051-1064.
114. Diele, S.; Oelsner, S.; Kuschel, F.; Hisgen, B.; Ringsdorf, H.; Zentel, R., X-ray investigations of liquid crystalline homo- and copolysiloxanes with paired mesogens. *Die Makromolekulare Chemie* **1987,** *188* (8), 1993-2000.
115. Wang, Q.; Yang, C.-a.; Xie, H.; Wang, X.; Zhang, H., Effect of mesogenic density on liquid-crystalline behaviours of polymethacrylates bearing azobenzene mesogen. *Liquid Crystals* **2010,** *37* (4), 435 - 443.
116. Barny, P.; Dubols, J.-C.; Friedrich, C.; Noël, C., Polymers with terminally cyanobiphenyl-substituted side chains. *Polymer Bulletin* **1986,** *15* (4), 341-348.
117. Charcosset, C., A review of membrane processes and renewable energies for desalination. *Desalination* **2009,** *245* (1–3), 214-231.
118. Lin, H.; Van Wagner, E.; Raharjo, R.; Freeman, B. D.; Roman, I., High-Performance Polymer Membranes for Natural-Gas Sweetening. *Advanced Materials* **2006,** *18* (1), 39-44.
119. Han, S.; Rabie, F.; Marand, E.; Martin, S. M., Enantioselective Separations Using Chiral Supported Liquid Crystalline Membranes. *Chirality* **2012**, n/a-n/a.
120. Loth, H.; Euschen, A., Diffusion flux control by liquid-crystalline side-chain polysiloxane elastomer foils. *Die Makromolekulare Chemie, Rapid Communications* **1988,** *9* (1), 35-38.
121. Barrer, R. M.; Rideal, E. K., Permeation, diffusion and solution of gases in organic polymers. *Transactions of the Faraday Society* **1939,** *35* (0), 628-643.
122. Serrette, A.; Carroll, P. J.; Swager, T. M., Tuning the intermolecular dative interactions in vanadium-oxo linear chain compounds: formation of a new type of liquid crystalline polymer. [Erratum to document cited in CA116(12):117814y]. *Journal of the American Chemical Society* **1993,** *115* (24), 11656-11656.
123. Koros, W. J.; Fleming, G. K., Membrane-based gas separation. *Journal of Membrane Science* **1993,** *83* (1), 1-80.

124. Li, Y.; Kröger, M.; Liu, W. K., Primitive chain network study on uncrosslinked and crosslinked cis-polyisoprene polymers. *Polymer* **2011,** *52* (25), 5867-5878.